CHAPTER 6

Wet Etching of III–V Semiconductors

Walter P. Gomes

LABORATORIUM VOOR FYSISCHE CHEMIE, UNIVERSITEIT GENT, BELGIUM

1. INTRODUCTION 215
2. SEMICONDUCTOR ELECTROCHEMISTRY: BASIC PRINCIPLES AND EXPERIMENTAL METHODS 218
   2.1. *Semiconductors* 218
   2.2. *The Semiconductor–Liquid Solution Interface* 220
   2.3. *Electrochemical Reactions at Semiconductors in Indifferent Electrolytes* . . 228
   2.4. *Electrochemical Reactions at Semiconductors in Redox Electrolytes* 233
3. TYPES OF ETCHING REACTIONS 238
   3.1. *(Photo)Electrochemical Etching* 238
   3.2. *Photoetching* 239
   3.3. *Electroless Etching* 241
   3.4. *Chemical Etching* 243
4. SOME SOLID-STATE AND ELECTROCHEMICAL DATA ON III–V SEMICONDUCTORS . 244
5. KINETICS AND MECHANISMS OF ETCHING REACTIONS AT III–V SEMICONDUCTORS 246
   5.1. *(Photo)Electrochemical Etching* 246
   5.2. *Photoetching* 253
   5.3. *Electroless Etching* 257
   5.4. *Chemical Etching* 259
   5.5. *Electroless and Chemical Etching Occurring in Parallel* 266
6. MATERIAL-SELECTIVE ETCHING 268
7. ETCH MORPHOLOGIES AND PROFILES 275
   7.1. *Etch Morphologies at Macroscopic Size Surfaces* 275
   7.2. *Profile Etching* 284
8. CONCLUSIONS 292
   ACKNOWLEDGMENT 292
   REFERENCES 293

1. Introduction

In the last two decades, III–V compound semiconductors have become increasingly important for various applications in microelectronics, optoelectronics, and optical telecommunication. Devices such as light-emitting diodes (LEDs), semiconductor laser diodes (LDs), and optical waveguides consist of III–V semiconducting materials [1]. Gallium arsenide is used in field effect

Copyright © 2001 by Academic Press
All rights of reproduction in any form reserved.
ISBN 0-12-752182-8
ISSN 0080-8784/01 $35.00

transistors because of the higher mobility of electrons in GaAs as compared to silicon, leading to devices that can operate faster [2]. In recent years, semiconducting group III nitrides have received great interest because they allow the wavelength range of LEDs and LDs to be extended into the green and the blue, which allows full color displays to be achieved through mixing of the three primary colors [3, 4].

The processing of III–V compound semiconductors for component fabrication involves steps in which material is removed in a controlled way, that is, etching steps. Both dry and wet etching methods are employed. This chapter pertains to wet etching, which is the controlled dissolution of the semiconductor as a consequence of a chemical or an electrochemical reaction. In addition to the controlled dissolution of semiconducting material as such, wet etching also has more specific applications. Whereas the etch morphology often depends on the crystal face, etching is used as a means to identify crystal faces. So-called polishing etchants are used to obtain samples with perfectly smooth surfaces, which is essential in certain process steps [5]. Wet etchants may in many cases react specifically at crystallographic defects such as dislocations, impurity striations, and microprecipitates, and hence have defect-revealing properties [6]. Because the performances of III–V devices are influenced by these defects, etching may hence be used for quality control of semiconducting materials. In many applications, multilayer structures of different III–V semiconductors that are grown epitaxially on a III–V substrate by techniques such as metal–organic chemical vapor deposition (MOCVD) are used. In the processing of these multilayer structures, it is often necessary to remove epitaxial layers selectively with respect to other layers [7]. Wet etchants that exhibit this material selectivity, based upon a difference in reactivity of the etchant with respect to different semiconductor materials, are available. Finally, in device fabrication, mask etching is often employed. It allows well-defined patterns of etch grooves with predetermined shapes to be obtained. For these process steps, wet etching is also appropriate, because it is known that the shape of the etch grooves is determined not only by crystallographic factors, but also by the etching kinetics and mechanisms.

For many years, etching recipes have been proposed mainly on an empirical basis, that is, as the result of trial-and-error experiments. As a consequence of the increasing variety in materials used (i.e., mixed III–V semiconductors composed of more than one group III and/or group V element and with varying composition) and in view of the quite different but very stringent requirements of etching agents for various applications, it has been gradually realized that for an efficient design of etching procedures, a deeper insight is needed into the factors governing the rates of etching reactions and the resulting morphologies, and hence into the mechanisms of etching of semiconductors. Obviously, this objective is not only important from the technological point of view, but also from the scientific. It was further realized that this fundamental approach to the

etching of semiconductors should be electrochemical. Indeed, wet etching processes in general take place at a semiconductor–electrolyte interface. Moreover, in certain cases, etching is achieved by integrating the semiconductor as an electrode into an electrochemical circuit and by drawing (mostly anodic) current through the semiconductor–electrolyte interface. Even when the etching is performed by simply immersing the semiconductor into the electrolyte solution, the net dissolution reaction may be the result of electrochemical steps compensating each other electrically, but not chemically. Gerischer and co-workers [8–11], on the occasion of their electrochemical studies on III–V semiconductors such as GaAs, were probably the first to recognize the potential of semiconductor electrochemistry for investigating the mechanisms of etching processes taking place without any net current flow. In the last 15 years or so, the strategy that consists of combining etch rate measurements with electrochemical studies on the individual steps of etching reactions has been successfully applied to many etching systems, mostly involving III–V semiconductors (for earlier reviews, see, e.g., [12, 13]). The main reasons why III–V semiconductors are especially suited for this line of research is first that most III–V compounds (in contrast to most II–VI compounds) are available both as n-type and p-type semiconductors, allowing identification of the charge-transfer mechanism of electrochemical steps (see further). Second, in contrast to silicon, where one is for a greatly restricted in aqueous media to fluoride or NaOH solutions, at III–V semiconductors a large variety of chemicals can be investigated. Later in this chapter we reveal how electrochemical studies may also help to unravel etching mechanisms that are purely chemical; that is, that do not consist of electrochemical partial reactions.

The outline of this chapter is as follows. Section 2 is devoted to the basic principles and experimental methods of semiconductor electrochemistry. The necessity of such a section is obvious from the foregoing considerations. In Section 3, the four types of etching reactions—(photo)electrochemical etching, photoetching, electroless etching, and chemical etching—are introduced. Section 4 is a short survey of relevant solid-state and electrochemical data on III–V semiconductors. Section 5 contains a detailed discussion on the kinetics and mechanisms of various etching reactions, representative of the previously cited four types of reactions and taking place at different III–V semiconductor materials. In Section 6, the discussion pertaining to the etching kinetics and mechanisms is focussed specifically on the problem of material selectivity, which is important with respect to the etching of multilayer structures as previously mentioned. It is thereby demonstrated that it is essential to know the etching mechanisms to understand and predict material-selective etching. Section 7 pertains to the resulting macroscopic (i.e. at single crystal faces) as well as microscopic (i.e. on the micrometer scale at mask edges) etch morphologies. Both subjects are shown to be closely related; that is, the macroscopic etching kinetics usually constitutes a good guideline for understanding and predicting the shapes of etch profiles near mask edges.

2. Semiconductor Electrochemistry: Basic Principles and Experimental Methods

In this section, the basic principles of semiconductor electrochemistry are briefly recalled. The discussion mainly is restricted to those aspects that are relevant to the wet etching of semiconductors. We refer to the literature [14–17] for more detailed treatments of this subject.

2.1. SEMICONDUCTORS

The electronic energy levels in semiconductors are grouped into energy bands. The highest (nearly) occupied band is denoted as the valence band and is separated from the lowest (nearly) unoccupied band, the conduction band, by a forbidden region of energy called the bandgap. The width of the bandgap E_g is thus given by

$$E_g = E_c - E_v \tag{1}$$

where E_c is the energy at the bottom of the conduction band and E_v is the energy at the top of the valence band. Common values for the bandgap of semiconductors are between 1 and 3 eV. This range of values implies that under equilibrium conditions at room temperature, only a minor fraction of the valence band electrons will be able to get thermally excited from the valence band to the conduction band and hence to create positive holes h^+ (empty levels in the valence band) and conduction band electrons e^- (occupied levels in the conduction band). Because these valence band holes and conduction band electrons are mobile and therefore responsible for the electrical conductivity of the solid, the band structure of most semiconductors is such that they normally are expected to behave as insulators. However, impurities or imperfections in the solid often give rise to localized energy levels in the bandgap. Two types of levels are important with respect to semiconductivity. The first type is that of a donor level; that is, a level close to the conduction band edge E_c and filled with an electron at 0 K. The majority of such levels will have donated their electron to the conduction band at room temperature. If the crystal contains a typical donor density N_D of 10^{16} cm^{-3} and the donor level is close enough to E_c, the density of conduction band electrons n will hence be approximately 10^{16} cm^{-3} at room temperature, giving rise to so-called n-type semiconductivity. The second type of localized level is that of an acceptor level; that is, a level not far above the valence band edge E_v and being empty at 0 K. At room temperature, most acceptor levels will have extracted an electron from the valence band and thus created a density of holes p, approximately equal to the acceptor density N_A. A material in which the conductivity is due to holes is denoted as a p-type semiconductor. In certain cases, a solid material will be either an n- or a p-type

semiconductor because it unintentionally contains a certain density of donors or acceptors, respectively, due to the circumstances under which the crystal was grown. Mostly, however, the material is made semiconducting by intentionally doping it with impurities. For example, gallium arsenide can be made an n-type semiconductor by doping with silicon and p-type by doping with zinc. Note that it is not always possible to achieve a given type of semiconductivity by doping.

The distribution of electrons among the available energy levels of a solid at thermodynamic equilibrium is described by Fermi statistics and characterized by a parameter, the Fermi energy or Fermi level E_F. An electronic level at the Fermi energy has a probability of 0.5 of being filled. The chemical significance of E_F is the electrochemical potential of the electrons divided by the Avogadro constant (i.e., expressed per particle). Usually, the Fermi level is within the bandgap and sufficiently distant ($> 2kT$) from the band edges. In that case, the Fermi distribution can be approximated by the following Boltzmann-type expressions for the densities of conduction band electrons and of holes:

$$n = N_c \exp[-(E_c - E_F)/kT] \tag{2}$$

or

$$E_F = E_c + kT \ln(n/N_c) \tag{3}$$

and

$$p = N_v \exp[(E_v - E_F)/kT] \tag{4}$$

or

$$E_F = E_v - kT \ln(p/N_v) \tag{5}$$

N_c and N_v represent the effective density of states at the bottom of the conduction band and at the top of the valence band, respectively.
From Eqs. (1), (2), and (4), it follows that

$$n\,p = N_c N_v \exp(-E_g/kT) \tag{6}$$

Equation (6) implies that at equilibrium, when n is relatively high (n-type semiconductor), p will be negligibly small and vice versa. However, nonequilibrium conditions also must be considered. For example, when illuminating the semiconductor with photons that have an energy $h\nu$ greater than E_g, electrons will be excited from the valence band to the conduction band, leading to an excess of both electrons and holes but affecting, on a relative scale, primarily the density of minority carriers (holes in an n-type and electrons in a p-type semiconductor). Under constant illumination, a steady-state density of minority carriers

will build up, depending on the generation and recombination rates of electrons and holes.

2.2. THE SEMICONDUCTOR–LIQUID SOLUTION INTERFACE

Wet etching of semiconductors implies reactions that occur at a semiconductor–liquid solution interface. In most cases, an (aqueous) electrolyte solution is involved. Therefore, we will first deal with the properties of the semiconductor–electrolyte interface, and more specifically with the charge and potential distribution at this interface.

2.2.1. *Charge and Potential Distribution*

Consider an electrochemical cell containing a semiconductor electrode SC, and a large area counterelectrode consisting of a metal ME (e.g., Pt) and a reference electrode RF. For the sake of simplicity, assume that all three electrodes are connected to wires consisting of the metal ME. The potential difference φ(right)$-\varphi$(left) in the circuit

ME/RF/EL/SC/ME

is called the electrode potential V of the semiconductor. It is the sum of the potential differences at the individual interfaces of the circuit. In what follows, the potential differences across ME/RF/EL are considered to be constant. Also the contact potential SC/ME can be considered to be constant for a given combination of materials. The potential difference of interest here is $\varphi_{sc/el}$, defined as the potential in the bulk of the semiconductor minus that in the bulk of the electrolyte, and hence related to V by

$$V = \varphi_{sc/el} + ct \tag{7}$$

or, under varying V, by

$$dV = d\varphi_{sc/el} \tag{8}$$

An accumulation of charges at both sides of the SC/EL interface corresponds to a given $\varphi_{sc/el}$. In what follows, assume that the electrolyte solution is concentrated ($c > 0.1$ mol l^{-1}). In that case, the charge at the electrolyte side of the interface can be considered to be concentrated in the (outer) Helmholtz plane, that is, the plane of closest approach of solvated ions to the semiconductor surface, which is located at about 0.3 nm from the surface. The layer between the surface and Helmholtz plane is called the Helmholtz layer H. It contains primarily solvent molecules which are more or less oriented in the electric field at

the surface. Therefore, the dielectric constant of the Helmholtz layer ε_H is generally assumed to be less than that of the free solvent; for water, for example, a value of $\varepsilon_H \cong 6$ is commonly accepted.

The charge at the semiconductor side of the interface extends over a much larger distance (see further), especially in the most important cases for semiconductor electrochemistry, that is, when $\varphi_{sc/el}$ is either greater than 0 for an n-type semiconductor or less than 0 for a p-type semiconductor electrode. A so-called space–charge layer is present here. In the former case, this space–charge consists of uncompensated ionized (positive) donors; in the latter case, it consists of filled (negative) acceptors. One also speaks of a depletion region in these cases, since the subsurface region and the surface of the semiconductor are depleted of free charge carriers (conduction band electrons e^- for n-type; valence band holes h^+ for p-type).

For a depletion layer in an n-type semiconductor, let us express the equilibrium number of conduction band electrons per unit volume n as a function of depth into the semiconductor x; the x axis is taken perpendicular to the surface, with the origin $x = 0$ at the surface (s) and the positive sense directed toward the bulk (b) of the semiconductor.

Using Eq. (2), we can write for n at any value of the coordinate x,

$$n(x) = N_c \exp(-[E_c(x) - E_F]/kT) \tag{9}$$

with $E_c(x)$ the energetic position of the conduction band edge at x.

Writing the expression, analogous to Eq. (9), for the bulk concentration of electrons, n_b, and dividing Eq. (9) by this expression, we obtain

$$n(x) = n_b \exp(-[E_c(x) - E_{c,b}]/kT) \tag{10}$$

The energy difference $E_c(x) - E_{c,b}$ is correlated to the corresponding potential difference through

$$E_c(x) - E_{c,b} = -e[\varphi(x) - \varphi_b] \tag{11}$$

where e is the positive elementary charge. From Eqs. (10) and (11), it follows that

$$n(x) = n_b \exp(e[\varphi(x) - \varphi_b]/kT) \tag{12}$$

Specifying to the conduction band concentration at the surface $n_s(x = 0)$, we obtain

$$n_s = n_b \exp([e(\varphi_s - \varphi_b)]/kT) \tag{13}$$

or, defining the potential drop in the space–charge layer of the semiconductor φ_{sc} as

$$\varphi_{sc} = \varphi_b - \varphi_s \tag{14}$$

$$n_s = n_b \exp(-e\varphi_{sc}/kT) \tag{15}$$

The analogous expression for the equilibrium concentration of holes at the surface of a p-type semiconductor, p_s, is

$$p_s = p_b \exp(e\varphi_{sc}/kT) \tag{16}$$

Whereas the separation of charges at the interface SC/EL involves two regions, that is, the space–charge layer within the semiconductor and the Helmholtz layer, we can write

$$\begin{aligned}\varphi_{sc/el} &= (\varphi_b - \varphi_s) + (\varphi_s - \varphi_{el}) \\ &= \varphi_{sc} + \varphi_H \end{aligned} \tag{17}$$

Here, φ_{el} represents the potential in the bulk of the electrolyte and φ_H represents the potential drop across the Helmholtz layer. From Eqs. (8) and (17), it follows that, when one changes the semiconductor electrode potential V, for example, by an external voltage supply connected between the semiconductor and the counterelectrode, one changes, in principle, φ_{sc} as well as φ_H. Subsequently, we will see that in many cases the change in φ_H is negligible. Anyway, according to Eqs. (15) and (16), this allows the concentrations of free charge carriers at the surface to change. This point is important as far as semiconductor electrode kinetics is concerned.

The change of the potential $\varphi(x)$ with distance into the semiconductor electrode corresponds to a change in the position of the energy bands. The relationship is given by an expression of the type of Eq. (11); that is, the energy bands are bent in the space–charge layer. Figure 1 shows schematically the charge and potential distribution as well as the band-bending in the case of an n-type semiconductor electrode that is positively charged with respect to the electrolyte. In Figure 1c, the Fermi level is drawn horizontally, because it is assumed that no current flows and hence the system is at equilibrium.

Let us now describe the potential distribution over the interface SC/EL more quantitatively. We again consider the case of an n-type semiconductor polarized positively, that is, $\varphi_{sc/el} > 0$. The starting point of the derivation is the one-dimensional form of the Poisson equation

$$d^2\varphi(x)/dx^2 = -\rho(x)/\varepsilon_0\varepsilon \tag{18}$$

where $\rho(x)$ is the charge density at the position x. Integration of Eq. (18) from $x = 0$ to $x \to \infty$ leads to an expression for the total charge per unit of surface area in the space–charge layer Q_{sc},

$$Q_{sc} = \varepsilon_0\varepsilon[d\varphi(x)/dx]_{x=0} \tag{19}$$

in which ε represents the dielectric constant of the semiconductor (note that $[d\varphi(x)/dx]_{x\to\infty} = 0$).

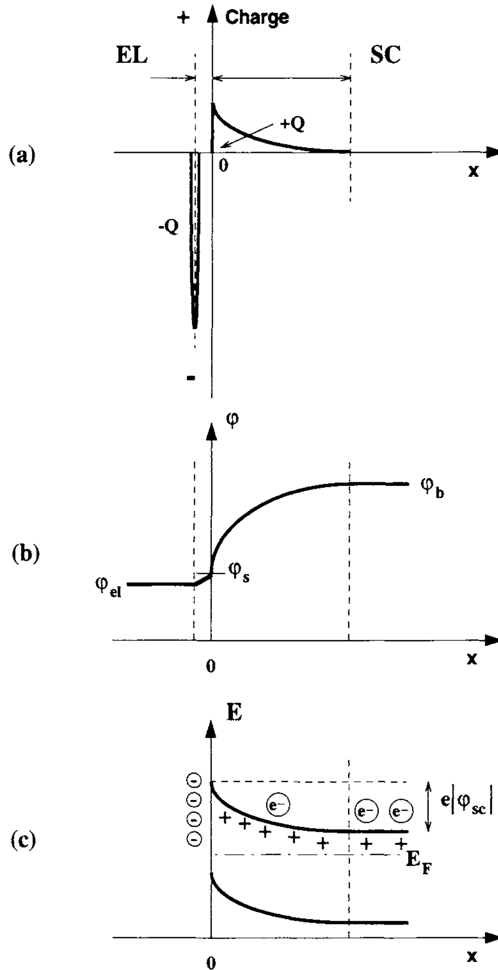

FIG. 1. Schematic representation of (a) charge distribution, (b) potential distribution, and (c) band-bending at an n-type semiconductor electrode under depletion conditions.

On the other hand, $\rho(x)$ can be expressed as

$$\rho(x) = e[N_D - n(x)] \tag{20}$$

where N_D is the donor density. Assuming that all donors in the bulk of the semiconductor are ionized ($n_b = N_D$), it follows from Eqs. (12) and (20) that

$$\rho(x) = eN_D\left[1 - \exp\left(\frac{e[\varphi(x) - \varphi_b]}{kT}\right)\right] \tag{21}$$

Combining Eqs. (18) and (21) yields

$$\frac{d^2\varphi(x)}{dx^2} = -\frac{eN_D}{\varepsilon_0\varepsilon}\left[1 - \exp\left(\frac{e[\varphi(x) - \varphi_b]}{kT}\right)\right] \tag{22}$$

Now consider the mathematical expressions

$$\frac{d}{dx}\left(\frac{d\varphi}{dx}\right)^2 = 2\frac{d^2\varphi}{dx^2}\frac{d\varphi}{dx} \tag{23}$$

and hence

$$\left(\frac{d\varphi}{dx}\right)^2 = 2\int \frac{d^2\varphi}{dx^2}\, d\varphi \tag{24}$$

Application on Eq. (22) yields

$$\left(\frac{d\varphi}{dx}\right)^2 = -\frac{2eN_D}{\varepsilon_0\varepsilon}\left[\varphi(x) - \frac{kT}{e}\exp\left(\frac{e[\varphi(x) - \varphi_b]}{kT}\right)\right] + ct \tag{25}$$

The value of the integration constant follows from the condition $(d\varphi/dx) = 0$ for $\varphi = \varphi_b$:

$$0 = -\frac{2eN_D}{\varepsilon_0\varepsilon}\left(\varphi_b - \frac{kT}{e}\right) + ct \tag{26}$$

Hence

$$\left(\frac{d\varphi}{dx}\right)^2 = \frac{2eN_D}{\varepsilon_0\varepsilon}\left\{[\varphi_b - \varphi(x)] - \frac{kT}{e}\left[1 - \exp\left(\frac{e[\varphi(x) - \varphi_b]}{kT}\right)\right]\right\} \tag{27}$$

Specifying to $x = 0$ and in view of Eq. (14),

$$\left(\frac{d\varphi}{dx}\right)^2_{x=0} = \frac{2eN_D}{\varepsilon_0\varepsilon}\left\{\varphi_{sc} - \frac{kT}{e}\left[1 - \exp\left(-\frac{e\varphi_{sc}}{kT}\right)\right]\right\} \tag{28}$$

In the so-called Mott–Schottky approximation, it is assumed that $e\varphi_{sc} \gg kT$, so that the exponential term can be neglected, and Eq. (28) reduces to

$$\left(\frac{d\varphi}{dx}\right)_{x=0} = \left(\frac{2eN_D}{\varepsilon_0\varepsilon}\right)^{1/2}\left(\varphi_{sc} - \frac{kT}{e}\right)^{1/2} \tag{29}$$

Combination of Eqs. (19) and (29) yields

$$Q_{sc} = (2\varepsilon_0\varepsilon eN_D)^{1/2}(\varphi_{sc} - kT/e)^{1/2} \tag{30}$$

The countercharge of the space–charge is located in the Helmholtz plane:

$$|Q_H| = Q_{sc} \tag{31}$$

According to Eq. (18), because no charges are present within the Helmholtz layer, the potential drop over this layer is linear,

$$d\varphi/dx = ct = \varphi_{\mathrm{H}}/d_{\mathrm{H}} \tag{32}$$

where d_{H} is the width of the Helmholtz layer ($\cong 3 \times 10^{-10}$ m). Application of Eq. (19) to the Helmholtz layer yields

$$|Q_{\mathrm{H}}| = \varepsilon_0 \varepsilon_{\mathrm{H}} \varphi_{\mathrm{H}}/d_{\mathrm{H}} = Q_{\mathrm{sc}} \tag{33}$$

From Eqs. (30) and (33), it finally follows that

$$\varphi_{\mathrm{H}} = (2\varepsilon_0 \varepsilon e N_D)^{1/2} \frac{d_{\mathrm{H}}}{\varepsilon_0 \varepsilon_{\mathrm{H}}} \left(\varphi_{\mathrm{sc}} - \frac{kT}{e} \right)^{1/2} \tag{34}$$

The discussion of the relative contributions of φ_{sc} and φ_{H} to $\varphi_{\mathrm{sc/el}}$ [see Eq. (17)] is somewhat hampered by the fact that the relationship (34) is not linear. As an example, consider typical values of $\varphi_{\mathrm{sc}} = 0.2$ V, $N_D = 10^{16}$ cm^{-3} $= 10^{22}$ m^{-3}, and $\varepsilon = 5$. Equation (34) then yields a value of $\varphi_{\mathrm{H}} = 8.8 \times 10^{-4}$ V $\cong 1$ mV, which is negligible with respect to φ_{sc}. In most cases, $\varphi_{\mathrm{sc/el}}$ can hence be approximated by φ_{sc} and Eq. (7) can be approximated by

$$V = \varphi_{\mathrm{sc/el}} + ct \cong \varphi_{\mathrm{sc}} + ct \tag{35}$$

The fact that the potential drop $\varphi_{\mathrm{sc/el}}$ occurs practically exclusively over the space–charge region of the semiconductor is due to the relatively low concentration of charge carriers $n_{\mathrm{b}} \cong N_D$ in the semiconductor. This can easily be seen by repeating the preceding calculation for a typical metal such as silver, with $n_{\mathrm{b}} \cong 6 \times 10^{28}$ m^{-3}. Here, the potential drop is found to be predominantly over the Helmholtz layer.

Note that in many cases the Helmholtz potential contains a potential-dependent contribution that has not been considered in the foregoing derivation, because surface charges are involved that are not due to the application of a potential difference $\varphi_{\mathrm{sc/el}}$, but to the establishment of an acid–base or an adsorption equilibrium at the surface (see further). This V-independent contribution is hence included in the constant term of Eq. (35). It should be kept in mind that this contribution can vary with the composition of the electrolyte (e.g., with pH).

In addition to depletion, other situations may occur at a semiconductor electrode surface, depending on bias. In Figure 2, depletion, flat-band situation, and accumulation are depicted for an n- as well as for a p-type electrode. One more possible situation is not shown in the figure, that is, inversion. By inversion we mean the following. In the case of an n-type electrode, for example, when the positive bias is so large that the Fermi level at the surface is below the middle of the bandgap, the equilibrium surface concentration of holes should exceed that of electrons; that is, holes should be created at the surface. When the band-bending is not too large, this inversion phenomenon is usually not observed with wide-bandgap semiconductors.

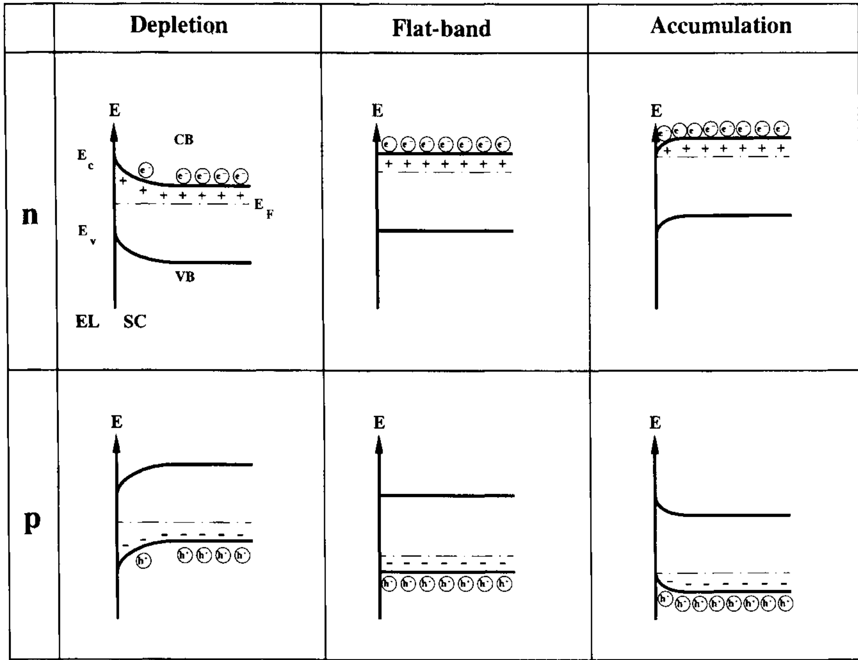

FIG. 2. Depletion, flat-band, and accumulation at n- and p-type semiconductor electrodes.

Note that when changes in the applied bias may be assumed to have no effect on the Helmholtz potential drop, the potential at the electrode surface, φ_s, can be considered to be fixed with respect to a reference level in the electrolyte or to the potential of the reference electrode, meaning that the band edges remain fixed with respect to the corresponding reference level. Hence the bands in the bulk of the semiconductor move up or down when the electrode potential is varied. As will become clear in the following sections, knowledge of the energetic position of the band edges at the surface $E_{c,s}$ and $E_{v,s}$ is of crucial importance to understanding the reactivity at the semiconductor–liquid interface. This position can be determined from knowledge of the flat-band potential V_{fb}, that is, the potential of the semiconductor electrode with respect to the reference electrode corresponding to the flat-band situation. Whereas in that case $\varphi_{sc} = 0$, V_{fb} corresponds to the constant term in Eq. (35), so that

$$V - V_{fb} = \varphi_{sc} \tag{36}$$

The flat-band potential measures the Fermi level of the semiconductor at the flat band with respect to that in the reference electrode:

$$E_{F,fb} = -eV_{fb} \tag{37}$$

From $E_{F,\text{fb}}$, the position of E_c can be determined (for an n-type semiconductor), provided that n ($\cong N_D$) and N_c are known [see Eq. (3)]. At values of the electrode potential different from V_{fb}, the position of the conduction band edge at the surface, $E_{c,\text{s}}$, remains the same at the surface. The corresponding value of $E_{v,\text{s}}$ is then deduced from Eq. (1).

The flat-band potential of a semiconductor electrode can be determined from differential capacitance measurements at the circuit containing the semiconductor electrode and the counterelectrode, performed under conditions of depletion, as will be explained in the next section.

2.2.2. *Differential Capacitance*

An electrical capacitance can be attributed to each of the interfaces of an electrochemical cell and describes their ability to accumulate charges under the influence of an applied potential difference. The different interfaces of the electrical circuit that comprise the cell can be considered to be connected in series, so that the total cell capacitance C is given by

$$C^{-1} = \sum_i C_i^{-1} \tag{38}$$

where the C_is are the capacitances of the individual interfaces.

The way the cell capacitance is experimentally determined is usually by applying a dc bias as well as a superimposed small ac signal between the semiconductor and the metal counterelectrode. Therefore, the circuit to be considered in a three-electrode cell for capacitance considerations is the current-carrying circuit

and the capacitance of interest is the differential capacitance $dQ/d\varphi$.

Assuming that the SC/ME contact is low ohmic, so that the corresponding capacitance is short-circuited, and that the surface area of the contact ME/EL is sufficiently large, so that, according to Eq. (38), the corresponding capacitance can be neglected, the only capacitance to be considered is that of the SC/EL junction.

In view of the foregoing considerations and of the approximate Eq. (35), the cell capacitance per unit of surface area C can be written as

$$C \cong C_{\text{sc/el}} = dQ_{\text{sc}}/d\varphi_{\text{sc/el}} \cong dQ_{\text{sc}}/d\varphi_{\text{sc}} \tag{39}$$

By taking the derivative of Eq. (30) with respect to φ_{sc}, the following expression for C is hence obtained:

$$C = \left(\frac{\varepsilon_0 \varepsilon e N_D}{2}\right)^{1/2} \left(\varphi_{\text{sc}} - \frac{kT}{e}\right)^{-1/2} \tag{40}$$

or

$$\frac{1}{C^2} = \frac{2}{\varepsilon_0 \varepsilon e N_D}\left(\varphi_{sc} - \frac{kT}{e}\right) \tag{41}$$

Inserting Eq. (36) into Eq. (41), the so-called Mott–Schottky relationship is obtained:

$$\frac{1}{C^2} = \frac{2}{\varepsilon_0 \varepsilon e N_D}\left(V - V_{fb} - \frac{kT}{e}\right) \tag{42}$$

This equation predicts a linear relationship between C^{-2} and the electrode potential V, which, in principle, allows the following data that are essential to the study of electrode kinetics, to be obtained:

1. The point of extrapolation of the Mott–Schottky plot with the V-axis leads to the determination of V_{fb}.
2. The slope of the Mott–Schottky plot yields the donor density N_D, provided that ε and the surface area of the electrode are known (remember that C is the capacitance per unit area).
3. The knowledge of V_{fb} allows determination of φ_{sc} at given V [see Eq. (36)] and hence n_s [see Eq. (15)].
4. Still under the assumption that the variation of φ_H with V is negligible, the (fixed) position of the band edges at the surface $E_{c,s}$ and $E_{v,s}$ can be determined; see Section 2.2.1.

Considerations that are analogous to the preceding can be held for a p-type semiconductor electrode. The form of the Mott–Schottky relationship in this case is

$$\frac{1}{C^2} = \frac{2}{\varepsilon_0 \varepsilon e N_A}\left(-V + V_{fb} - \frac{kT}{e}\right) \tag{43}$$

Experimentally, it is often found that C at fixed electrode potential V depends on the frequency f of the ac signal used, indicating that the foregoing assumptions made for an ideal Schottky barrier and on which this simple derivation was based are not always fulfilled. Whereas usually Mott–Schottky plots recorded at different measuring frequencies more or less converge to a common point on the potential axis, the flat-band potential can still be approximately determined in such cases. For a recent discussion on this problem, see [18].

2.3. ELECTROCHEMICAL REACTIONS AT SEMICONDUCTORS IN INDIFFERENT ELECTROLYTES

We now briefly discuss the current–potential behavior of semiconductor electrodes immersed in an indifferent electrolyte solution, that is, in a solvent

containing ions that do not react electrochemically. The discussion is restricted to aqueous medium.

Figure 3a shows typical current density (j) vs. potential (V) curves for an n-type semiconductor in darkness (curve 1) and under illumination with photons having an energy $h\nu \geq E_g$ (curve 2). Curve 1 demonstrates the rectifying characteristics of a semiconductor–electrolyte contact: in the anodic sense, a low nearly constant current is observed (j typically between 1 nA cm^{-2} and 1 μA cm^{-2}), whereas in the cathodic sense, the current rises exponentially when the potential becomes more negative. Whereas the latter sense is that in which the electron concentration at the surface increases exponentially [Eq. (15)], the electrochemical reaction involved obviously requires the participation of conduction

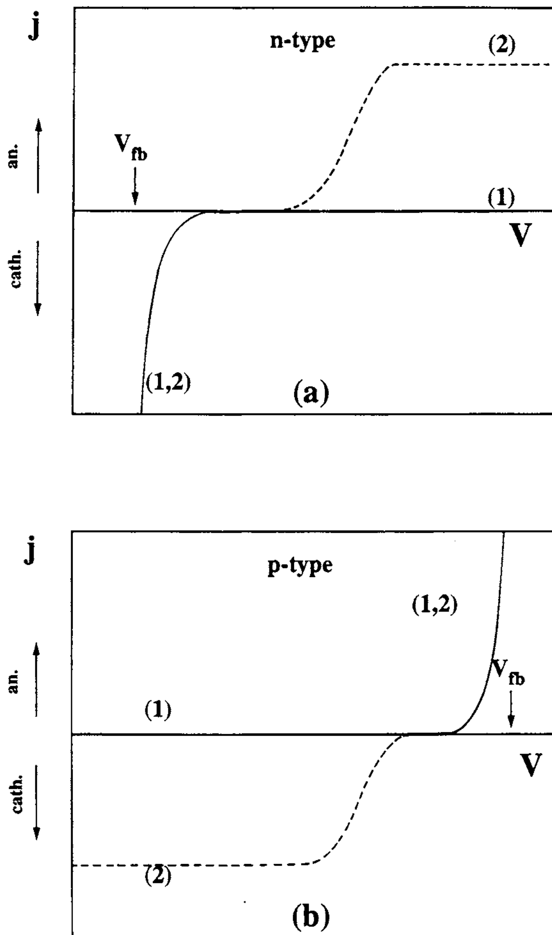

FIG. 3. Schematic current density vs. potential curves. (a) n-type electrode; (b) p-type electrode; 1, darkness, 2, light.

band electrons (*electron capture*). [Note that usually this exponential current range is found under depletion ($V > V_{fb}$), due to the relatively high electron capture rate constant.] The corresponding reaction appears to be the reduction of water molecules or of protons, resulting in hydrogen evolution. In certain cases, a small fraction of the cathodic current is associated with the reduction of the semiconductor material itself; for example, in the case of InP, the formation of some metallic In is observed.

Curve 2 shows that the anodic current is greatly enhanced by illumination. The difference between the current under illumination and that in darkness is denoted as the *photocurrent*. The onset of the photocurrent curve is in a potential range that is positive to the flat-band potential. Considering the sense in which the energy bands are bent under these circumstances, the occurrence of a photocurrent can be interpreted as follows (Fig. 4a). The electrons and holes, which are formed by absorption of photons, are separated by the electric field in the depletion layer. The holes move to the surface, where they undergo electrochemical reactions, and the electrons are drawn into the bulk and from there into the external circuit (at $V \leq V_{fb}$, the holes formed by light immediately recombine with electrons due to the large density of majority carriers at and near the surface). Because the photoinduced charge carriers have a finite lifetime before recombining, holes created in a region behind the depletion layer, denoted as the diffusion layer, also may reach the depletion layer and hence the surface. In most cases, the reaction associated with the photocurrent is found to be the anodic oxidation of the semiconductor material; in some cases, in aqueous media, the oxidation of the solvent to O_2 is involved (TiO_2, $SrTiO_3$). In view of the scope of this chapter, we restrict the discussion to the anodic oxidation of the semiconductor. Apparently, because this reaction does not occur in darkness at n-type electrodes, at least the first step of this multiequivalent

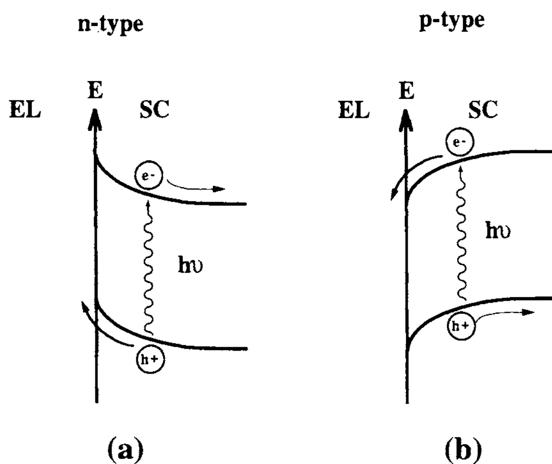

FIG. 4. Mechanism of photocurrent generation at n- and p-type semiconductor electrodes.

oxidation reaction requires a valence band hole. Since the valence band is composed of the bonding states of the semiconductor, holes at the surface correspond to electrons being removed from surface bonds. The problem of whether or not the subsequent steps are so-called hole-capture steps will be addressed subsequently. The photocurrent curve exhibits an onset region (normally rather close to the flat-band potential), the shape of which is mainly determined by surface charge-carrier recombination, followed, at not too high light intensities, by a saturation region in which the current density is governed by the rate at which the holes are created by light and, therefore, it is proportional to the light intensity. At higher light intensities, various types of alternative behavior may occur. When the dissolution rate of the oxidation products is relatively low, the photocurrent may go through a maximum with increasing potential and then drop to a lower level, where this typical passivating behavior is due to the formation of a product layer on the surface. Under certain circumstances, the anodic oxidation reaction may require the participation of ions from solution for the formation of soluble products (e.g., OH^- ions to form oxyanions); in that case, at high light intensities, diffusion of these ions toward the electrode surface may become rate-determining (see subsequent text).

Figure 3b shows typical j vs. V curves for a p-type semiconductor in darkness (curve 1) and under illumination (curve 2). The cathodic current density is low in darkness, but enhanced by light. Whereas under the given circumstances, photogenerated conduction band electrons are drawn toward the electrode surface (see Fig. 4b), it can again be concluded that the hydrogen evolution reaction is a conduction band process. In the anodic sense, the current rises exponentially. This can easily be understood by keeping in mind that the first step of the anodic dissolution reaction occurs by hole capture. If the various steps of this multiequivalent reaction are irreversible, the steady-state current density can be written as

$$j = nFkp_s c_s \tag{44}$$

where n is the equivalence of the reaction, F is the Faraday constant, k is the rate constant of the first step, and c_s is the surface concentration of the reactant needed to form the soluble oxidation products. The exponential rise of j is then attributable to that of p_s with φ_{sc} [Eq. (16)] and hence with V [Eq. (36)]. From these equations, a rise of j by a factor of 10 per 60 mV potential increase is expected. In most cases, for reasons that are not clearly established, the curve is less steep than expected. Also here, passivation effects may occur at higher current densities, due to layer formation.

It should be stressed that in case the anodic oxidation products are soluble, the (photo)anodic reaction under consideration amounts to the electrochemical etching of the semiconductor.

The equivalence n of the anodic dissolution reaction can be determined, based on Faraday's law, from the total amount of (photo)anodic charge drawn over a

certain amount of time and the corresponding amount of semiconductor material dissolved. The latter quantity can be determined after the passage of current, either by analyzing the cell solution or by measuring the etch depth (using a mask to cover part of the surface from the solution to make the difference between the etched and the unetched surface visible). The value of n for a given reaction in a given medium, combined with chemical considerations, then leads to information on the oxidation products.

The question arises whether or not the subsequent steps of the (photo)anodic oxidation reaction of semiconductors are hole-capture steps. Indeed, let us represent the capture of a hole in a surface bond of a semiconductor AB by the reaction equation

$$A:B + h^+ \rightarrow A \bullet B \tag{45}$$

The surface species A • B is then an oxidation intermediate that has an unpaired electron that is no longer in a valence band level, but in a surface state, that is, an energy level in the bandgap at the surface [19]. Therefore, A • B may, in principle, be further oxidized either by capture of a second hole,

$$A \bullet B + h^+ \rightarrow \text{products} \tag{46}$$

or by injection of an electron into the conduction band,

$$A \bullet B \rightarrow e^- + \text{products} \tag{47}$$

[We do not specify here the nature of the surface products formed in reactions (46) and (47). In most cases, several electrochemical steps are needed before soluble products are formed.] Electron injection [reaction (47)] is expected to occur only if the corresponding surface state is sufficiently close to the conduction band edge, which in many cases seems to be rather improbable [19].

Several methods may be used to investigate the contribution of electron injection to (photo)anodic dissolution. An appropriate technique for the photoanodic dissolution of n-type semiconductors is intensity-modulated photocurrent spectroscopy (IMPS). At a constant potential in the photocurrent saturation region, a harmonically modulated light source is superimposed upon the base illumination, creating a modulated hole flux toward the n-type semiconductor surface. It has been shown that, due to the extremely fast separation of photogenerated electron–hole pairs, the harmonically varying concentration of holes at the surface is always in phase with the light source. In the absence of reaction step (47), the current in the external circuit also is in phase with the light intensity. If, however, the second step of the photoanodic dissolution reaction is reaction (47) (for simplicity, we assume here that the overall reaction is two-equivalent), the fact has to be taken into account that such an electron injection step is characterized by a time constant, so that the current may lag behind with respect to the modulated light intensity over a certain phase angle. Only at very low

frequencies of the modulated light is the modulated injection current density in phase with the light source. In contrast, at very high frequencies, the hole current [reaction (46)] is measured exclusively. Hence by measuring the photoresponse as a function of frequency, the contribution of electron injection steps to photoanodic dissolution can be detected. More quantitative considerations on this method can be found in the literature [20, 21] and in further sections of this chapter.

In addition to IMPS, electron injection during anodic dissolution of semiconductors may be investigated by other methods, which are summarized, for example, in [13], some of which are discussed further in this text.

2.4. ELECTROCHEMICAL REACTIONS AT SEMICONDUCTORS IN REDOX ELECTROLYTES

From the electronic point of view, an oxidizing agent in solution, ox^z, can be considered as an empty energy level, and the corresponding reducing agent red^{z-1} can be considered as a filled energy level (for simplicity in what follows, one-equivalent redox couples are considered). Cathodic reduction of an oxidizing agent at a semiconductor electrode then amounts to electron transfer from a semiconductor level to an empty level in solution; anodic oxidation of a reducing agent amounts to electron transfer from a filled level in solution to an empty level in the semiconductor. The generally accepted theory for these processes was developed by Gerischer [14, 15]. The basic idea is that electron transfer occurs by tunneling through the Helmholtz layer, and thus occurs between electron levels at equal energetic height. To understand electrochemical reactivity, the energy level distribution of the redox couple in solution with respect to that in the semiconductor must be known. Due to the difference in solvation structure between the oxidizing agent and the corresponding reducing agent, the energy of the most stable empty and filled redox states, E_{ox}^m and E_{red}^m, respectively, differs considerably. More specifically, it can be shown that the empty level is higher in energy than the filled level over an amount $2\lambda_r$,

$$E_{ox}^m - E_{red}^m = 2\lambda_r \tag{48}$$

in which λ_r, the rearrangement energy, is related to the rearrangement taking place in the solvation structure of the ion when this ion either takes up or gives off an electron. Reliable data on λ_r are not currently available; values reported in the literature often are between 0.4 and 1.2 eV, depending on the redox couple considered.

Owing to fluctuations of the solvation shell of the ions, the redox energy states do not constitute discrete levels, but are distributed over a certain energy range. In Gerischer's theory, the densities of energy functions are described by

Gaussian functions, D_{ox} and D_{red}, the widths of which are again determined by the rearrangement energy of the redox couple

$$D_{\text{ox}} \sim \exp\left[-\left(E - E_{\text{ox}}^{m}\right)^{2}/4\lambda_{r}kT\right] \tag{49}$$

and

$$D_{\text{red}} \sim \exp\left[-\left(E - E_{\text{red}}^{m}\right)^{2}/4\lambda_{r}kT\right] \tag{50}$$

(see Fig. 5). It can be shown that the Fermi level of the redox couple at equal activities of the oxidizing and the reducing agent, $E_{F,\text{redox}}^{\circ}$, is energetically midway between the maxima of the empty and filled level curves:

$$E_{F,\text{redox}}^{\circ} = E_{\text{red}}^{m} + \lambda_{r} = E_{\text{ox}}^{m} - \lambda_{r} \tag{51}$$

Whereas $E_{F,\text{redox}}^{\circ}$ [measured with respect to the Fermi level in the standard hydrogen electrode (SHE)] is related to the standard redox potential of the couple U° by

$$E_{F,\text{redox}}^{\circ} = -eU^{\circ} \tag{52}$$

the U° value can be used as a rough measure for the energetic position of the redox levels. When also expressing the position of the semiconductor band edges at the surface $E_{c,s}$ and $E_{v,s}$ with respect to the SHE, mutual comparison between energy level positions at both sides of the semiconductor–redox electrolyte interface becomes possible, which is essential for discussing electrochemical reactivity.

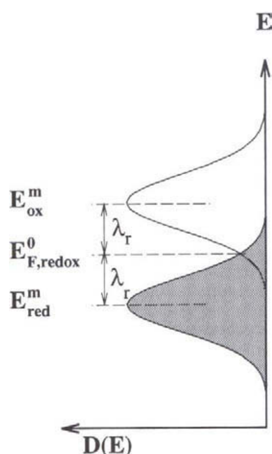

FIG. 5. Gaussian curves that represent the energetic distribution of redox levels in solution.

Since in principle, electrons for cathodic charge transfer may originate either from the conduction band or from the valence band of the semiconductor electrode, two types of cathodic reactions are possible:

$$\mathrm{ox}^z + \mathrm{e}^- \xrightarrow{k_{c,c}} \mathrm{red}^{z-1} \tag{53}$$

and

$$\mathrm{ox}^z \xrightarrow{k_{c,v}} \mathrm{red}^{z-1} + \mathrm{h}^+ \tag{54}$$

The first type is the capture of a conduction band electron, a process that was discussed previously (Section 2.3). Reaction (54) describes the uptake by the oxidizing agent of an electron from the valence band of the semiconductor, leading to the creation of a hole in that band; therefore this process is denoted as hole injection.

Similarly, two types of anodic oxidation reactions may occur, depending on whether the conduction or the valence band is involved, that is, electron injection and hole capture [reactions (55) and (56), respectively]:

$$\mathrm{red}^{z-1} \xrightarrow{k_{a,c}} \mathrm{ox}^z + \mathrm{e}^- \tag{55}$$

$$\mathrm{red}^{z-1} + \mathrm{h}^+ \xrightarrow{k_{a,v}} \mathrm{ox}^z \tag{56}$$

Whether or not cathodic or anodic current flow can occur depends on the relative positions of the Fermi levels in the semiconductor and in the redox electrolyte. If a reaction is thermodynamically possible and if the surface reaction is rate-determining, the current densities corresponding to reactions (53)–(56) can be expressed by the following respective equations, taking into account the sign conventions for electrochemical currents:

$$-j_{c,c} = ek_{c,c}c_{\mathrm{ox}}n_{\mathrm{s}} \tag{57}$$

$$-j_{c,v} = ek_{c,v}c_{\mathrm{ox}} \tag{58}$$

$$j_{a,c} = ek_{a,c}c_{\mathrm{red}} \tag{59}$$

$$j_{a,v} = ek_{a,v}c_{\mathrm{red}}p_{\mathrm{s}} \tag{60}$$

(c_{ox} and c_{red} represent concentrations in the outer Helmholtz plane.)

The rate constants in these equations evidently depend on the relative positions of electron energy levels at both sides of the interface. For example, hole injection requires that the empty redox levels overlap with the valence band of the semiconductor and hence have a relatively low position in the energy diagram. Considering Eq. (52), such behavior may be, in general, expected for a (one-equivalent) redox couple that has a high standard redox potential; that is, a relatively strong oxidizing agent.

It also follows from these equations that the rate of the injection processes (54) and (55) is expected to be independent of the electrode potential V (as long as the position of the band edges at the surface is independent of V; see subsequent sections). This means, for example, that hole injection, when it occurs cathodically, also is expected to occur anodically. Anodically, however, the consumption of the oxidizing agent cannot be measured as an external current, but has to be detected by other methods. An appropriate method is rotating ring-disk voltammetry (see, e.g., [22, 23]). In this method, the semiconductor, in the shape of a circular disk, is concentrically surrounded by a thin metal ring. Ring and disk are electrically insulated from each other and are incorporated in separate electrochemical circuits. This electrode setup can be rotated at a controlled speed around an axis, perpendicular to the plane of the ring and the disk and passing through the center of the disk. Due to the rotation, the solution flows from the bulk to the disk and from there to the ring, so that products formed electrochemically at the semiconductor disk may be detected quantitatively through electrochemical reaction at the ring, that is, by measuring the ring current.

The rates of the electron and hole capture reactions are proportional to the surface concentration of electrons and holes, respectively [Eqs. (57) and (60)]. At p-type semiconductors, reaction (53) therefore does not occur in darkness, since virtually no conduction band electrons are available. This reaction becomes possible under bandgap illumination however (cathodic photocurrent). The shape of the photocurrent curve is analogous to that discussed in Section 2.3. At n-type electrodes, the rate of reaction (53) is expected to increase exponentially when V is lowered. [Also here, in many cases $k_{c,c}$ is sufficiently large so that the reaction may occur under depletion ($V > V_{fb}$) at considerable rates.] Similarly, hole capture can occur in darkness at p-type electrodes only; at n-type electrodes, illumination is required (anodic photocurrent).

In the case of two-equivalent electrochemical reactions, a particular class of reactions—so-called current-doubling reactions—deserves special attention. The current-doubling effect was first observed at the (n-type) ZnO electrode [24, 25]. At given light intensity, the limiting (anodic) photocurrent was found to be approximately doubled when certain two-equivalent reducing agents were added to the indifferent electrolyte solution. This effect was explained by a mechanism analogous to that described by Eqs. (45) and (47) for the photoanodic oxidation of n-type semiconductors (chronologically, the latter was observed experimentally much later). The assumption is that the two-equivalent reducing agent A captures a photogenerated hole from the electrode to form a radical-type intermediate $A^{+\bullet}$ that has highly reducing properties so that the corresponding filled redox levels are close to or above the conduction band edge so that in a second step, the intermediate injects an electron into the conduction band to form A^{2+}:

$$A + h^+ \rightarrow A^{+\bullet} \qquad (61)$$

$$A^+ \rightarrow A^{2+} + e^- \qquad (62)$$

In this way, for each photogenerated hole reacting at the surface, two electrons flow through the external circuit. If, in an indifferent electrolyte, the photoanodic reaction involves hole capture steps only, the saturation photocurrent is doubled by adding the reactant.

Shortly after photoanodic current-doubling was detected, its cathodic counterpart was also reported [26] on p-type GaP with two-equivalent oxidizing agents (B) such as hydrogen peroxide and the persulfate ion. The reduction mechanism can be denoted here as

$$B + e^- \rightarrow B^{-\bullet} \tag{63}$$

$$B^{-\bullet} \rightarrow B^{2-} + h^+ \tag{64}$$

where $B^{-\bullet}$ is a strongly oxidizing radical such as $OH^{\bullet}$ with empty redox levels located near or below the valence band edge. In view of the electrochemical approach for studying etching mechanisms, the latter type of current-doubling reaction is especially important in the framework of this chapter on etching of III–V compounds, because current-doubling oxidizing agents are often found to be etchants for III–V compounds.

Two important remarks have to be made at this point. The first one is that complications may arise in semiconductor electrode reactivity due to surface states. As an alternative route to direct charge transfer as described previously, charge transfer may occur in two steps, that is, first from the semiconductor bands to surface states and then from surface states to redox species in solution or vice versa. Furthermore, the filling or emptying of surface states may lead to charge accumulation at the electrode surface and hence to the unpinning of the band edges, with evident consequences on the magnitude of the electrochemical rate constants.

The second remark is that at high current densities, mass transport may become the rate-limiting factor of electrochemical reactions. Indeed, due to the high reaction rate, the surface concentration of the oxidizing or the reducing agent may become considerably less than the bulk concentration, so that the electrochemical reactant has to be transported to the surface by diffusion. This leads to a potential-independent current density j_{diff} that, for rotating electrodes in which the transport is by convective diffusion, obeys to the Levich equation [23]

$$j_{\mathrm{diff}} = 0.155\, nFD^{2/3}(\rho/\eta)^{1/6} w^{1/2} c \tag{65}$$

In this equation, j_{diff} is the limiting current density in amperes per centimeter squared, n is the number of charge carriers involved in the reaction, D is the diffusion coefficient (in meters squared per second), and c is the concentration (in moles per liter) of the rate-limiting species, ρ is the density (in kilograms per cubic meter) and η is the viscosity (in kilograms per meter per second) of the electrolyte solution, and w is the rotation rate of the electrode (per second).

Hence, a limiting current can be identified as diffusion-limited if, at a rotating (ring-) disk electrode, it is found to be proportional to the square root of the rotation rate of the electrode. We recall that diffusion limitation may also occur in an indifferent electrolyte; for example, in the (photo)anodic dissolution of semiconductors in an alkaline medium, the current density may be limited by diffusion toward the electrode of the OH^- ions necessary to form soluble anions of the lattice constituents (see Section 2.3).

3. Types of Etching Reactions

3.1. (PHOTO)ELECTROCHEMICAL ETCHING

(Photo)electrochemical etching amounts to the (photo)anodic oxidation of the semiconductor under conditions in which the oxidation products are soluble (see Section 2.3). This type of etching has the practical disadvantage that the semiconductor has to be incorporated into an electrochemical circuit; that is, that electrical contact has to be made to connecting wires. On the other hand, (photo)electrochemical etching also offers certain advantages. The amount of semiconductor removed by etching can be controlled coulometrically, that is, through the total anodic charge drawn, provided that the equivalence of the reaction involved is known [cf. Eq. (44)]. Also, as mentioned later in this chapter, well-determined morphologies (e.g., porous surfaces) may be induced by choosing the appropriate range of applied potentials. Because holes are needed for the anodic dissolution of semiconductors, this process occurs in darkness with p-type semiconductors, whereas for n-type semiconductors, illumination with photons of the appropriate energies is required; that is, the dissolution is photoelectrochemical. Special advantages are in principle inherent to the latter procedure. Indeed, local photoelectrochemical etching of well-defined areas on the semiconductor surface may be achieved either by using a thin light beam or by covering chosen parts of the surface from the light. Also, when multilayer structures consisting of semiconductor materials with different bandgaps are involved, material-selective etching of a semiconductor with a narrower bandgap with respect to one having a wider bandgap may be performed by choosing the wavelength range of the light such that only in the former case are electron–hole pairs produced.

Next to (photo)electrochemical etching, three types of etching reactions can be distinguished that involve no net current flow, which is obviously more attractive from the technological point of view: the semiconductor sample is simply immersed in the etchant solution and, in certain cases, illuminated with light of appropriate wavelengths. These three types of etching are photoetching, electroless etching, and chemical etching. The first type occurs under illumination; the other two in darkness. The first two involve an electrochemical mechanism; the third one does not. We now briefly introduce the principles and characteristics of these three types of etching reactions.

3.2. PHOTOETCHING

Consider again photoelectrochemical etching as depicted in Figure 4a, which shows an n-type semiconductor under anodic bias and illuminated by photons with energy larger than the bandgap. The photogenerated holes are assumed to oxidize and hence to etch the semiconductor. The electrons flow through the external circuit and reduce some oxidizing agent at the counterelectrode. In the case of photoetching, there is no external circuit. (It should be noted here that a certain confusion in terminology exists in the literature; therefore it is stressed that by photoelectrochemical etching and by photoetching, we mean etching under illumination with and without external current flow, respectively.) Hence in photoetching, the photogenerated electrons have to be consumed at the semiconductor–electrolyte interface; that is, they react with an oxidizing agent. The levels of the oxidizing agent required for photoetching should hence overlap with the conduction band of the semiconductor (Fig. 6). The net photoetching process thus proceeds by an electrochemical mechanism that consists of two partial currents (photoanodic dissolution of the semiconductor and cathodic reduction of the oxidizing agent; Fig. 7a) that compensate each other electrically but not chemically.

The corresponding reactions can be written as

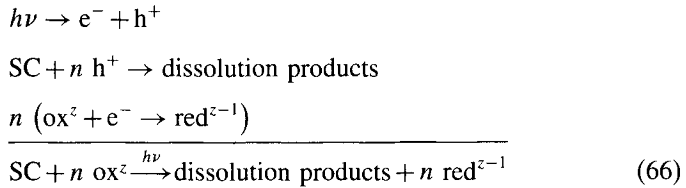

$$h\nu \rightarrow e^- + h^+$$

$$SC + n\ h^+ \rightarrow \text{dissolution products}$$

$$n\ \left(ox^z + e^- \rightarrow red^{z-1}\right)$$

$$SC + n\ ox^z \xrightarrow{h\nu} \text{dissolution products} + n\ red^{z-1} \qquad (66)$$

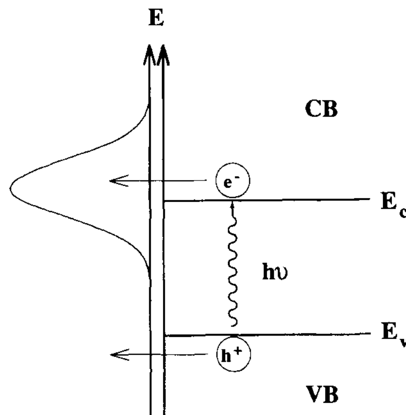

FIG. 6. Mechanism of photoetching.

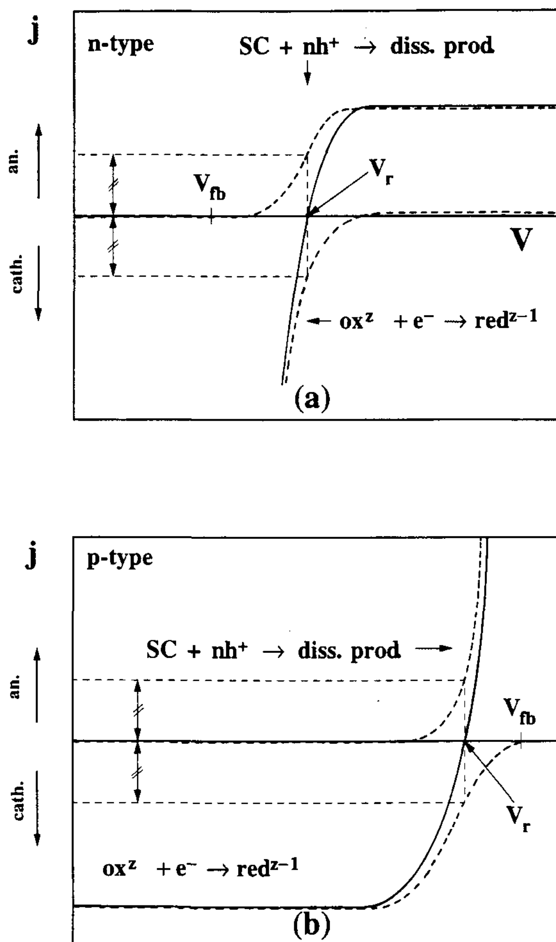

FIG. 7. Schematic representation of partial and total current density curves at an illuminated semiconductor electrode in an electrolyte solution that contains an electron-capturing oxidizing agent. (a) n-type; (b) p-type. Photoetching occurs at V_r.

(for simplicity, one formula unit of the semiconductor SC is assumed to be oxidized by n holes, whereas the reduction of the oxidizing agent is assumed to be one-equivalent).

Combination of etch rate and electrochemical measurements in principle allows us to check whether this simple photoetching model holds. Indeed, in this case, the open-circuit etch rate should correlate with the cathodic current density at open-circuit potential under illumination V_{oc} (see Fig. 7a), which can be measured separately (e.g., by working with chopped light). From Figure 7a, it is obvious that the open-circuit photoetch rate is determined by the relative positions of both partial current curves. A high photoetch rate, at given light intensity and oxidizing agent concentration, implies a steep onset of the photocurrent

curve and hence a relatively low surface electron–hole recombination rate and a high electron capture rate constant k_{cc} [see Eq. (57)].

Figure 6 equally applies to the photoetching mechanism at p-type semiconductors. The corresponding partial current density curves are schematically represented in Figure 7b. The comments are analogous to those applying to n-type samples.

The particular advantages of light-assisted etching are essentially the same as those enumerated in the previous section.

3.3. ELECTROLESS ETCHING

Electroless etching occurs in darkness but is otherwise rather analogous to photoetching as far as the mechanism is concerned. Indeed, here also the net etching reaction is the sum of two electrochemical steps that cancel each other electrically but not chemically. The anodic step is the same as in photoanodic etching or in photoetching; that is, hole capture leads to dissolution of the semiconductor. The cathodic step is the injection of holes by an oxidizing agent. The empty levels of the etching reactant must hence overlap with the valence band of the semiconductor in this case. Under the same assumptions as those accompanying reaction Eq. (66), the electroless mechanism can be symbolized by

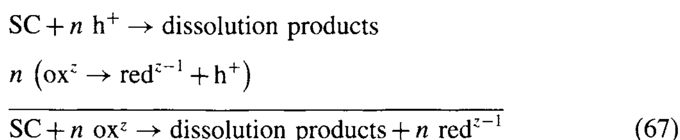

$$\begin{array}{l} \mathrm{SC} + n\ \mathrm{h}^+ \rightarrow \text{dissolution products} \\ n\ \left(\mathrm{ox}^z \rightarrow \mathrm{red}^{z-1} + \mathrm{h}^+\right) \\ \hline \mathrm{SC} + n\ \mathrm{ox}^z \rightarrow \text{dissolution products} + n\ \mathrm{red}^{z-1} \end{array} \quad (67)$$

that is, the holes injected by the oxidizing agent are consumed in the oxidation reaction of the semiconductor. This mechanism is illustrated in Figure 8a by a current density vs. potential diagram pertaining to a p-type semiconductor. The diagram is based on the simple assumption that the hole injection current is potential-independent (see Section 2.4). The actual etching conditions correspond to the rest potential V_r, which is a mixed potential, and imply that the anodic dissolution current adjusts itself to the constant cathodic reduction current. At $V \geq V_r$, all injected holes are consumed in the etching reaction. At potentials sufficiently negative with respect to V_r, the injected holes lead to cathodic current flow. In the case of an n-type semiconductor, where the current is transported by conduction band electrons, the graphical representation of electroless etching requires more attention. Indeed, in that case, the injected holes constitute the minority carriers, so that the situation is similar to that under illumination, where the holes are created by light. Hence, one has to construct a fictitious anodic curve in the current-potential diagram (Fig. 8b) that has a shape analogous to the photocurrent curve. At potentials close to the flat-band

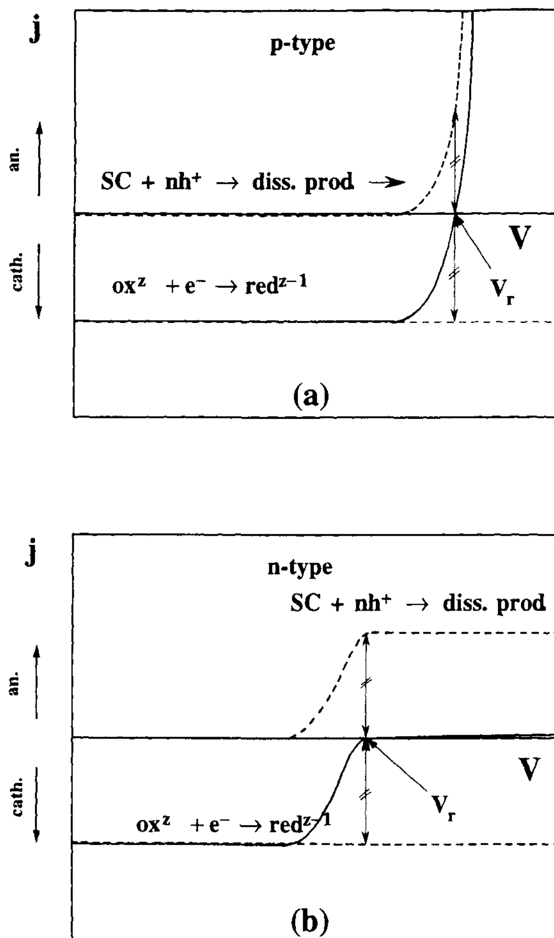

FIG. 8. Schematic representation of partial and total current density curves at a dark semiconductor electrode in an electrolyte solution that contains a hole-injecting oxidizing agent. (a) p-type; (b) n-type. Electroless etching occurs at V_r.

potential the injected holes recombine with electrons, which are here the majority charge carriers. At more positive potentials, the injected holes remain at the surface, where they oxidize the semiconductor. We note that, in contrast to the case of photoanodic dissolution, in electroless etching, current flow takes place when the holes recombine with electrons (the current is transported through the n-type sample by conduction band electrons), whereas no net current flows when the holes do not recombine. The fictitious anodic current-potential curve in Figure 8b reaches a limiting value that is equal to the absolute value of the limiting cathodic hole injection current (it is again assumed that the hole injection rate is potential-independent). The resulting current-potential curve does not

tend to zero at positive potentials due to the contribution of electron injection to the anodic dissolution reaction (see Sections 2.3 and 5.1) that causes a small net anodic current. As a result, also with n-type semiconductors, a rest potential V_r is defined (see Fig. 8b), at which the actual electroless etching occurs. It can be seen from Figure 8b that the etch rate at V_r corresponds to the limiting current density of the fictitious anodic dissolution curve. This point will be important in the discussion of the etch morphologies (see Section 7).

It is obvious for electroless etching also that combining etch rate and electrochemical measurements may lead to detailed insight into the reaction mechanism. This will be illustrated by selected examples further on in this chapter.

3.4. CHEMICAL ETCHING

In a chemical etching mechanism, no free charge carriers from the semiconductor (i.e., neither conduction band electrons nor valence band holes) are involved. The etching reaction amounts to the breaking of surface bonds of the semiconductor by the etchant and the formation of new bonds between the semiconductor constituents and species from solution. For example, the first step of the etching of InP by HCl can be represented by

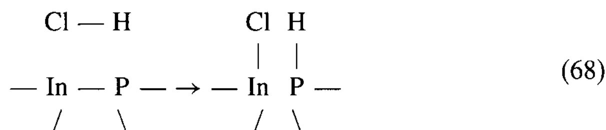

(68)

As this example shows, etchants operating by a chemical mechanism are not necessarily oxidizing agents, although they mostly are. For instance, oxidizing agents such as H_2O_2 and dihalogens act as chemical etchants.

Although chemical etching reactions are not composed of electrochemical steps, electrochemical measurements can yield useful mechanistic information. Thus, electrochemical data may allow us to decide whether the attack of a semiconductor by an oxidizing agent in darkness is electroless or chemical, especially when p-type samples are available. Indeed, if a given oxidizing agent is found to etch the p-type sample under open-circuit conditions but not to enhance the cathodic dark current and, hence, not to inject holes, then electroless etching can be excluded, so therefore the mechanism must be chemical. If, on the other hand, the etchant does inject holes, it is informative to measure the etch rate under limiting cathodic current flow, that is, under circumstances in which the injected holes are drawn into the semiconductor by the electric field so that they cannot participate in etching. If the p-type sample is etched under these circumstances, this must involve a chemical mechanism, so that at rest potential, the etching will occur by both mechanisms in parallel. If, on the other hand, the p-type sample is not etched cathodically, this does not necessarily mean that chemical etching at rest potential can be excluded. Indeed, if the cathodic

hole injection current is diffusion-limited, the competition for oxidizing species between hole injection and chemical reaction may be such that the rate of the latter becomes negligible.

These principles of investigation will be further illustrated by specific examples. As will be demonstrated later, identification of the etching mechanism(s) is important in tackling problems of material-selective etching and of etch morphology.

In case it is somehow established that an etching mechanism is chemical, semiconductor electrochemistry may yield further details on this mechanism, in the sense that it may distinguish between a concerted reaction [such as in the example of Eq. (68)] and a sequential reaction. Indeed, if the etchant is an oxidizing agent, it may first extract one electron from a surface bond, leaving a radical-type surface intermediate. Anodically, in a second step, the remaining surface electron may either be removed by the etchant or, if the position of the corresponding surface level allows, be injected into the conduction band. In certain cases, an increase in the anodic dark limiting current has been observed with n-type semiconductors in contact with a chemical etchant (see further), and this effect has been attributed to electron injection by surface oxidation intermediates of the semiconductor and hence to a sequential etching mechanism.

4. Some Solid-State and Electrochemical Data on III–V Semiconductors

The binary and mixed III–V semiconductors to which this chapter pertains are listed in Table I, together with their crystal structures and their bandgap values E_g at room temperature. All these materials can be made either n-type or p-type semiconducting by appropriate doping, although there are presently still problems in making good quality p-type GaN samples.

In Figure 9, the unit cell of the zincblende structure is represented. This structure belongs to the cubic system (class $\bar{4}3m$) and has three inversion tetrad

TABLE I

III–V SEMICONDUCTOR MATERIALS

Semiconductor	Crystal structure	Bandgap E_g (eV)
GaAs	Zincblende	1.43
GaP	Zincblende	2.25
InP	Zincblende	1.35
$Al_{0.25}Ga_{0.75}As$	Zincblende	1.75
$In_{0.53}Ga_{0.47}As$	Zincblende	0.75
GaN	Wurtzite	3.39
	(when grown on sapphire)	

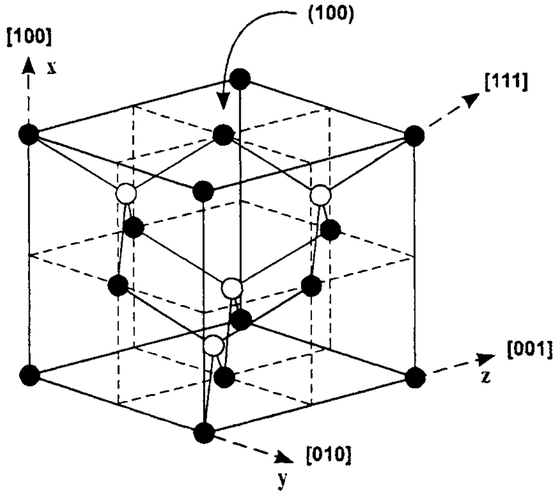

FIG. 9. The zincblende unit cell.

axes ([100], [010], and [001]) and four triad axes such as the [111] axis shown in the figure. In view of the discussion on etch morphology, it is important to note that the triad axes are polar, so that a sample cut perpendicular to the [111] axis has two faces that have different properties. The (111) face consists of group III atoms and the $(\bar{1}\bar{1}\bar{1})$ face consists of group V atoms exclusively. The (100)-type faces, on the other hand, are mixed; that is, they contain group III as well as group V atoms.

The wurtzite structure belongs to the hexagonal system (class 6*mm*). The hexagonal axis is polar. A sample cut perpendicularly to this axis has a (0001) face consisting of atoms of one constituent (Ga in the case considered) and a $(000\bar{1})$ face consisting of the other constituent (N in the given case). In both structures, each atom is surrounded by four atoms of the other kind.

Figure 10 is an energy scheme that shows the energetic position of the band edges (referred to the SHE scale) of the six semiconductor materials considered. The data pertain to an indifferent aqueous medium at pH = 0 and were obtained from differential capacitance measurements, as explained in Section 2. The sources are as follows: for GaAs, [18, 27]; for GaP, [27]; for InP, [18, 28]; for $Al_{0.25}Ga_{0.75}As$, [29]; for $In_{0.53}Ga_{0.47}As$, [30]; for GaN, [31]. In all these cases, the band edges were found to shift upward over about 0.06 eV per unit pH increase, indicating that acid–base equilibria are established at the semiconductor–electrolyte interface [27]. The positions shown should be considered as approximate only. Indeed, in certain cases the flat-band potential and, hence, the energy band positions were found to differ, depending on the crystal face exposed to the electrolyte. Also several cases have been observed in which the bands may shift by adding redox components to the electrolyte solution, due either to adsorption at the semiconductor surface or to more complex processes

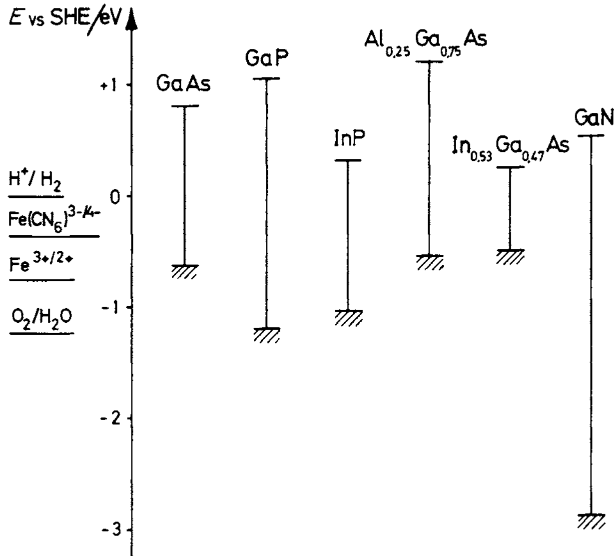

FIG. 10. Energy band edge positions for different III–V semiconductors and standard Fermi levels for different redox couples referred to the SHE; aqueous medium; pH = 0.

such as holes being injected by an oxidizing agent and being held at the surface. Such cases will be discussed on the occasion of the specific examples given further in the text.

The left-hand side of Figure 10 shows the standard Fermi level [see Eq. (52)] of some common redox couples. Mutual comparison of the energy levels at both sides of the interface is essential for discussing the possibility of charge-transfer reactions. As far as the kinetics are concerned, it should be kept in mind that for one-equivalent redox couples, the empty levels are mainly above and the filled levels are mainly underneath the levels drawn [see Eqs. (49) to (51)], and that for two-equivalent redox couples, the $E^{\alpha}_{F,\,\mathrm{redox}}$ values shown are actually values averaged over the two steps of the reaction, each of which is characterized by a Fermi level and by two Gaussian level distribution curves of the type of Eqs. (49) and (50).

5. Kinetics and Mechanisms of Etching Reactions at III–V Semiconductors

5.1. (PHOTO)ELECTROCHEMICAL ETCHING

Anodic current flow at p-type and photoanodic current flow at n-type III–V compound semiconductors at either low or high pH and not too high current

densities lead mostly (see subsequent text) to the anodic dissolution and hence to etching of the semiconductor. At high current densities or in the intermediate pH range, the electrochemical oxidation of the semiconductor may lead to precipitation of products upon the surface and hence to passivation of the electrode.

Several studies have been devoted to the electrochemical equivalence of the anodic dissolution reaction, that is, to the number of elementary charges n flowing through the external circuit per formula unit of semiconductor dissolved. Values of $n = 6$ have been reported for GaAs [8], GaP [32, 33], and InP [34, 35], as well as for the mixed semiconductors $Al_{0.25}Ga_{0.75}As$ [36] and $In_{0.53}Ga_{0.47}As$ [37]. It hence follows that in all these cases the elements involved go into solution in the +3 oxidation state. This result is somewhat surprising as far as phosphorus is concerned, considering the negative standard redox potential of the (H_3PO_4, H_3PO_3) couple ($U° = -0.276$ V vs. SHE). Since PO_4^{3-} and PH_3 have been detected in solution [32, 38] in the anodic dissolution of GaP, it has been suggested that the H_3PO_3 or HPO_3^{2-} formed electrochemically reacts further homogeneously in solution by chemical disproportionation to H_3PO_4 and PH_3. As far as GaN is concerned, recent results demonstrate that $n = 3$ [31, 39], indicating that the oxidation products are Ga in the trivalent state and N_2. It should be mentioned that certain authors claim that the photoanodic reaction at n-GaN in aqueous indifferent (H_2SO_4) electrolyte is H_2O oxidation [40]. This apparent contradiction in the data may be due to a difference in behavior between the two polar faces perpendicular to the [0001] axis [31] in the sense that, presumably, the N-terminated $(000\bar{1})$ face is etched photoanodically, whereas the Ga-terminated (0001) face is not. Whether the free surface is the $(000\bar{1})$ or the (0001) face seems to depend on the circumstances under which the GaN film is grown. The growth occurs by MOCVD from $(CH_3)_3Ga$ and NH_3 upon a sapphire substrate. Gallium-terminated films can apparently be obtained only when, at the initiation of growth, all traces of ammonia have been removed from the reactor.

On the basis of these summarized results and taking into account the chemistry of the elements involved in strong acidic and alkaline aqueous media [41], the following overall reaction equations can be proposed for the anodic dissolution of the binary III–V semiconductors under consideration:

At low pH,

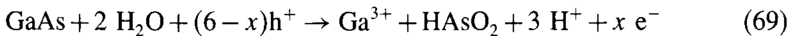

$$GaAs + 2\ H_2O + (6-x)h^+ \rightarrow Ga^{3+} + HAsO_2 + 3\ H^+ + x\ e^- \quad (69)$$

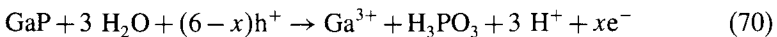

$$GaP + 3\ H_2O + (6-x)h^+ \rightarrow Ga^{3+} + H_3PO_3 + 3\ H^+ + xe^- \quad (70)$$

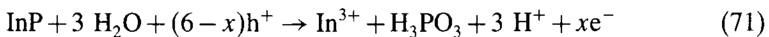

$$InP + 3\ H_2O + (6-x)h^+ \rightarrow In^{3+} + H_3PO_3 + 3\ H^+ + xe^- \quad (71)$$

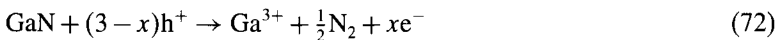

$$GaN + (3-x)h^+ \rightarrow Ga^{3+} + \tfrac{1}{2}N_2 + xe^- \quad (72)$$

At high pH,

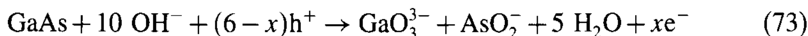

$$\mathrm{GaAs} + 10\ \mathrm{OH^-} + (6-x)\mathrm{h^+} \rightarrow \mathrm{GaO_3^{3-}} + \mathrm{AsO_2^-} + 5\ \mathrm{H_2O} + x\mathrm{e^-} \qquad (73)$$

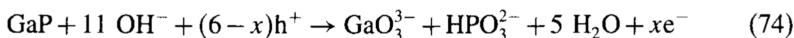

$$\mathrm{GaP} + 11\ \mathrm{OH^-} + (6-x)\mathrm{h^+} \rightarrow \mathrm{GaO_3^{3-}} + \mathrm{HPO_3^{2-}} + 5\ \mathrm{H_2O} + x\mathrm{e^-} \qquad (74)$$

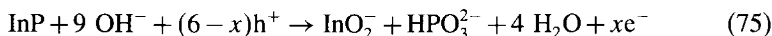

$$\mathrm{InP} + 9\ \mathrm{OH^-} + (6-x)\mathrm{h^+} \rightarrow \mathrm{InO_2^-} + \mathrm{HPO_3^{2-}} + 4\ \mathrm{H_2O} + x\mathrm{e^-} \qquad (75)$$

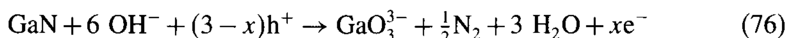

$$\mathrm{GaN} + 6\ \mathrm{OH^-} + (3-x)\mathrm{h^+} \rightarrow \mathrm{GaO_3^{3-}} + \tfrac{1}{2}\mathrm{N_2} + 3\ \mathrm{H_2O} + x\mathrm{e^-} \qquad (76)$$

The symbol x is used to take into account the possible participation of electron injection into the anodic oxidation reaction, a problem that is discussed subsequently.

In parallel with the foregoing reactions, other reactions may contribute to the anodic current to a minor extent. Thus, an enrichment in As at the GaAs electrode surface after anodic current flow has been demonstrated by various experimental techniques [42, 43]. Hence, it must be concluded that three-equivalent oxidation of GaAs occurs to a small extent in parallel to the six-equivalent oxidation. In the intermediate pH range, the formation of an anodic oxide film on the electrode surface is often observed; that is, on GaAs, film formation in a weakly alkaline medium (pH = 11.5) was reported and attributed to slow dissolution of the Ga_2O_3 and As_2O_3 formed anodically under these circumstances [44]. Thicker passivating layers on GaAs have been produced under various conditions. At n-GaN, a photoanodic current decrease due to Ga_2O_3 formation has been observed even in strongly acidic or alkaline media, indicating slow dissolution kinetics [31]. In view of the scope of this chapter, the focus is primarily on circumstances in which layer formation does not occur.

From various experiments (see subsequent text), it follows that electron injection into the conduction band contributes to the (photo)anodic dissolution reaction only to a minor fraction in the case of GaAs [10, 45], GaP [33, 38, 46], and GaN [31]; that is, that $x \ll 1$ in Eqs. (69), (70), (72), (73), (74), and (76). In the case of n-InP, IMPS studies (see Section 2.3) have demonstrated that this fraction depends on the total photocurrent density and may be very significant [47, 48]. Indeed, the ratio of the total photocurrent density j vs. the part of it due to hole capture j_h has been found, for n-InP in an acidic medium, to range from 1.2 at high light intensities [implying $x = 1$ in Eq. (71)] to 2 at very low light intensities [implying $x = 3$ in Eq. (71)]; see, for example, Figure 11. This means that at low light intensities, three of the six electrochemical steps are hole-capture steps and three are electron-injection steps. At first, this suggests a sequence consisting of a hole-capture step leading to the formation of a radical-type oxidation intermediate, followed by the injection of an electron by that intermediate, again followed by hole capture in a new surface bond, etc. However, from a detailed analysis of the IMPS data [47], it follows that three subsequent electron-injection steps are involved, indicating a more complex anodic dissolution mechanism. The decrease in j/j_h from 2 to 1.2 with increasing light

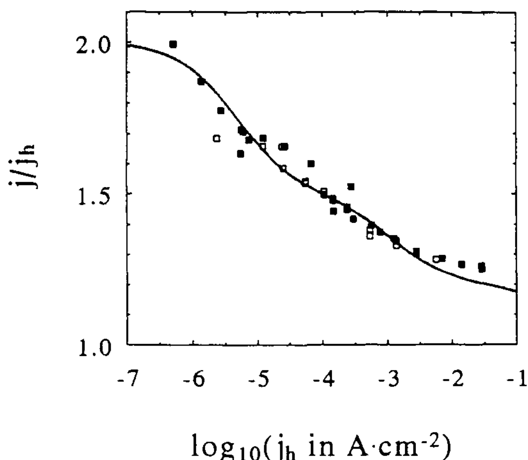

FIG. 11. Ratio of the total photocurrent density vs. the hole current density, j/j_h, as a function of the hole current density, j_h, measured by IMPS at n-InP in 1.2-mol l^{-1} HCl. The solid and the open symbols refer to measurements on two different electrodes. The curve has been calculated based on the assumptions mentioned in the text. Reprinted from *Electrochim. Acta* 38, B. H. Erné, D. Vanmaekelbergh, and I. E. Vermeir, pp. 2559–2567, ©1993, with permission from Elsevier Science.

intensity can be understood by assuming that for two electrochemical oxidation steps, a competition exists between electron injection and hole capture, the latter step being increasingly favored when the hole concentration at the surface, and hence the total photocurrent density, increases. The fact that even at very high photocurrent densities one step still occurs exclusively by electron injection leads to the conclusion that for this step, competition with hole capture is absent, the reason presumably being that the corresponding electron level (surface state) is located above the conduction band edge. The IMPS data also allow us to estimate the magnitude of the electron-injection rate constants associated with the photoanodic dissolution of n-InP. It was found that in 1-mol l^{-1} HCl medium, the rate constants are significantly larger (over a factor of 20–200) than in 1.3 mol l^{-1} H_2SO_4 [48]. Apparently, the presence of Cl^- ions gives rise to decomposition intermediates with positions more favorable for electron injection as compared to those formed in SO_4^{2-} containing solutions. It can hence be concluded that the properties of the surface states associated with the anodic decomposition intermediates of InP are influenced by the surface chemistry. The same conclusion follows from the observed enhanced electron-injection rate during photoanodic dissolution of n-InP in the presence of H_2O_2 [48].

Experimental results obtained at the n-$In_{0.53}Ga_{0.47}As$ electrode in aqueous 1.3 mol l^{-1} H_2SO_4 solution indicate that here, also the contribution of conduction band electron injection to the photoanodic dissolution reaction may be important when the photocurrent density is low [37]. All this suggests that efficient

electron injection during photoanodic dissolution of III–V compound semiconductors may be connected to indium-related surface states.

There are strong indications that, in certain cases, a mixed chemical–electrochemical dissolution mechanism of III–V semiconductors occurs. As far back as 1969, Gerischer et al. [10, 11] reported an accelerating effect of Br_2 upon the anodic dissolution of p-type GaAs, in the sense that the onset of the anodic current density curve was shifted toward less positive potentials as compared to the curve in an indifferent electrolyte. If the position of the band edges is unaffected by adding the oxidizing agent, this implies that at the same band-bending (i.e., the same hole concentration at the surface p_s) the anodic current and hence the corresponding rate constant is larger (see Section 2). The authors interpreted this effect as follows. It is generally accepted that the first hole-capture step in the anodic oxidation reation is rate-determining as a consequence of the high activation energy for breaking an intact surface bond. Since Br_2 is known to be a chemical etchant for GaAs, Gerischer et al. then assumed that, in the presence of Br_2, the slow first electrochemical step is substituted by a faster chemical bond-breaking step (or more likely, that the first two steps are substituted). Afterward, the same effect was observed with several other systems, including p-GaP–aqueous Br_2 [49], p-GaP–methanolic Br_2 [50], and p-InP–aqueous HIO_3 [51]. Such a negative shift of the anodic dissolution curve may serve as an indication that the oxidizing agent involved acts as a chemical etchant under open-circuit conditions. It should be checked by performing impedance measurements, however, whether the observed shift is due to an artefact, that is, to a shift in flat-band potential caused by the interaction of the oxidizing agent with the semiconductor surface. A particularly interesting case is that of p-GaP–Br_2 in methanol [50]. By adding Br_2 to the methanolic solution, the anodic dissolution curve of $(\bar{1}\bar{1}\bar{1})$ p-GaP was found to shift up to 0.6 V on the potential scale referred to the flat-band potential, indicating that the preceding interpretation holds. At the (111) p-GaP face, however, no such effect was observed, in agreement with the observation that the open-circuit rate of etching by Br_2 at the (111) face is much lower than at the opposite polar face [i.e. the $(\bar{1}\bar{1}\bar{1})$ face]. However, rotating ring-disk experiments showed an increased Br_2 consumption at the (111) face under anodic current flow. Moreover, the electrochemical equivalence of the anodic dissolution reaction was found to be about 4 in the presence of Br_2, in contrast to the value of 6 measured in an indifferent electrolyte. All these data strongly indicate that a mixed dissolution mechanism holds here also, but the first oxidation steps are hole-capture steps, and two further steps are chemical; that is, chemical attack of the (111) face by Br_2 can occur only after bond cleavage has been initiated by holes.

It is evident that formulas such as Eq. (69) or (73) merely describe the overall anodic etching reactions and that these reactions involve various decomposition intermediates as well as chemical steps in which (in an aqueous medium) H_2O molecules or OH^- ions participate. Several experimental approaches based on

electrode kinetics have been used to obtain more detailed information on the anodic or photoanodic dissolution mechanisms of III–V semiconductors.

One of these approaches consists of studying the kinetics of the competition between the (photo)anodic dissolution reaction of the semiconductor and the capture of holes by a one-equivalent reducing agent such as the Fe^{2+} ion or a Fe(II)-based complex. Interest in this subject was originally connected with the field of electrochemical solar energy conversion. Indeed, in 1975, Gerischer [52] proposed a type of solar cell based on a semiconductor electrode, called a regenerative or photovoltaic electrochemical cell, in which a dissolved reducing agent was photoanodically oxidized by holes at an n-type semiconductor electrode, while the corresponding oxidizing agent was reduced back at a dark counterelectrode, the net result being the conversion of solar energy into electrical energy. In view of the matching of the bandgap of the semiconductor with the spectral distribution of sunlight, GaAs and InP seemed to be the most suitable candidates for use as photoactive electrode materials. However, it was soon realized that one of the main problems with such cells was the stability of the semiconductor material with respect to photocorrosion, that is, in addition to hole capture by the dissolved reducing agent, reactions such as (69) or (71) take place also. To optimize the competition between both reaction types in favor of the added reducing agent, thorough kinetic studies were made in which the competing rates were investigated as a function of reducing agent concentration, pH, solvent composition, and light intensity. These investigations were carried out mainly by rotating ring-disk measurements; see Section 2.2. For a review on the results, see, for example, [13]. The fact that in nearly all cases the competition was more in favor of the photoanodic dissolution reaction when the light intensity was higher turned out to be an especially important clue as far as the competition mechanism is concerned. Indeed, if both reactions were simply occurring in parallel, they both would be first order in photogenerated holes [see Eqs. (44) and (60)], so that the competition would be light-intensity independent. A detailed analysis revealed the central role of the decomposition intermediate X_I^+, formed when an intact surface bond of the semiconductor captures a hole from the valence band. For example, for GaAs,

$$\mathrm{GaAs} + h^+ \rightarrow X_I^+ \tag{77}$$

where X_I^+ is a surface bond with one electron missing. Many of the kinetic data could be explained by assuming that the dissolved reducing agent is not oxidized by a hole, but by donating an electron to X_I^+, hence restoring the surface bond. More importantly in the present context, in most cases involving GaAs the kinetics indicated that the intermediate X_I^+ and not the free hole h^+ constitutes the mobile species participating in the consecutive steps of the dissolution reaction, so that it must be concluded that the intermediate X_I^+ is mobile within a two-dimensional layer; in other words, that a bonding electron may jump from an unbroken surface bond to a neighboring electron-deficient bond.

More insight into the surface chemistry involved in the anodic dissolution reaction was obtained by studying the competition kinetics under conditions of varying pH and water activity, the latter being varied by adding large concentrations of a highly hydrated salt such as LiCl or by using mixed solvents such as water–methanol or water–acetonitrile. The results, which were primarily obtained on GaAs and GaP, led to a comprehensive model, proposed in [53]. The model assumes that after reaction (77), a chemical reaction between X_1^+ and water occurs:

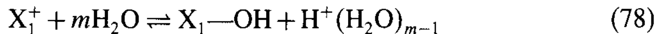

$$X_1^+ + mH_2O \rightleftharpoons X_1\text{—}OH + H^+(H_2O)_{m-1} \tag{78}$$

In this reaction, m water molecules react with the mobile and positively charged intermediate X_1^+, giving rise to a neutral intermediate X_1—OH and a solvated proton. The intermediate X_1—OH is then supposed to be immobile since it contains an OH group attached to the surface. The equilibrium (78) is thought to play a key role in the dissolution mechanism. For GaAs in an acidic aqueous medium, this equilibrium is supposed to be positioned somewhere in the middle, so that the second step of the photoanodic dissolution reaction is between X_1—OH and X_1^+. In contrast, for GaP, this equilibrium is assumed to be positioned far to the right (i.e., practically no mobile intermediates are available), so that here the second oxidation step is between X_1—OH and a free hole. The observed changes in competition mechanism induced by decreasing the water activity can then be explained as consequences of equilibrium (78) being shifted toward the left.

The conclusions just mentioned were largely confirmed from independent data obtained by quantitatively studying the enhancement of the anodic dark current density at n-type electrodes, caused by hole injection. Indeed, as mentioned in earlier sections, under anodic bias, holes injected into an n-type semiconductor by an oxidizing agent in darkness are consumed, just like at rest potential, in the anodic dissolution reaction of the semiconductor. If the latter reaction involves the valence band solely, the anodic blocking current will remain unchanged by adding the hole-injecting reactant. Any participation of conduction band electrons in the dissolution reaction will show up as an increase in the dark anodic limiting current density. By this method, it has been demonstrated that the conduction band contributes considerably to the anodic dissolution reaction in the case of InP and $In_{0.53}Ga_{0.47}As$ (as confirmed later by IMPS measurements; see preceding text), but only to a minor fraction (on the order of per thousand to per hundred) to the anodic dissolution of GaAs and GaP. Because j_a, the anodic current density increase, was found to increase with temperature (for GaAs and GaP) [45, 46], this process is believed to be activated; that is, the electron must be thermally excited from the surface state associated with the decomposition intermediate to the conduction band before injection can occur.

Measuring the relationship between the additional anodic current density j_a and the cathodic hole injection current density j_c constitutes a powerful probe

for investigating the dissolution mechanism. The basic assumption used in the interpretation of such relationships, obtained on GaAs and GaP, is that the anodic current increase is due to injection of an electron by the first decomposition intermediate, X_1^+, into the conduction band. Analysis of the results by standard steady-state kinetic treatment then leads to conclusions that confirm those obtained by studying the competition kinetics [54].

Recall at this point that anodic electron injection by dissolution intermediates can be observed not only as a consequence of hole injection (i.e., of electroless etching), but alternatively as a consequence of chemical etching (see Sections 3.4 and 5.4). Analogously, as before, quantitative studies of the relationship between the injection current density j_a and the chemical etch rate may yield important information on the etching mechanism, as will be shown further.

5.2. PHOTOETCHING

The simple model for electroless photoetching, as proposed in Section 3.2, appears to hold in the case of the InP–Fe^{3+} system in an acidic medium [55, 56]. The partial current densities at the rest potential were determined as follows. The illuminated n- or p-type InP electrode in an Fe^{3+}-containing solution was held at the potential at which the net current was zero (rest potential). Then the light was abruptly shut off. The value of the current density immediately after interruption of the light yields the partial "dark" current density, corresponding to cathodic Fe^{3+} reduction in the n-type case and to anodic dissolution of the InP in the p-type case (see Fig. 7). The reason the light has to be shut off abruptly is that the energy bands may shift under illumination, so that the "dark" partial current density under illumination may be different from that in darkness. An alternative procedure consists of working with chopped light (see subsequent text). The (photo)anodic partial electrical current density at rest potential j_{el} was then compared to the photoetch rate, the latter being determined analytically. To enable the comparison between both quantities, the photoetch rate r_{etch} was converted into an etch current density j_{etch} through the relationship

$$j_{etch} = nFr_{etch} \tag{79}$$

where n is the number of charge carriers involved in the anodic dissolution of one formula unit of InP, equal to 6 [see Eq. (71)]. Figure 12 demonstrates the good quantitative correlation between the electrical and the etch current densities and hence the validity of the simple photoetch model of two compensating partial currents. Also according to this model, the photoetch rate is expected to be higher as the onset of the anodic dissolution curve is shifted toward negative potentials and the onset of the cathodic reduction curve is shifted toward positive potentials. This prediction is fulfilled in the given case, because the photoetch rate was found to be considerably higher in a HCl medium than in H_2SO_4 or

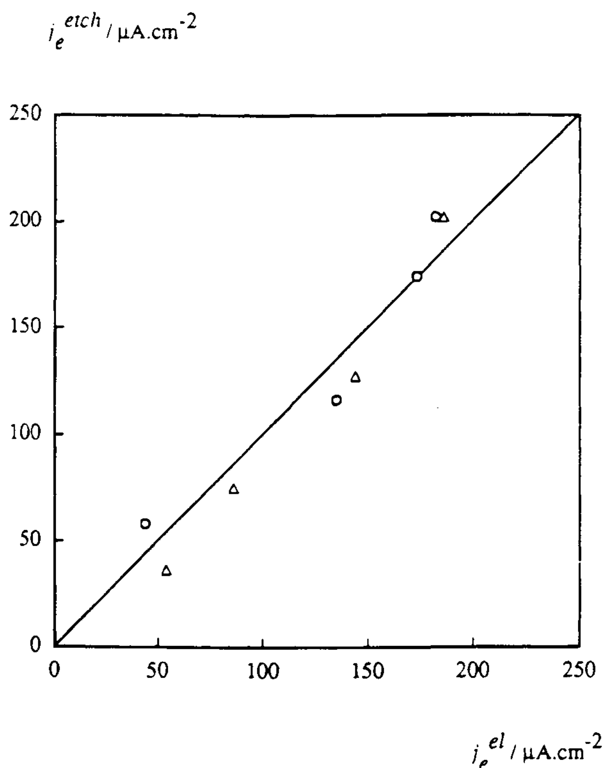

FIG. 12. Photoetch current density obtained form etch rate measurements, j_e^{etch}, vs. partial electrical current density, j_e^{el} measured at rest potential at n-InP in aqueous $FeCl_3 + HCl$ (pH = 0). O, $(\bar{1}\bar{1}\bar{1})$ face; Δ, (111) face. Reprinted from *J. Electrochem. Soc.* 142, I. E. Vermeir, W. P. Gomes, and P. Van Daele, pp. 3226–3232, 1995. Reproduced by permission of the Electrochemical Society, Inc.

in $HClO_4$, and corresponding voltammetric results show that in a HCl medium, both currents are shifted favorably as compared to H_2SO_4 or $HClO_4$ media. Considering the general reaction scheme for simple photoetching [Eq. (66)], the anodic reaction here is Eq. (71) and the cathodic reaction is

$$Fe^{3+} + e^- \rightarrow Fe^{2+} \qquad (80)$$

In view of the discussion in Section 7, it is worth mentioning that at the same light intensity, the photoetch rate at the (111) face is much lower than that at the $(\bar{1}\bar{1}\bar{1})$ face [56]. This difference between both polar faces is well known for dark etching, but rather surprisingly holds as well for photoetching in the given case.

Results similar to those outlined previously were obtained for GaP in alkaline OBr^- solution [57]. The partial reactions are now Eq. (74) and the reduction of OBr^-, which appears to involve the current-doubling mechanism

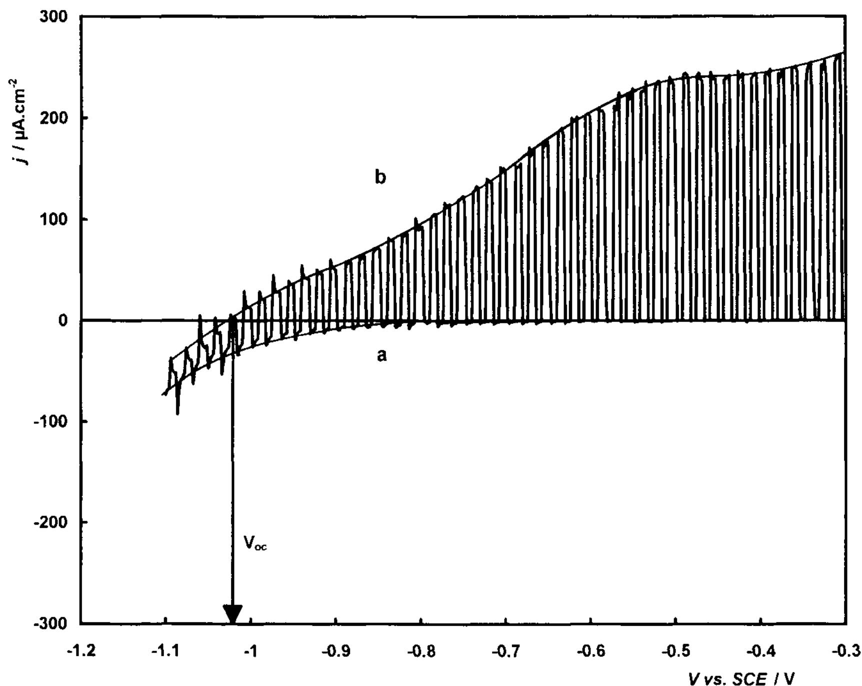

FIG. 13. Voltammograms, obtained at n-GaN in aqueous 1-mol l^{-1} KOH with chopped illumination. Curve a, light off; curve b, light on. V_{oc} is the open-circuit potential under illumination. Courtesy of I. M. Huygens, unpublished results.

(see Section 2.4):

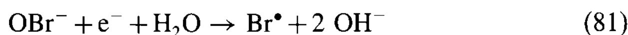

$$OBr^- + e^- + H_2O \rightarrow Br^\bullet + 2\,OH^- \tag{81}$$

$$Br^\bullet \rightarrow Br^- + h^+ \tag{82}$$

Also in the case of $(000\bar{1})$ n-GaN, photoetching can be achieved in aqueous alkaline-indifferent electrolyte [31]. This is visualized in Figure 13, which shows voltammetric results in 1-mol l^{-1} KOH obtained with chopped illumination. Curves a and b connect the points with the light off and on, respectively. The potential indicated in the figure represents zero net current under illumination. This situation results from two mutually compensating currents, that is, the dark cathodic current and the photoanodic dissolution current, corresponding to reaction Eq. (76), the net result being the photoetching of GaN. The oxidizing agent in indifferent electrolyte is H_2O and/or residual dissolved O_2. This photoetching effect is essentially due to the fact that the onset of the dark cathodic j vs. V curve is situated in a potential range that is markedly positive with respect to the flat-band potential, implying a very high reactivity of conduction band electrons toward the oxidizing agent. Note that in acidic media, no such

high reactivity of conduction band electrons occurs and hence no photoetching of GaN is observed. Presumably, a special reaction pathway exists in alkaline media through surface states, the presence and/or activity of which is somehow controlled by the surface chemistry.

Due to the high chemical stability of GaN, etching recipes for this semiconductor material are scarce, so the proposed photoetching procedure constitutes an interesting possibility for wet processing of GaN in device technology. We recall, however, that it is very likely that this possibility may not exist as far as the (0001) face is concerned, because the photoanodic current does not involve dissolution of the GaN (see Section 5.1).

Photoetching processes do not always consist of a simple superposition of an anodic and a cathodic partial process, and may exhibit various types of complications. First, even in the "simple" case of the photoetching of GaP single crystals in alkaline OBr^- solutions, the situation is actually more complex than depicted, because in n-type crystals, the photoetching process itself induces a hole injection reaction and hence an electroless etching effect [57]. Initially, OBr^- is reduced at the GaP surface via the previously mentioned current-doubling mechanism. However, during the reduction of OBr^- ions, $Br^\bullet$ radicals are formed as intermediates [cf. reaction (81)], which appear to initiate an autocatalytic reaction mechanism: surface states are formed, through which holes are injected into the valence band (at least at not too high OBr^- concentrations). These surface states, which are experimentally detected as a peak in the capacitance–potential plot [57, 58], are believed to be associated with adsorbed OBr^-. Furthermore, voltammetric experiments demonstrate that these surface states can be annihilated by a sufficiently large concentration of holes at the surface. The latter effect may explain why this induced electroless etching effect is not observed at p-GaP, since in this case the holes are the majority carriers.

Another more complicated case is the photoetching of GaAs by several two- or multiequivalent oxidizing agents such as H_2O_2, Br_2, OBr^-, OCl^-, $S_2O_8^{2-}$, and CrO_3–HF [12, 59–66]. The mechanisms of the etching reactions appear to be rather complex. The oxidizing agent was found to react at the semiconductor through various pathways, such as chemical etching, hole injection, electron capture followed by hole injection (current doubling), and hence photoetching. A model has been proposed in which these reactions were supposed to be mutually linked via a common precursor, that is, a chemisorbed surface complex formed by transfer of an electron from a surface bond to the oxidizing agent. A more detailed discussion on the competing reactions subsequent to the formation of the precursor will be given later in this chapter.

Particularly interesting features have been observed in the photoetching of n-GaAs surfaces that are partially illuminated with laser light [65, 66]. Photoetching occurs only at the illuminated spots with a quantum efficiency that is considerably higher than under uniform illumination (in the latter case, the quantum efficiency is usually low because the rest potential is generally situated in the onset region of the photocurrent curve; see Figure 7). The quantum

efficiency increases with the ratio of dark vs. illuminated surface area and may reach a value of 1 when this ratio is sufficiently high. It was shown experimentally that anodic dissolution proceeds in the illuminated area only, whereas electron capture by the oxidizing agent necessary to maintain charge neutrality takes place all over the surface, the reason being that the electrons are the majority carriers so they are available anywhere at the surface. For that reason, a high dark vs. illuminated area ratio leads to high quantum efficiencies. The photoetching mechanism thus amounts to the operation of a corroding short-circuited photogalvanic element.

5.3. ELECTROLESS ETCHING

When a given oxidizing agent etches a semiconductor at the rest potential, it can be concluded that the etching mechanism is purely electroless if, first, the reactant is observed to cause a limiting cathodic dark current at a p-type electrode (demonstrating that hole injection takes place) and if, second, no etching occurs when this limiting cathodic dark current flows [indicating that no (chemical) etching occurs when all injected holes are drawn into the bulk of the sample]. In fact, the latter criterion is unambiguous only if the hole-injection current is not limited by diffusion of the oxidizing agent, since in the opposite case, the possibility should, in principle, be considered that chemical etching is prevented because of the competition for the diffusing species by the hole-injection reaction. Because cases have been observed where the hole-injection rate is lower at the rest potential than under limiting cathodic current flow (see subsequent text), a parallel chemical etching reaction could then participate at the rest potential.

Using the foregoing diagnostic criteria, it has been established that an electroless etching mechanism operates, for example, with $Fe(CN)_6^{3-}$ at GaAs [67] and GaP [68, 69] in an alkaline medium, with $Fe(CN)_6^{3-}$ at InP at pH = 14 (this high pH being necessary to avoid passivation) [70], with acidic Fe^{3+} solutions at GaAs [71, 72] and GaP [38], and with acidic Ce^{4+} solutions at GaAs [10, 71, 72] and GaP [38]. More examples are given in Section 5.5, pertaining to simultaneous electroless and chemical etching, and in Section 6, dealing with material-selective etching.

The simple mechanism of electroless etching was presented in Section 3.3 and illustrated by Figure 8. Various factors may complicate the kinetics and mechanisms of electroless etching reactions, however, as will be explained by taking the GaP–$Fe(CN)_6^{3-}$ system as an example [68, 69]. The behavior of the GaAs–$Fe(CN)_6^{3-}$ system is closely analogous. The complications are the following: First, the etch rate at pH = 13 was found to be dependent on the crystal face. More specifically, a difference was found between the two polar faces: whereas at the (111) face, the rate is kinetically controlled, at the $(\bar{1}\bar{1}\bar{1})$ it is controlled by diffusion, either of $Fe(CN)_6^{3-}$ (at concentrations below 0.3 mol l^{-1}) or of OH^-

(at $Fe(CN)_6^{3-}$ concentrations ≥ 0.3 mol l^{-1}). The faster kinetics at the $(\bar{1}\bar{1}\bar{1})$ face as compared to the (111) face can be related to the observed difference in valence band position. Indeed, the flat-band potential was found to be 0.1–0.2 V more negative for the $(\bar{1}\bar{1}\bar{1})$ face than for the (111) face [68]. The same observation was made with GaAs and can be rationalized from the structural point of view: the (111) face consists of Ga atoms that are triply bonded to the nearest atoms of the crystal, so that all valence electrons are used in these bonds; the $(\bar{1}\bar{1}\bar{1})$ face consists of *P* atoms, again triply bonded to their neighboring atoms so that one valence electron pair remains free. This leads to a higher surface electron density at the $(\bar{1}\bar{1}\bar{1})$ face as compared to the (111) face and hence to a more negative potential, that is, to a higher position of the band edges. It is interesting to note that the difference in electron density around group III and group V atoms in the zincblende lattice has been directly visualized by recording scanning tunneling microscopy (STM) images of the (110) GaAs surface [73]. The higher position of the $(\bar{1}\bar{1}\bar{1})$ valence band edge apparently leads to a better overlap with the empty redox levels of the ($Fe(CN)_6^{3-}$, $Fe(CN)_6^{4-}$) system and hence to a higher hole-injection rate. At $Fe(CN)_6^{3-}$ concentrations below 0.3 mol l^{-1}, the hole-injection rate and hence the open-circuit etch rate at the $(\bar{1}\bar{1}\bar{1})$ face are limited by diffusion of $Fe(CN)_6^{3-}$. At higher $Fe(CN)_6^{3-}$ concentrations, at which the hole-injection rate under cathodic polarization exceeds the diffusion-limited value of the anodic dissolution rate, the etch rate at rest potential is determined by the anodic partial current density and hence controlled by the diffusion rate of OH^- ions.

Second, from rotating ring-disk experiments, it was found that the hole-injection rate at the (111) face is not potential-independent, but is lower at anodic than at cathodic potentials [in the latter case, it corresponds to the cathodic $Fe(CN)_6^{3-}$ reduction current density]. An example is shown in Figure 14. This result implies that the plateau value of the cathodic current density cannot be used as a measure for the etch rate at the rest potential. The reason for this decrease in the hole-injection rate at higher potentials should be sought along the same lines as before. Indeed, when the potential is increased so that the cathodic current decreases, part of the injected holes are used in the oxidation of the semiconductor. In this reaction, positively charged decomposition intermediates such as X_1^+ are formed (see Section 5.1). Thus, positive charges are accumulated at the crystal surface, which causes a downward shift of the band edges and, hence, a poorer overlap with the empty redox levels. Whereas at the (111) face, the reaction is kinetically controlled, a lower hole-injection rate results.

A decrease of the hole-injection rate when the electrode potential is increased is commonly observed in III–V semiconductor electrochemistry. For example, in the case of GaAs–Fe^{3+}, it was shown by means of rotating ring-disk experiments that the reduction rate of Fe^{3+} in the anodic potential region is drastically decreased in comparison to that in the cathodic potential region. In the case of GaAs–Ce^{4+}, on the contrary, holes are injected at a diffusion-limited rate over

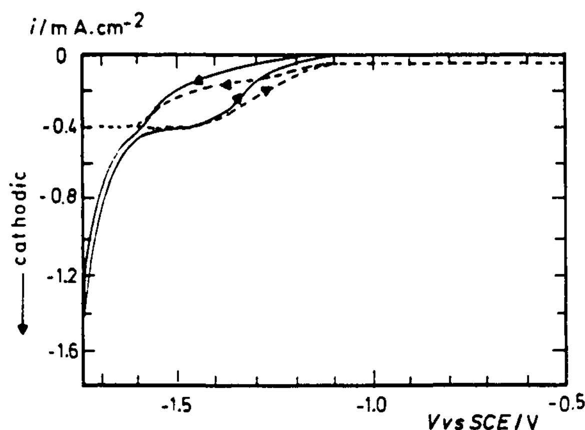

Fig. 14. Current density vs. potential curves at (111) n-GaP in aqueous 10^{-3}-mol l^{-1} $K_3Fe(CN)_6$ + 0.1-mol l^{-1} KOH. —, net current density; - - -, partial current density due to reduction of $Fe(CN)_6^{3-}$. Reprinted from *Electrochim. Acta* 35, H. H. Goossens, I. E. Vermeir, F. Vanden Kerchove, and W. P. Gomes, pp. 1351–1358, ©1990, with permission from Elsevier Science.

the whole potential region [71, 72]. This difference in behavior is explained on the basis of the positions of the redox levels concerned. Whereas the (Ce^{4+}, Ce^{3+}) standard Fermi level lies well below the valence band edge, the (Fe^{3+}, Fe^{2+}) standard Fermi level is located close to the valence band edge, so that the overlap of the unoccupied (Fe^{3+}) levels with the valence band, and hence the Fe^{3+} reduction rate, is very sensitive to the downward displacement of the valence band edge under anodic polarization caused by the accumulation of holes at the surface.

5.4. Chemical Etching

In a chemical etching mechanism, no free charge carriers (no valence band holes) are involved. Whereas most chemical etchants for III–V compound semiconductors are oxidizing agents, just as electroless etchants are, it is essential to distinguish between the two dark etching mechanisms. The obvious way to do this is by observing the cathodic behavior of the p-type semiconductor in darkness in the presence of the etchant: if no cathodic reduction of the etchant (hence no hole injection) occurs, the etching mechanism cannot be electroless and, hence, must be chemical.

In addition to allowing a decision on whether the etching mechanism is electroless or chemical, electrochemical measurements also yield essential information on chemical etching reactions, that is, on the stoichiometry of the surface reaction, on the problem of whether the mechanism is concerted (synchronous) or sequential, etc. This information will be explained by taking a study on the

etching of GaP by methanolic bromine solution [50, 74] as an example. This solution is commonly used for the etching various III–V and II–VI semiconductor materials. Considering that bromine–methanol mixtures may be hazardous at high Br_2 concentrations [75] and that methanol is toxic, one of the main objectives of this study was to find the possible advantages of using methanol instead of water as the solvent for bromine-based etching solutions.

Measurements were performed at the $(\bar{1}\bar{1}\bar{1})$ and the (111) GaP face. At the rest potential, the etch rate at the $(\bar{1}\bar{1}\bar{1})$ face appeared to be diffusion-limited, whereas that at the (111) face was low and independent of the rotation rate of the sample. The etch rate under given circumstances was the same for n- and p-type samples. The etch rate and the current density at the $(\bar{1}\bar{1}\bar{1})$ face were studied at an n-type $(\bar{1}\bar{1}\bar{1})$ GaP electrode as a function of electrode potential. The results are represented in Figure 15. A cathodic diffusion-controlled plateau is observed at sufficiently negative potentials. In this potential region, the etch rate is low. In Figure 15, the etch rates have been converted into etch current densities, based on Eq. (79), in which n has been put equal to 6. The underlying hypothesis here is that, similar to the anodic dissolution, the oxidation of GaP by Br_2 is a 6-equivalent redox reaction. When the electrode potential is increased, the cathodic current decreases and, simultaneously, the etch rate increases. Finally, at sufficiently positive potentials, a low limiting anodic current is observed and

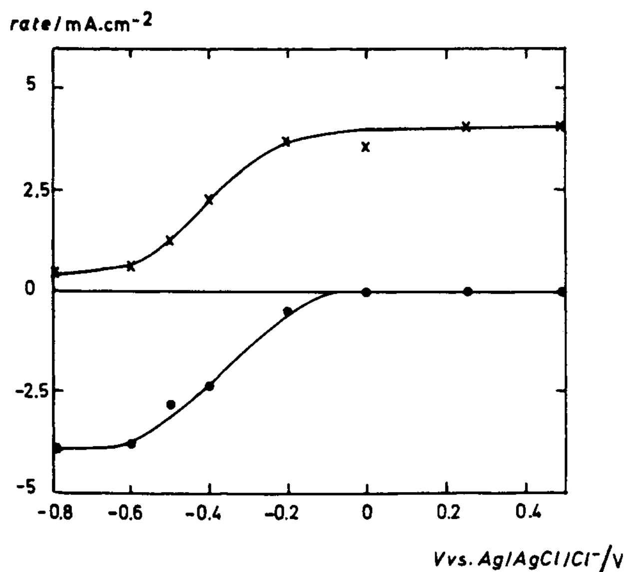

FIG. 15. Combined etch rate and current density vs. potential plots at $(\bar{1}\bar{1}\bar{1})$ n-GaP in methanolic 4×10^{-3}-mol l^{-1} $Br_2 + 0.25$-mol l^{-1} LiCl. ×, etch rate (expressed as an etch current density); •, electrical current density. Reprinted from *J. Electrochem. Soc.* 140, K. Strubbe and W. P. Gomes, pp. 3294–3300, 1993. Reproduced by permission of The Electrochemical Society, Inc.

the etch rate reaches a limiting value that is proportional to the square root of the rotation speed of the electrode. The sum of the etch rate and the absolute value of the electrical current density is found to be constant over the entire potential range. Rotating ring-disk experiments show that the Br_2 consumption at the GaP disk is potential-independent and equal to the diffusion-controlled value.

Measurements at the p-type $(\bar{1}\bar{1}\bar{1})$ face show that Br_2 is not reduced cathodically in darkness, which allows us to exclude electroless etching. Combined current–potential and impedance measurements reveal that the anodic dissolution current starts at a considerably lower surface hole concentration in the presence of Br_2 than in an indifferent electrolyte solution. Also this phenomenon points to a chemical etching mechanism, since it can be explained by assuming that in the presence of Br_2, the first (slow) anodic dissolution steps are replaced by faster chemical steps; the faster subsequent hole-capture steps can then occur at a higher rate for the same hole concentration than in a totally electrochemical mechanism (see Section 5.1).

The fact that the cathodic limiting current density $j_{c,\,\mathrm{lim}}$ in Figure 15 is found to be equal to the anodic limiting etch current density $j_{\mathrm{etch,\,lim}}$ confirms that this chemical etching process is a 6-equivalent redox reaction, as assumed. Indeed, because the cathodic reduction of Br_2 is 2-equivalent, $j_{c,\,\mathrm{lim}}$ can be written as

$$j_{c,\,\mathrm{lim}} = 2FJ_{\mathrm{Br}_2} \tag{83}$$

where J_{Br_2} is the diffusion flux of Br_2 toward the electrode surface. Putting Eq. (83) equal to $j_{\mathrm{etch,\,lim}} = 6Fr_{\mathrm{etch,\,lim}}$ yields

$$J_{\mathrm{Br}_2} = 3\; r_{\mathrm{etch,\,lim}} \tag{84}$$

that is, the number of moles of Br_2 arriving at the surface by diffusion is 3 times the number of moles of GaP consumed. Taking into account chemical considerations [76, 77], the reaction equation can then be proposed as

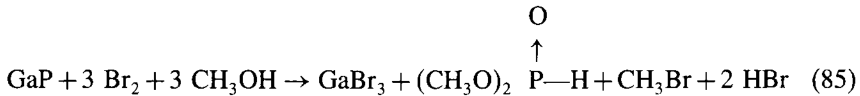

$$\mathrm{GaP} + 3\,\mathrm{Br_2} + 3\,\mathrm{CH_3OH} \rightarrow \mathrm{GaBr_3} + (\mathrm{CH_3O})_2\,\overset{\overset{\mathrm{O}}{\uparrow}}{\mathrm{P}}\mathrm{{-}H} + \mathrm{CH_3Br} + 2\,\mathrm{HBr} \tag{85}$$

Note that the experiments mentioned yield direct information on the stoichiometry of the *surface* reaction and that it cannot be excluded that $(CH_3O)_2PHO$ is further oxidized by Br_2 homogeneously in solution.

The fact that a small limiting current due to the presence of Br_2 is observed anodically at $(\bar{1}\bar{1}\bar{1})$ n-GaP allows us to conclude that the etching mechanism is not concerted, but sequential. Indeed, this anodic current can be attributed to electron injection by decomposition intermediates of GaP; see Section 5.1. If the chemical etching mechanism were synchronous, no such intermediates would be formed. More details on the reaction mechanism can be obtained by studying the relationship between this limiting anodic current and the consumption rate

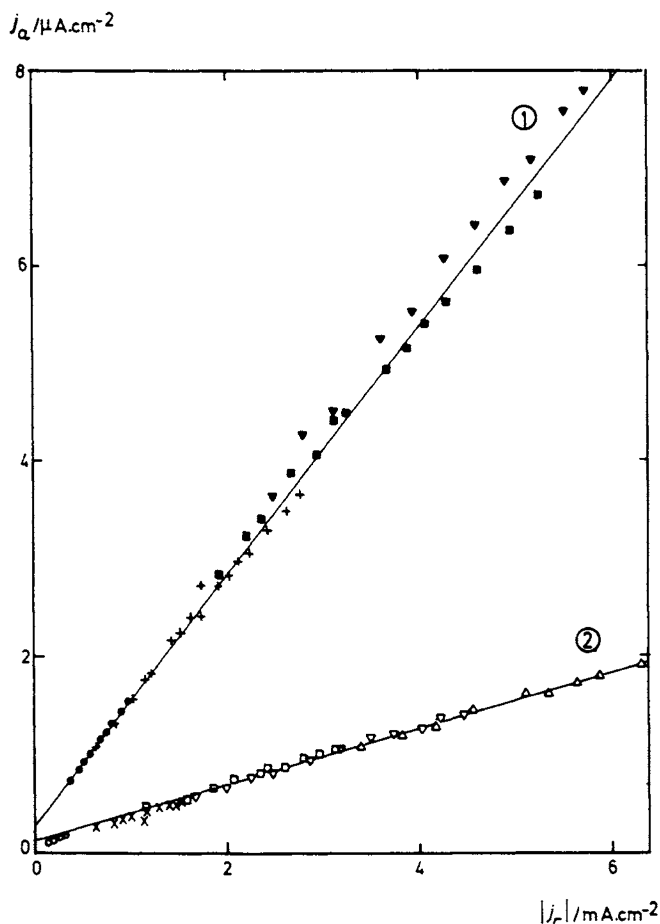

FIG. 16. Anodic j_a vs. cathodic $|j_c|$ current density at $(\bar{1}\bar{1}\bar{1})$ n-GaP in methanolic LiCl + various Br_2 concentrations; V_a and V_c equal 0.4 and −0.8 V vs. Ag–AgCl–Cl^-, respectively. The closed symbols refer to 0.25 mol l^{-1} LiCl; the open ones refer to 4-mol l^{-1} LiCl. Reproduced from *J. Electrochem. Soc.* 140, K. Strubbe and W. P. Gomes, pp. 3294–3300, 1993. Reproduced by permission of The Electrochemical Society, Inc.

of Br_2. As appears from the considerations mentioned previously for the latter, the cathodic limiting current density can be taken as a measure. Figure 16 shows the measured relationship between the anodic and the cathodic limiting current densities at two different concentrations of the indifferent electrolyte (LiCl). The relationship appears to be linear in both cases and the slope is lower at higher LiCl concentration. These data can be interpreted as follows [74]. Reaction of an unbroken surface bond with Br_2 first leads to the formation of a mobile surface intermediate X_1^+:

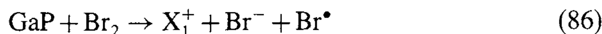

$$GaP + Br_2 \rightarrow X_1^+ + Br^- + Br^\bullet \tag{86}$$

(see Section 5.1). In the next step, the positively charged X_1^+ intermediate is converted into an immobile neutral intermediate X_1—A by the reaction

$$X_1^+ + A^- \underset{k_{-c}}{\overset{k_c}{\rightleftharpoons}} X_1\text{—}A \tag{87}$$

In principle, A^- may be either Cl^-, present in the indifferent electrolyte solution, or Br^-, formed during the chemical etching process [Eq. (86)], or methanolate [in which case a proton is released in reaction (87)]. Whereas P is more electronegative than Ga, the A^- anion is localized on the gallium.

We assume that the equilibrium (87) is positioned to the right, so that few mobile X_1^+ intermediates are present. The neutral species X_1—A is then further oxidized by the $Br^•$ radical to the intermediate X_2^+:

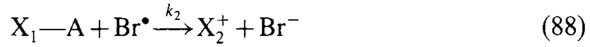

$$X_1\text{—}A + Br^• \xrightarrow{k_2} X_2^+ + Br^- \tag{88}$$

The anodic current increase is attributed to electron injection from X_1^+ into the conduction band of the semiconductor, occurring in parallel with reaction (87):

$$X_1^+ \xrightarrow{k_2^{\text{inj}}} X_2^{2+} + e^- \tag{89}$$

Whereas the chemical structure of the intermediate X_2^{2+} is obviously different from that of X_2^+, step (89) must be followed by other chemical reaction steps. However, since these steps do not influence the competition between reactions (87) and (89), they are not taken into account in the kinetic derivation.

Further oxidation of the semiconductor is then assumed to proceed in subsequent steps, in which two more Br_2 molecules per GaP formula unit are consumed. The small excess of $Br^•$ at the surface [formed during reaction (86), but not used up in reaction (89), since X_1^+ is converted into X_2^{2+} in reaction (89) without consumption of $Br^•$] is assumed to desorb from the surface and to react further in solution:

$$Br^• \xrightarrow{k_d} (Br^•)_{\text{solv}} \tag{90}$$

By a standard steady-state kinetic derivation, the proposed mechanism is shown to lead to the following relationship between the anodic current density j_a and the cathodic current density $|j_c|$:

$$j_a = \frac{k_2^{\text{inj}}}{6\,(k_c c_A + k_2^{\text{inj}})} |j_c| + \frac{e k_d k_{-c} k_c c_A}{k_2\,(k_c c_A + k_2^{\text{inj}})} \tag{91}$$

in which c_A represents the concentration of A.

Equation (91) predicts a linear relationship between j_a and $|j_c|$ for the $(\bar{1}\bar{1}\bar{1})$ face with a positive intercept on the j_a axis, as is found experimentally (Fig. 16). Equation (91) also predicts that an increase of the A concentration leads to a

decrease of the slope of the j_a vs. $|j_c|$ curve. In Figure 16, we see that the slope of the j_a vs. $|j_c|$ plot in 4-mol l^{-1} LiCl is lower than in 0.25-mol l^{-1} LiCl, indicating that step (87) occurs between X_1^+ and a Cl^- ion in that case. In practical etching conditions in which no LiCl is present, the anion reacting with X_1^+ is presumably the Br^- ion formed in the first step.

When comparing the results of this study on the etching of GaP by methanolic Br_2 to those by aqueous Br_2 [49], it appears that both processes occur quite similarly. Hence, there seems to be no clear advantage of using methanol as the solvent, except maybe for the fact that the solubility of bromine is higher in methanol than in water. However, especially at high concentrations, bromine solutions in methanol are hazardous. Moreover, it is possible to increase the solubility of bromine in aqueous solutions considerably by complexing it with bromide to form Br_3^- and Br_5^-.

Other oxidizing substances besides Br_2 that usually act as chemical etchants for III–V compound semiconductors are Cl_2, I_2, OCl^-, H_2O_2, and HIO_3. Most often it is found that the etch rate at the (100) and $(\bar{1}\bar{1}\bar{1})$ faces is comparable, whereas that at the (111) face is considerably lower. The difference in kinetics between both polar faces perpendicular to the [111] axis has been attributed to the fact that electrophilic reactants are concerned and that the electron density at the $(\bar{1}\bar{1}\bar{1})$ face is higher than that at the (111) face, due to the difference in orientation of the group III atom–group V atom surface dipole [78, 79]. By exception, the chemical etch rate of InP by HIO_3 is diffusion-controlled even at the (111) face [51]; otherwise, the electrochemical and etching behavior of this system is quite similar to that of GaP–methanolic Br_2 described previously.

Kelly and co-workers performed extensive studies on the etching of GaAs in acidic solutions containing Cl_2, Br_2, I_2, or H_2O_2 [60, 61] and in alkaline solutions containing the hypohalites ClO^- and BrO^- [62]. Their observations will be examplified by the case of GaAs–H_2O_2. An enhanced anodic dark current at n-type electrodes in the presence of the oxidizing agent was observed, as was an interdependence between the rate of chemical etching and that of cathodic reduction. Indeed, in darkness, the cathodic current at a p-type electrode is low, indicating weak hole injection by the oxidizing agent. Under the same circumstances, GaAs is etched at a potential-independent rate. When the p-type electrode is illuminated, a photocurrent is observed that involves the current-doubling mechanism (see Section 2.3), and the etch rate decreases by a corresponding amount. At high light intensities, the etching is completely suppressed cathodically even though no significant depletion of the oxidizing agent at the surface occurs. The conclusion was reached that hole injection, electron capture, and chemical etching are coupled through a common precursor: the oxidizing agent is thought to adsorb on the semiconductor surface under injection of a hole in a surface bond, so that an electron-deficient species of the type as depicted in Figure 17 is formed. Electronically, this species acts as a filled surface state, the electron of which can be injected into the conduction band or can participate in competing surface reactions (see the scheme of Figure 17, which

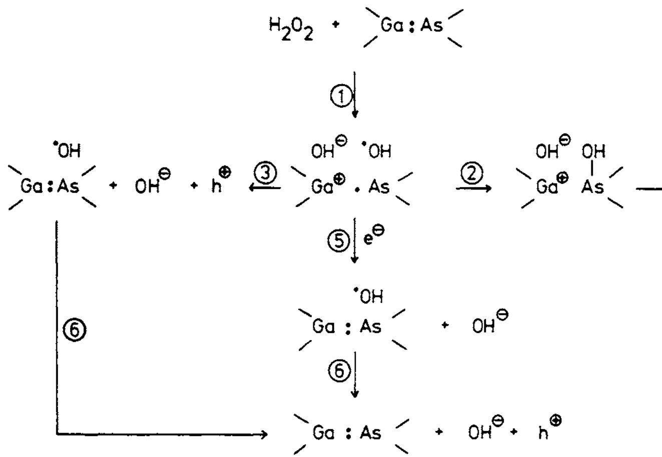

Fig. 17. Unified model for cathodic reduction of H_2O_2 at GaAs and chemical etching of GaAs in H_2O_2 solutions. Reproduced from *J. Electroanal. Chem.* 273, B. P. Minks, D. Vanmaekelbergh, and J. J. Kelly, pp. 133–145, ©1989, with permission from Elsevier Science.

represents the unified model proposed for these competing reactions). Although at first, this common precursor looks similar to the species X_1—Cl proposed in the work on GaP–methanolic Br_2 (see preceding text), there is a significant difference. Indeed, the intermediate represented in Figure 17 may be viewed as an immobilized hole, complexed with the anion that results from the etchant ($OH^-, Br^-, \ldots$) that, in a subsequent step, may react with the adsorbed radical ($OH^\bullet, Br^\bullet, \ldots$). Chemical reaction with Cl^- should hence not occur, and the Cl^- concentration should not influence the injection rate, in contrast to the experimental evidence in the case of GaP–methanolic Br_2 (Fig. 16).

Hydrogen peroxide is a very common etchant for GaAs in device fabrication. Several studies have been devoted to the etching mechanisms in different pH ranges. Kelly and Reynders [80] investigated the etching of GaAs in dilute aqueous H_2O_2 solutions in the higher pH range. Above $pH = 12$, where electrolytic dissociation of H_2O_2 to H^+ and HO_2^- takes place, the etch rate is low. Below $pH = 10$, etching is prevented by the formation of a Ga-rich oxide film on the GaAs surface. In the intermediate pH range, the etch rate is kinetically controlled. These findings were interpreted on the basis of a mechanism in which, first, the GaAs is oxidized by undissociated H_2O_2 molecules to As(III), which goes into solution, and to adsorbed $Ga(OH)_3$. In a second step, $Ga(OH)_3$ is desorbed. Depending on the pH, either the oxidation step or the desorption step is rate-determining. Similar reaction schemes involving oxidation and desorption have also been proposed for the etching of GaAs by H_2O_2 in acidic media [81–83].

The etch rate of GaP by H_2O_2 has found to be rather low [57]. The etching of InP by H_2O_2 also occurs at a low rate [48].

The etching behavior of InP is different from that of other III–V semiconductors in that InP is etched in concentrated aqueous HCl or HBr solutions [84, 85]. A significant etch rate is observed only at HCl or HBr concentrations above 5 mol l^{-1}. This strongly suggests that the etch rate depends on the degree of dissociation of the HCl or the HBr, and that, in fact, undissociated hydrogen halide molecules are involved. This hypothesis is confirmed by results obtained with HCl dissolved in acetic acid. Whereas the dissociation constant of HCl in CH_3COOH is many orders of magnitude lower than in water, undissociated HCl molecules are the prevailing species in acetic acid solutions, even at low HCl concentrations. Experiments in that medium show that the etch rate of InP is proportional to the HCl concentration, confirming that HCl molecules, and not protons, are the active species. Whereas neither HCl nor HBr is an oxidizing agent, the etching mechanism must be chemical and synchronous as depicted in Eq. (68) as far as the first step is concerned. This step is very likely the rate-determining one. To complete the dissolution of one formula unit of InP, two more HCl or HBr molecules are necessary; the end products are PH_3 gas and $InCl_3$ or $InBr_3$, which may undergo further hydrolysis reactions.

It is important to note that InP is normally covered by a native oxide layer, which is also removed in the HCl or HBr solutions used as etchants.

Since the etching mechanism is not sequential, no enhancement of the limiting anodic dark current at n-type InP electrodes upon addition of concentrated HCl solution is expected, because no decomposition intermediates are formed. This expectation appears to be fulfilled experimentally [51]. We recall here that if decomposition intermediates were formed, the electron-injection effect would be substantial in the case of InP (see Section 5.1).

A final remark is that it is hitherto not clear why InP is etched in concentrated HCl or HBr solutions, whereas other III–V compound semiconductors such as GaAs and GaP are not.

5.5. Electroless and Chemical Etching Occurring in Parallel

Complications may arise in assigning dark open-circuit etching mechanisms in that an electroless and a chemical mechanism may, in certain cases, operate in parallel. Here, electrochemical experiments also are crucial to unravel the mechanisms. An example—that of the etching of $In_{0.53}Ga_{0.47}As$ by H_2O_2—will be presented in Section 6. Another example involving $In_{0.53}Ga_{0.47}As$, that is, the etching by alkaline hypobromite solutions [86], will be discussed next.

The etch rate of $In_{0.53}Ga_{0.47}As$ by hypobromite in 1-mol l^{-1} aqueous NaOH solution at the rest potential appears to be diffusion-controlled at n- and p-type samples. At n-type samples, diffusion-controlled reduction of OBr^- is observed cathodically. Figure 18 shows dark voltammograms for p-$In_{0.53}Ga_{0.47}As$ without and with OBr^- added. The interesting point in an indifferent electrolyte is

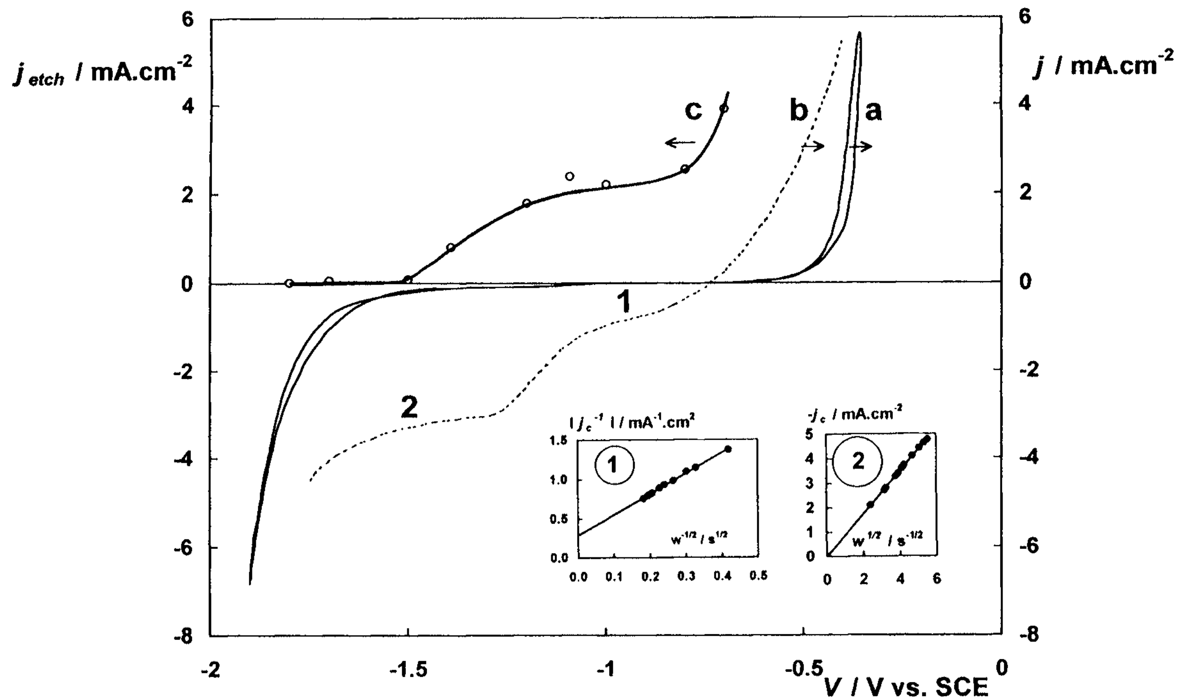

FIG. 18. Electrical and etch current density vs. potential curves at a dark rotating p- $In_{0.53}Ga_{0.47}As$ electrode. Curve a; Electrical current density in 1-mol l^{-1} NaOH. Curve b; Electrical current density in 1-mol l^{-1} NaOH + 5×10^{-3}-mol l^{-1} OBr^-. Inset 1: Koutecki–Levich plot of the cathodic current density at $V = -1$ V (region 1). Inset 2: Levich plot of the cathodic current density at $V = -1.4$ V (region 2). Curve c, etch current density in 1-mol l^{-1} NaOH + 5×10^{-3}-mol l^{-1} OBr^-. Reproduced from A. Theuwis, Ph.D. Thesis, University of Ghent, 1998, with permission of the author.

the water reduction curve. Apparently, because conduction band electrons are needed for this process, inversion is involved here, that is, electrons are thermally generated in this narrow-bandgap material at sufficiently negative bias. With hypobromite added, two current plateaus are observed. In the first plateau, the current is under mixed control; in the second, it is under diffusion control. The limiting current in region 1 appears to be enhanced by illumination. At low light intensities, this photocurrent is twice that in an indifferent electrolyte, indicating that OBr^- is photoreduced by a current-doubling mechanism. At high intensities, it reaches the same value as plateau 2 in darkness, that is, the OBr^- diffusion limit. These data can be interpreted by assuming that in plateau 1 for p-type samples, the first step is hole injection. Under illumination, addition reduction via a current-doubling mechanism occurs, in which the first step is electron capture and the second is hole injection. At sufficiently high supply rate of conduction band electrons, this process becomes diffusion-limited by hypobromite. Plateau 2 in darkness then corresponds to the same situation, but with thermally generated conduction band electrons. With n-type samples, we may again assume the same reaction scheme, but now electrons are the majority charge carriers. In conclusion, due to the narrow bandgap of $In_{0.53}Ga_{0.47}As$, hypobromite can be reduced via both bands. Considering the relative rates, the overlap of the empty hypobromite levels is apparently better with the conduction band than with the valence band. As far as dark etching at rest potential is concerned, the latter process is evidently the important one. The upper curve in Figure 18 represents the measured etch rate converted into an etch current density, taking into account that the dissolution of $In_{0.53}Ga_{0.47}As$ is 6-equivalent [37]. When hypobromite is consumed cathodically in region 2 at a diffusion-limited rate, we see that no etching occurs. In region 1, part of the OBr^- supplied at the surface is used in the cathodic hole-injection reaction and the remaining part is used in etching, which hence must be chemical. At the rest potential, all the hypobromite is consumed in etching. It hence follows that two etching mechanisms operate in parallel: in region 1, only a chemical mechanism operates; at the rest potential (i.e., under practical circumstances), the injected holes also participate in etching through an electroless mechanism.

6. Material-Selective Etching

Optoelectronics and optical telecommunication technology make widespread use of multilayer III–V structures. In the processing of these structures, it is often necessary to selectively dissolve one layer with respect to another, the selectivity being evidently based on the fact that materials of different composition are involved. Often, a thin etch-stop layer of different composition is incorporated into a layer structure to control the etch depth [87, 88]. An extreme

example of the use of selective etchants is the so-called epitaxial lift-off technique, which allows removal of thin epitaxial layers (on the order of 1 μm) from the original substrate and transplantation of them to a host substrate. In this way, different optoelectronic components may be integrated [89–91]. For example, in the case of GaAs-based multilayer structures, a thin AlAs film, which is selectively etched away from the sides, is used between the substrate and the epitaxial layer.

Material selectivity in wet etching can be achieved in various ways, depending on the type of etching reaction, the type of semiconductivity, etc.

Material-selective anodic etching is not frequently performed because it is impractical to incorporate the sample into an electrical circuit. For n-type materials, material selectivity can be achieved based on the difference in bandgap: by polarizing the sample anodically and illuminating it with photons of energy in between the bandgap values of the two materials, only the material with the narrower bandgap will dissolve photoanodically. For p-type materials, one may speculate that the two semiconductors have a different flat-band potential and hence a different onset potential of the anodic dissolution curve: by selecting a potential in between both onset potentials, if the potentials are sufficiently apart, the semiconductor with the more negative onset potential (the "less noble" one) will be selectively dissolved.

Selective electroless etching is essentially based on the same principle. Consider, for example, two p-type III–V semiconductors in electrical contact with each other and with the same electrolyte solution, containing a hole-injecting oxidizing reactant. The reduction of the oxidizing agent is assumed to be diffusion-limited. Figure 19 is a schematic representation of the partial current–potential curves at the separate semiconductor surfaces and for both surfaces brought together. For simplicity, the surface areas of both materials are assumed to be the same.

In the figure, semiconductor 1 is the "less noble" one; that is, it has the more negative onset potential, normally due to the fact that it has a more negative flat-band potential. The respective rest potentials $V_r(1)$ and $V_r(2)$ for the separate semiconductors correspond to the situations in which the anodic dissolution current is compensated by the cathodic hole-injection current. Whereas the latter is diffusion-limited in both cases, the etch rates of both materials are equal. However, when the two semiconductors are in electrical contact, as is the case in the etching of a multilayer structure, the total anodic and cathodic $(1+2)$ curves must be considered to determine the new rest potential $V_r(1+2)$. As can be seen in the figure, $V_r(1+2)$ is situated between $V_r(1)$ and $V_r(2)$, and at that potential, the etch rate of semiconductor 1 is increased and that of semiconductor 2 is decreased as compared to the case in which the semiconductors were separate. Mechanistically, this means that part of the holes that are injected into semiconductor 2 are transported to semiconductor 1, which they then dissolve. The total process amounts to a cathodic protection mechanism.

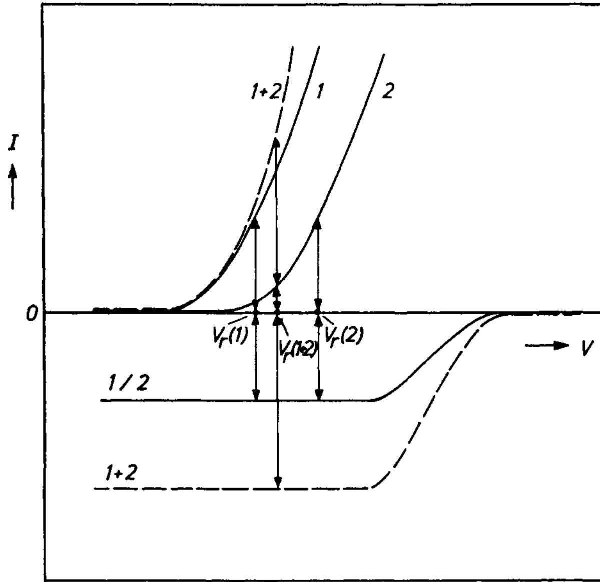

FIG. 19. Schematic representation of galvanic element formation between two p-type semiconductors 1 and 2 under diffusion-controlled hole injection by an oxidizing agent. The solid lines represent the current–potential curves for the individual semiconductors; the dashed lines refer to the total currents for the two semiconductors in electrical contact. Reprinted from P. H. L. Notten, J. E. A. M. van den Meerakker, and J. J. Kelly, "Etching of III–V Semiconductors: An Electrochemical Approach," ©1991, with permission from Elsevier Science.

A well-known case in which material-selective etching based on cathodic protection was achieved is that of the system p-GaAs–p-$Al_{0.3}Ga_{0.7}As$ in a Ce^{4+}-containing acidic solution [7]. The flat-band potential of p-$Al_{0.3}Ga_{0.7}As$ is more negative than that of p-GaAs [the same is true for p-$Al_{0.25}Ga_{0.75}As$ (see Fig. 10), showing that $Al_{0.25}Ga_{0.75}As$ has a higher value of the valence band edge], so that in the given combination, GaAs is the more "noble" material, which is cathodically protected.

When the etching reaction involves a chemical mechanism, material selectivity should be based on a difference in chemical rate constant. Striking examples of material-selective chemical etching can be found when InP is involved. Indeed, as mentioned in Section 5, concentrated HCl or HBr solutions are specific etchants for InP, and do not etch other binary or mixed III–V semiconductors. This fact has been used to selectively etch InP with respect to the quaternary III–V semiconductor $In_{0.7}Ga_{0.3}As_{0.7}P_{0.3}$ in multilayer structures.

In all this, the importance of passivation effects (i.e., the formation of product layers preventing further reaction) should be kept in mind. The products formed by oxidative etching of GaAs and GaP are soluble at sufficiently low or high pH. In contrast, the products of InP appear to be soluble only at very high pH [70].

Selective etching of other III–V semiconductors with respect to InP can therefore be performed in oxidative etchants, based on oxide layer formation on the InP surface. In general, in view of the fact that the solubility or the dissolution rate of oxide products layers is very sensitive to pH, the pH of the solution is a key parameter that influences material selectivity through passivation.

The role of the various factors enumerated in the preceding text in controlling the material selectivity of etching will be further illustrated by some examples taken from recent work in the author's laboratory.

The first example pertains to the selective etching of $Al_{0.25}Ga_{0.75}As$ with respect to GaAs by acidic iodine ($I_2 + I^-$) solutions. This procedure is frequently used in device technology [92–94], but the origin of the etch selectivity until recently had not been thoroughly studied. In the present investigation [36, 95], current–potential curves were registered at p-type $Al_{0.25}Ga_{0.75}As$ rotating disk electrodes in an indifferent electrolyte solution (0.5 mol l^{-1} H_2SO_4) and in the presence of 10^{-2} mol l^{-1} I_2 (Fig. 20, curves 1 and 2, respectively). It can be seen that a limiting cathodic current density (j_c) is measured in I_2, indicating that holes are injected by I_2 into the valence band of $Al_{0.25}Ga_{0.75}As$. This limiting current is diffusion-controlled, as can be deduced from the proportionality between j_c and the square root of the rotation rate $\sqrt{w}$ (inset of Fig. 20).

Etching experiments were performed on the $Al_{0.25}Ga_{0.75}As$ electrode as a function of potential. To compare the etch rate at given applied potentials with

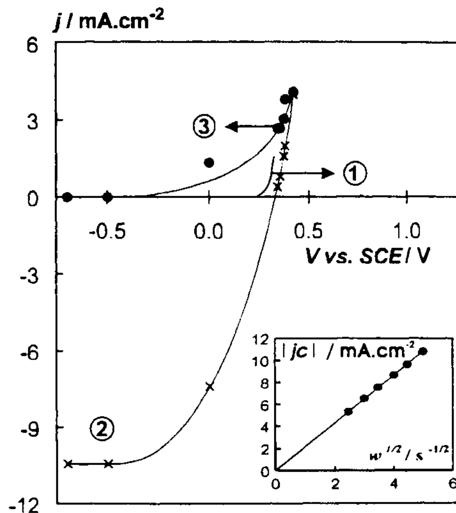

FIG. 20. Current density vs. potential curves at (100) p-$Al_{0.25}Ga_{0.75}As$ electrode. (1) Electrical current density in 0.5-mol l^{-1} H_2SO_4. (2) Electrical current density in 0.5-mol l^{-1} $H_2SO_4 + 10^{-2}$-mol l^{-1} $I_2 + 4 \times 10^{-2}$-mol l^{-1} KI. (3) Etch current density in 0.5-mol l^{-1} $H_2SO_4 + 10^{-2}$-mol l^{-1} $I_2 + 4 \times 10^{-2}$-mol l^{-1} KI. Inset: Cathodic limiting current density $|j_c|$ vs. square root of rotation rate $\sqrt{w}$ at −0.5 V vs. SCE. Reproduced from *Bull. Soc. Chim. Belg.* 105, P. J. Verpoort, pp. 805–808, 1996, with permisssion.

the electrical current density, the etch rate can be converted into an equivalent etch current density according to Eq. (79), with n=6 (see Section 5.1). This etch current density is also depicted in Figure 20 (curve 3). In the cathodic potential region, iodine is reduced electrochemically in a diffusion-limited way. Since all iodine molecules reaching the surface are consumed by hole injection, no etching is measured. When the potential is increased, the cathodic current density j_c decreases and the etch current density j_{etch} increases simultaneously. Finally, at more positive potentials, both current densities j_c and j_{etch} coincide. Experiments at n-$Al_{0.25}Ga_{0.75}As$ showed that iodine is cathodically reduced in a diffusion-limited way.

Etching experiments at $Al_{0.25}Ga_{0.75}As$ were also performed at the rest potential (i.e., without making electrical contacts) as a function of the iodine concentrations (c_{I_2}) (Fig. 21). In solutions containing less than 0.05-mol l^{-1} I_2, the etch rate r is proportional to c_{I_2}. In more concentrated solutions, the etch rate decreases. The composition of the etched $Al_{0.25}Ga_{0.75}As$ surface was investigated by X-ray photoelectron spectroscopy (XPS) measurements, leading to the conclusion that an oxide layer (consisting of oxides of gallium and arsenic, but not of aluminum) is formed during etching.

The combination of all these results points to an electroless etching mechanism occurring at $Al_{0.25}Ga_{0.75}As$ in iodine solutions. At the rest potential, the (anodic) oxidation of $Al_{0.25}Ga_{0.75}As$ (hole capture) is electrically compensated by the (cathodic) reduction of iodine to iodide ions (hole injection). The proportionality between r and c_{I_2} at lower concentrations is in agreement with

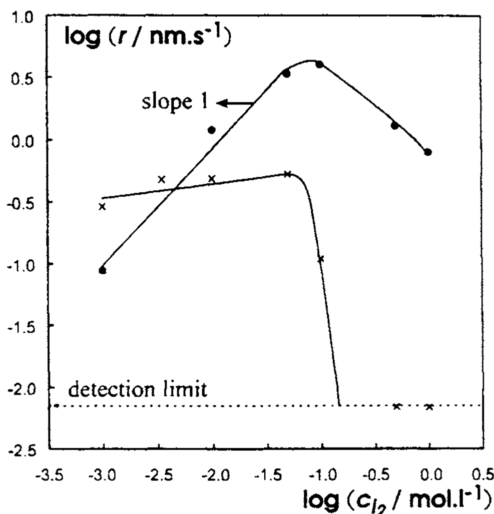

FIG. 21. Double-logarithmic plot of the etch rate r vs. the I_2 concentration c_{I_2} at the rest potential. The aqueous solution contained 0.5-mol l^{-1} $H_2SO_4+I_2+KI$ ($c_{KI}=4c_{I_2}$). •, $Al_{0.25}Ga_{0.75}As$; ×, GaAs. Reproduced from *Bull. Soc. Chim. Belg.* 105, P. J. Verpoort, pp. 805–808, 1996, with permisssion.

the assumption of an electroless mechanism, since this does not necessitate adsorption of the etchant at the semiconductor surface. That the etching also occurs, although at a lower rate, when an oxide film covers the surface is explained by the ability of holes to tunnel through this film [16].

Similar experiments were performed at p- and n-type GaAs rotating disk electrodes. At p-type GaAs, no cathodic reduction current is measured when adding I_2 to the indifferent electrolyte solution. This implies that no hole injection occurs, so that an electroless etching mechanism can be excluded. The fact that iodine can inject holes into $Al_{0.25}Ga_{0.75}As$ but not into GaAs can be explained as follows. The energetic position of the valence band edge is higher at the $Al_{0.25}Ga_{0.75}As$ surface as compared to the GaAs surface (see Fig. 10). Although no reduction current is measured at p-GaAs in contact with iodine solution, GaAs does get etched at open circuit by iodine (Fig. 21). Current–potential diagrams registered at p-GaAs with and without iodine added show a negative shift in the onset of the anodic dissolution curve (as referred to the flat-band potential). All this is indicative of a chemical etching mechanism. In Figure 21, it is seen that the concentration dependence of the etch rate is less than linear for iodine concentrations below 0.05 mol l^{-1}. This points to adsorption of iodine at the surface (Freundlich isotherm), in agreement with the fact that interaction between iodine and the GaAs surface is chemical. This difference in concentration dependence of the etch rate between $Al_{0.25}Ga_{0.75}As$ and GaAs leads to inversion of the selectivity at $\sim 5 \times 10^{-3}$-mol l^{-1} I_2.

At both $Al_{0.25}Ga_{0.75}As$ and GaAs, the etch rate decreases with increasing c_{I_2} in highly concentrated iodine solutions ($> 5 \times 10^{-2}$ mol l^{-1}). As can be seen from Figure 21, the decrease is much more drastic for GaAs than for $Al_{0.25}Ga_{0.75}As$, so that at 0.5-mol l^{-1} I_2, the etch rate of GaAs becomes negligible. From the XPS measurements, it was found that oxides are formed during the dissolution of both semiconductors and that the oxide layer thickness d_{ox} is larger when etching for the same time in solutions in which the iodine concentration is higher. It is reasonable to assume that for both materials, the oxide passivates the surface with respect to etching. The question then arises as to why, although the layer thickness is on the same order of magnitude in both cases, this passivating effect is much more pronounced for GaAs than for $Al_{0.25}Ga_{0.75}As$. A possible explanation may be offered by the difference in etching mechanism. Electroless etching of $Al_{0.25}Ga_{0.75}As$ implies that holes are injected into the valence band of the semiconductor. Since holes are able to tunnel through an oxide layer, electroless etching can still take place when the surface is covered with an oxide. However, the tunneling probability decreases with increasing oxide layer thickness. Since d_{ox} increases with increasing iodine concentration, the decreasing etch rate may be attributed to a smaller tunneling probability. A thickness of $\sim$3 nm, which is found after etching in 1-mol l^{-1} I_2, seems to be a reasonable value for tunneling. In view of the observed high roughness after etching, the oxide layer thickness may be assumed to be highly position dependent. Tunneling may preferentially occur at sites where the layer is thinner. Since the etch

rate was time independent, the oxide layer thickness is probably controlled by steady-state conditions. In contrast, at GaAs, purely chemical etching by iodine occurs. To react with GaAs surface bonds, I_3^- ions must adsorb at the surface. The presence of an oxide layer then hinders the contact of the I_3^- ions with the surface, so that the etch rate may become almost zero when the oxide layer is sufficiently thick, that is, in highly concentrated iodine solutions.

The reason the oxide layer is thicker in solutions with high iodine concentrations presumably is connected with the low solubility of the oxidation products in these media. In 1-mol l^{-1} I_2, for example, the KI concentration is 4 mol l^{-1}, so that the influence of the decrease in water activity on the solubility of the products must be taken into account.

In the fabrication process of optoelectronic devices, concentrated ($\cong$ 1 mol l^{-1}) iodine solutions are used in $\cong$0.1-mol l^{-1} H_3PO_4 (pH = 1.6), that is solutions in which the pH is higher than in the previously described experiments (pH = 0.3). Therefore, for comparison, in the foregoing fundamental study, etching experiments were also carried out in concentrated $I_2 + I^-$ solutions containing less H_2SO_4, that is, 0.02 mol l^{-1} (pH = 1.7). At 1-mol l^{-1} I_2, the etch rate of $Al_{0.25}Ga_{0.75}As$ at pH = 1.7 is, rather surprisingly, found to be about six times higher than at pH = 0.3. The increase in the etch rate of GaAs associated with this increase in pH is even more pronounced, that is, about 2 orders of magnitude. As a consequence, the selectivity ratio is significantly lower at pH = 1.7 than at pH = 0.3. This initially unexpected decrease in the etch rate caused by increasing the H_2SO_4 concentration may be explained along the same lines as that caused by increasing the I_2 + KI concentration, that is, by considering the effect of the lowering of the water activity on the solubility of the oxidation products.

An alternative mechanism that leads to material-selective etching, that is, galvanic element formation (cathodic protection), can be excluded in the present case. Selective etching of $Al_{0.25}Ga_{0.75}As$ with respect to GaAs implies that holes are injected into GaAs and consumed in the dissolution of $Al_{0.25}Ga_{0.75}As$. Since no holes are injected into GaAs by iodine during etching, this mechanism can be rejected.

Two other examples of material-selective etching pertain to the selective etching of $In_{0.53}Ga_{0.47}As$, lattice-matched on InP, with respect to the InP substrate.

In one case, the etchant was acidic aqueous H_2O_2 [37]. Hydrogen peroxide does not inject holes into p-InP, so here also, cathodic protection can be ruled out as the origin of the selective etching. At p-type $In_{0.53}Ga_{0.47}As$, hole injection by H_2O_2 is observed. Under the same circumstances, the semiconductor is also etched, obviously due to a chemical mechanism, since, cathodically, the injected holes are drawn toward the bulk of the sample and hence cannot contribute to etching. Both processes appear to be kinetically controlled. At open circuit, the measured etch rate is approximately the sum of the cathodic rate plus the hole current density converted into an etch rate [see Eq. (79)]. All this shows that at the rest potential, two etching mechanisms operate in parallel, that is, a chemical

one and an electro-chemical one. As far as InP is concerned, the measured etch rate in H_2O_2 was very small. Since no hole injection takes place, the mechanism must be chemical. The selective etching is here essentially a consequence of the fact that H_2O_2 is a very poor etchant for InP, due to the fact that the InP surface is passivated in an oxidizing medium.

In a second case, hexacyanoferrate(III) in an aqueous medium at pH = 14 was tried as a possible selective etchant for $In_{0.53}Ga_{0.47}As$ vs. InP [30]. Both separate semiconductors appear to be etched by $Fe(CN)_6^{3-}$, the former at a higher rate than the latter at the same concentration. This can be rationalized on the basis of the relative positions of energy levels. Whereas the valence band edge is located considerably higher for the ternary compound (see Fig. 10), the overlap with the empty $Fe(CN)_6^{3-}$ levels is better. The material-selectivity factor, which is the ratio of the etch rates of $In_{0.53}Ga_{0.47}As$ vs. InP, was calculated from the data obtained at the separate semiconductors to be around 15 and to be independent of the $Fe(CN)_6^{3-}$ concentration. Electrochemical experiments along the lines explained previously helped to establish that the etching mechanism is purely electroless in both cases. With the two semiconductor materials in contact (i.e., when etching the multilayer structure), the selectivity factor appeared to reach values over 2000. Apparently a cathodic protection mechanism is operating here. This is not surprising, since hole injection by $Fe(CN)_6^{3-}$ occurs in both semiconductors and since InP is much more "noble" than $In_{0.53}Ga_{0.47}As$ (the latter point is again illustrated by the relative positions of the valence band edges of both semiconductors as represented in Fig. 10, which constitutes a rough estimate of their flat-band potentials for p-type samples: V_{fb} is considerably more positive for InP).

7. Etch Morphologies and Profiles

7.1. Etch Morphologies at Macroscopic Size Surfaces

This section on the morphologies that result from wet etching processes at III–V semiconductors starts with a discussion on morphologies obtained at single crystal faces of macroscopic size, that is, obtained by one-dimensional etching. Afterward, the shapes of etch profiles will be considered at the edges of mask grooves, in which case essentially two-dimensional etching is concerned.

7.1.1. (Photo)Electrochemical Etching

The problem of the etch morphology obtained after (photo)anodic etching of III–V compound semiconductors will be discussed primarily on the basis of results obtained on GaP single crystals [69, 96]. The case of strongly alkaline

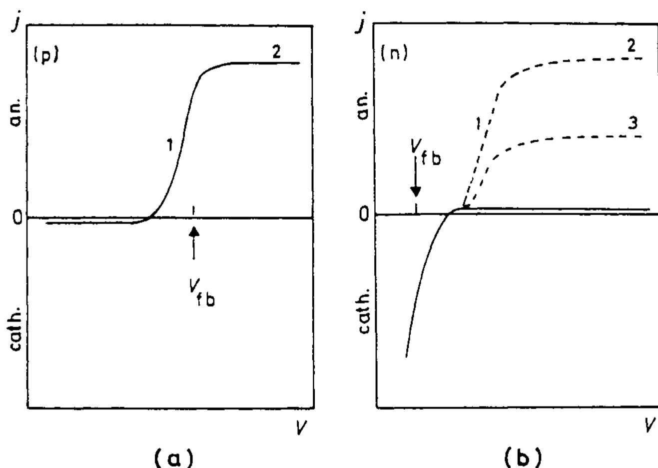

FIG. 22. Schematic representation of voltammograms for (a) p-type and (b) n-type GaP electrodes in a strongly alkaline aqueous medium.

solutions will be treated first. For the sake of the discussion, the voltammograms for p- and n-type electrodes are schematically represented in Figure 22. For p-type GaP (Fig. 22a), distinction has to be made between the exponential region 1 of the j–V curve, in which the current density is determined by the hole-capture rate, and the plateau region 2, in which the anodic current density and hence the etch rate are determined by diffusion of OH^- ions toward the surface. For n-GaP (Fig. 22b), distinction has to be made between the photocurrent onset region 1, in which surface recombination of the charge carriers is important, and the photocurrent plateau region, in which the current density is controlled either by OH^- diffusion (region 2; high light intensities) or by the light-intensity-dependent creation of electron–hole pairs (region 3; low light intensities). The morphological results for the (photo)anodic etching of p- and n-GaP under different circumstances are summarized in Table II.

This table clearly shows that for all three crystal faces studied, etching at a diffusion-limited rate leads to a flat surface (cases A and E). This is due to the fact that for a diffusion-limited process, the etch rate is the same over the entire surface and is hence unaffected by solid-state factors.

When etching at a rate below the diffusion limit, specific etch patterns develop at the surface due to local differences in the rate of the surface reaction. As a consequence of etching p-GaP in the rising part of the j–V curve (cases B, C, and D), etch pits develop at the surface that have a density of 10^5–10^6 cm^{-2} and a geometry depending on the crystal orientation: the pits at the $(\bar{1}\bar{1}\bar{1})$ and (111) faces exhibit a more or less triangular shape, whereas those at the (100) face are roughly rectangular. Furthermore, it is important to note that at the (111) face, the etch pits are more readily developed than at the $(\bar{1}\bar{1}\bar{1})$ and (100) faces. The etch pit formation and the difference in selectivity are rationalized as

TABLE II

MORPHOLOGY AFTER (PHOTO)ANODIC ETCHING OF GaP IN AQUEOUS 0.1 MOL L^{-1} KOH

Case	Type	Face	Etching conditions	Rate-determining step	Surface morphology
A	p	$(\bar{1}\bar{1}\bar{1})$ (111) (100)	Anodic current plateau (Fig. 22a, region 2)	OH^- diffusion	Smooth
B	p	$(\bar{1}\bar{1}\bar{1})$	Rising part of j–V curve (Fig. 22a, region 1)	Surface reaction (kinetically controlled)	Triangular etch pits
C	p	(111)	See B	See B	See D, but more selective
D	p	(100)	See B	See B	Rectangular pits
E	n	$(\bar{1}\bar{1}\bar{1})$ (111) (100)	Photocurrent plateau, high light intensity (Fig. 22b, region 2)	OH^- diffusion	Smooth
F	n	$(\bar{1}\bar{1}\bar{1})$	Photocurrent plateau, low light intensity (Fig. 22b, region 3)	Hole supply, controlled by e^- and h^+ photogeneration	Microrough
G	n	(111)	See F	See F	Etch pits
H	n	(100)	See F	See F	Microrough
I	n	$(\bar{1}\bar{1}\bar{1})$ (111) (100)	Photocurrent onset (Fig. 22b, region 1)	Hole supply, controlled by e^- and h^+ photogeneration and recombination	Etch hillocks and ridges

follows. In a p-type semiconductor, holes are the majority carriers, constituting a quasiequilibrium cloud at the surface. Surface bonds at dislocations and impurity sites may be assumed to be weaker than those at intact sites, resulting in an enhanced hole-capture rate and, hence, in the formation of etch pits at these sites. Assuming that the reactivity at these defect sites is unaffected or hardly affected by the crystal orientation, the observed difference in selectivity can be attributed to differences in the hole-capture rate between the three crystal faces at *intact* sites, the higher selectivity at the (111) face corresponding to a lower "normal" rate. Remembering that the [111] axis is polar (see Section 4), the difference in the hole-capture rates between the (111) and the $(\bar{1}\bar{1}\bar{1})$ faces can be associated with the GaP surface dipole orientation, which in the case of the $(\bar{1}\bar{1}\bar{1})$ face is in an energetically favorable direction for holes to reach the surface, in contrast to the (111) face [96]. As to the similar reactivity of the (100) face in comparison to the $(\bar{1}\bar{1}\bar{1})$ face, the assumption is made, based on experimental results, that the etching of the (100) face actually proceeds perpendicularly to the {111} face pairs from the side of the group V element, hence at a rate comparable to that of the $(\bar{1}\bar{1}\bar{1})$ face [69].

When etching n-GaP photoanodically in the onset region 1 of the photocurrent–potential curve (case I), etch hillocks and ridges are observed at the surface after removal of only a small amount of material. In this region of the j–V curve, recombination of the photogenerated charge carriers predominates. As dislocations and damaged sites locally enhance the recombination rate, the local surface concentration of holes will be lower than that of the surroundings, resulting in the formation of etch hillocks. This interpretation of the occurrence of elevations has been evidenced directly in the case of n-GaAs anodes by laser scanning of the electrode surface after photoanodic etching, which demonstrated that at elevated lines, apparently associated with mechanical damage, the local photocurrent is indeed lower than elsewhere on the surface [97]. The fact that the etch rate is controlled by the supply of holes, not by their reactivity, explains the similarity in the morphologies obtained at the three faces considered. In the photocurrent plateau region 3, in which the current density is controlled by the light intensity, etching of n-GaP leads either to a large quantity of small etch pits [$(\bar{1}\bar{1}\bar{1})$ and (100) face, cases F and H] or to large geometrically shaped etch pits [(111) face, case G]. In contrast to p-GaP, the holes at the n-GaP surface do not necessarily constitute a quasiequilibrium cloud. Instead, they are created in the semiconductor by light and move through the space–charge region to the surface where they react. Etch pits may then reflect sites of higher reactivity and/or be a consequence of an inhomogeneous flow of holes through the space–charge layer [98–100].

In acidic solutions, surface morphologies analogous to the corresponding cases in alkaline solutions are obtained. In contrast to alkaline solutions, however, a steady-state condition in which the anodic current density is diffusion-limited does not exist. Instead, in acidic solutions at sufficiently high anodic current densities, passivation of the GaP surface occurs. Etching in this region

does not lead to homogeneously flat surfaces; scratches are observed on p-GaP, whereas large-sized etch pits as well as a few scratches form on n-GaP. The development of these etch figures must obviously be related to the physical and chemical properties of the passivation layer, such as the adherence of the layer, the rates of electron and ion transport through this layer, the optical absorption, etc., which are still poorly understood.

Although there are, to our knowledge, no similar systematic studies on the morphology of the (photo)anodically etched surface of GaAs and InP, it seems that several of the conclusions drawn for GaP also hold for these materials. For example, it was found that photoanodic etching of n-GaAs and n-InP in the photocurrent onset region leads to very selective etching and formation of etch hillocks [101, 102], whereas (photo)anodic etching in the (photo)current plateau region of n-GaAs under OH^- diffusion limitation leads to smooth and structureless surfaces. In the case of InP, diffusion-controlled anodic etching is not feasible due to passivation of the electrode as a result of the formation of an insoluble oxidation product layer involving In(III) compounds [70].

Electrochemical dissolution of n-GaP single crystals under high anodic bias in darkness leads to particular etch morphologies with interesting photoelectrochemical properties [103, 104]. Indeed, when applying a potential on the order of +10 V to an n-GaP electrode, the band bending is such that inversion occurs at the semiconductor surface (see Section 2.2) and, hence, the GaP is dissolved by the holes created. The optical and electrical properties of the GaP change dramatically during this anodic dissolution process. The dark anodic current at given potential (+10 V) increases strongly as a function of the charge passed, and the interfacial capacitance at lower anodic potentials, which is a measure of the surface area of the electrode, increases in parallel over more than 2 orders of magnitude. These data suggest that a highly porous structure is formed, a fact that is confirmed by scanning electron microscopy. Pore formation is apparently initiated by preferential attack, probably through avalanche breakdown at a small number of localized sites on the surface such as dislocations, and from these initial pores, a radial system of pores with structural details in the 50–200-nm range develops. These microporous electrodes appear to exhibit a quantum efficiency for bandgap (green) light close to unity, in contrast to a value near 0.01 for nonporous GaP. This effect can be ascribed to two reasons: enhanced light scattering that gives rise to a more effective absorption of photons in the porous layer and the fact that even at a considerable depth, the photogenerated holes have to travel only over a short distance to reach the semiconductor–electrolyte interface. Subbandgap photocurrents also have been observed [105]. These results are clearly important for improving the photoresponse of junctions based on semiconductors in which the light absorption coefficient and the diffusion length of minority carriers are small. Pore formation in GaAs has also been reported, but was less extensively studied [106].

7.1.2. *Photoetching*

Photoetching has been reported to lead to etch hillocks (see, e.g., [12, 107]). This can be explained as follows. As mentioned previously, the rest potential is generally situated in the onset region of the photocurrent curve, where a considerable fraction of the photogenerated minority carriers are consumed in surface recombination. The latter process is favored at surface defects, so that the reaction rate and hence the etching is lower at defect sites. Photoetching can thus be used for defect-revealing purposes.

An interesting case is that of the photoetching of GaAs by H_2O_2 [12]; see also Section 5.2. The formation of the surface precursor at n-GaAs is kinetically controlled. In the dark, this reaction is followed by chemical etching, by which a rough surface is obtained. Under illumination, photoetching takes place. Whereas the etch rate is controlled by the formation rate of the precursor, it is the same for photoetching as for dark etching. Nevertheless, under illumination, the resulting etch morphology is entirely different: lattice defects are clearly revealed as etch hillocks.

The situation may, however, be more complex, such as in the case of the photoetching of GaP by hypobromite [96] (see also Section 5.2). Photoetched (111) and $(\bar{1}\bar{1}\bar{1})$ faces of GaP in alkaline OBr^- solutions show a remarkable difference in morphology depending on the type of semiconductivity: etch hillocks develop on n-GaP, whereas etch pits are formed on p-GaP. To explain these facts, it is assumed that on the microscale, the two partial reactions under consideration do not necessarily take place at the same sites. The morphology thus reflects local differences in the hole supply rate for n-GaP and local differences in the hole-capture reactivity for p-GaP. At n-GaP, the anodic partial reaction proceeds by the minority carriers. Whereas at the rest potential, recombination processes determine the availability of holes and hence the value of the current density, the hillocks formed by photoetching correspond to sites where the recombination rate is high (dislocation sites, damaged areas). In the case of p-GaP, however, where the holes are the majority carriers, locally enhanced recombination leads to a local decrease of the cathodic partial current density (and hence to a decrease of the overall etch rate), but does not significantly influence the local anodic partial current density. Here, however, the holes are at quasiequilibrium at the surface, so etch pits develop at sites with an enhanced reactivity for hole-capture.

In contrast, in the case of GaAs photoetching in CrO_3-HF solutions, etch hillocks are formed both on n- and p-type samples [107, 108]. Hillocks are also observed when etching in darkness, and their occurrence has been explained on the basis of a complex reaction scheme. The CrO_3–HF photoetch has been found to be very sensitive to defects at GaAs and even more so at InP crystals [109].

Another fact that demonstrates the complexity of the phenomena that control the photoetch morphologies is that, in contrast to the cases mentioned previously, photoetching of n-InP in Fe^{3+}-containing aqueous HCl solutions leads to

etch pits [56]. Obviously, the structural defects that determine the etch morphology must be entirely different in the latter case.

7.1.3. *Electroless Etching*

Similarly as for the kinetics and mechanisms of electroless etching (Section 5.3), the GaP–$Fe(CN)_6^{3-}$ system will be used to illustrate the factors that determine the macroscopic morphology in electroless etching. Alkaline $K_3Fe(CN)_6$ solutions are often used to differentiate between the two polar faces of GaP, that is, the (111) and $(\bar{1}\bar{1}\bar{1})$ faces [110]. In fact, in most cases triangular etch pits develop at the (111) face, whereas the $(\bar{1}\bar{1}\bar{1})$ face is etched homogeneously. The situation, however, is slightly more complex, since triangular etch pits were also observed at $(\bar{1}\bar{1}\bar{1})$ p-GaP, but only at $Fe(CN)_6^{3-}$ concentrations below 0.3 mol l^{-1} and after a very long etching time. For the purpose of the discussion of these observations, the morphological results on electroless etching by $Fe(CN)_6^{3-}$ are summarized in Table III.

The morphology of etched surfaces can be rationalized on the basis of the electroless mechanism and hence of electrochemical principles. It is thereby assumed that the two partial electrochemical reactions that constitute the electroless process do not necessarily take place at the same sites. Furthermore, since only the anodic partial current involves dissolution of the semiconductor, it is important to realize that the surface morphology reflects only local differences in the anodic partial current density. In p-GaP, the holes, which are the majority carriers, are at quasiequilibrium at the surface. The anodic partial reaction rate at a given site is thus determined by the local hole-capture reactivity, which hence determines the surface morphology, except when the anodic partial reaction rate is limited by OH^- diffusion: in the latter case, the rate is the same

TABLE III

MORPHOLOGY AFTER ELECTROLESS ETCHING OF GaP IN $Fe(CN)_6^{3-}$ SOLUTIONS (pH = 13)

Face	Type	$Fe(CN)_6^{3-}$ concentration (mol. l^{-1})	Rate-determining step	Morphology
(111)	p, n	$c \le 1$	Injection of h^+, kinetically controlled	Triangular pits
$(\bar{1}\bar{1}\bar{1})$	p	$c < 0.3$	$Fe(CN)_6^{3-}$ diffusion	Triangular pits after long etching time
$(\bar{1}\bar{1}\bar{1})$	p	$0.3 \le c \le 1$	OH^- diffusion	Smooth
$(\bar{1}\bar{1}\bar{1})$	n	$c < 0.3$	$Fe(CN)_6^{3-}$ diffusion	Smooth
$(\bar{1}\bar{1}\bar{1})$	n	$0.3 \le c \le 1$	OH^- diffusion	Smooth

over the entire surface. The case of n-GaP is quite different. Here, holes are the minority carriers, and since they can be assumed to be very rapidly captured in surface bonds, it is now the availability of holes at the surface that determines the anodic partial reaction rate and hence the surface morphology. In electroless etching, holes are supplied by injection from solution, so that for n-GaP, the anodic partial reaction is expected to take place near the sites where the holes are injected by $Fe(CN)_6^{3-}$. The morphology hence reflects local differences in the hole-injection rate. If either the injection rate is limited by $Fe(CN)_6^{3-}$ diffusion or the anodic partial reaction rate is limited by OH^- diffusion, the anodic partial current density is the same over the entire surface.

Keeping these principles in mind, the interpretation of the morphology data in Table III is straightforward. At the (111) face, the overall etch rate is kinetically controlled. The j–V curves for the p-type (111) GaP face are schematically shown in Figure 8a (omitting the potential dependence of the hole-injection rate), which demonstrates that the situation at the rest potential V_r corresponds to the rising part of the anodic partial current density. Etch pits are formed due to local differences in hole-capture reactivity, analogously to the anodic etching of p-GaP in the rising part of the j–V curve (see Table II, case C). The j–V behavior of the n-type (111) GaP face is schematically represented in Figure 8b. Etch pits are formed at sites with a locally higher hole-injection rate, due to a locally higher position of the valence band edge (dislocation sites). In this case, the situation is analogous to the photoanodic etching of n-GaP in the photocurrent plateau (Table II, case G) in that the morphology is determined by local differences in the availability of holes at the surface. For the p-type $(\bar{1}\bar{1}\bar{1})$ GaP face and at low $Fe(CN)_6^{3-}$ concentrations (<0.3 mol l^{-1}), the overall etch rate is determined by diffusion of $Fe(CN)_6^{3-}$. The rest potential V_r is thus located in the rising part of the anodic partial current density curve, and etch pits are similarly formed as a result of local differences in the hole-capture reactivity. The fact that these pits are only visible after a long etching time may be ascribed either to the low etch rate at these low concentrations or, alternatively, to the low selectivity of the $(\bar{1}\bar{1}\bar{1})$ face, as discussed in Section 7.3.1. At high $Fe(CN)_6^{3-}$ concentrations, the overall etch rate at p-GaP is determined by the diffusion rate of OH^-. The rest potential V_r thus corresponds to the diffusion-limited plateau region of the anodic partial current density curve, so that etching leads to a homogeneously flat surface, as in the case of anodic etching of p-GaP in the diffusion-limited regime (Table II, case A). For the n-type $(\bar{1}\bar{1}\bar{1})$ GaP face at low $Fe(CN)_6^{3-}$ concentrations (<0.3 mol l^{-1}), the overall etch rate is determined by $Fe(CN)_6^{3-}$ diffusion. The etched surface is homogeneously flat, since the hole supply, that is, the hole-injection rate, is the same all over the surface. At high $Fe(CN)_6^{3-}$ concentrations (>0.3 mol l^{-1}), the overall etch rate at n-type $(\bar{1}\bar{1}\bar{1})$ GaP is limited by OH^- diffusion. A flat surface is obtained, analogously to the diffusion-limited, photoanodically etched surface.

In summary, the interpretation of the morphology of electroless etching processes at GaP is analogous to the proposed interpretation of (photo)anodic etching. In electroless etching, however, the potential is not applied by an external

source, but it is imposed as a rest potential through addition of $Fe(CN)_6^{3-}$ to the solution.

In the case of open-circuit etching of GaAs in $K_3Fe(CN)_6$ solutions, it was found that etch pits develop at both n- and p-GaAs when etching is diffusion-limited through the cathodic partial reaction [12]. The fact that with GaAs, in contrast to GaP, a distinction between diffusion limitation by the cathodic and by the anodic partial reactions is also observed at n-type crystals may be due to the higher hole mobility in GaAs, which might enable the holes, injected at a diffusion-limited rate, to move along the surface before being captured selectively.

7.1.4. Chemical Etching

In chemical etching of III–V compound semiconductors, differences in the etch morphology that depend on the crystal face have been reported. For example, a homogeneously flat $(\bar{1}\bar{1}\bar{1})$ surface is obtained, whereas triangular etch pits are formed on the (111) face in the case of GaP–aqueous Br_2 [49], GaP–methanolic Br_2 [74], and InP–HIO_3 [51]. These chemical etchants hence can be used to differentiate between the two surfaces perpendicular to the [111] axis. Considerations involving free charge carriers are evidently irrelevant in the interpretation of these differences. Rather, one should consider that in all these cases, the etch rate at the $(\bar{1}\bar{1}\bar{1})$ face is diffusion-controlled and hence equal at all sites, whereas the etch rate at the (111) face is limited by the surface reaction itself, the rate of which is locally higher at defect sites. The triangular shape of the pits evidently reflects the symmetry of the (111) face. Interpretations for the difference in kinetics were presented in Section 5.4.

The interpretation of the morphology of chemical etching is not always that simple, however. A more complicated case, for example, is the etching of InP by HIO_3 [51]. In this case, it was found that although the etch rate is diffusion-controlled at all three crystal faces investigated [(111), $(\bar{1}\bar{1}\bar{1})$, and (100)], triangular etch pits develop at the (111) face, whereas the $(\bar{1}\bar{1}\bar{1})$ and (100) faces are etched more or less homogeneously. The following explanation has been proposed. The etching mechanism consists of different consecutive steps that involve the formation of decomposition intermediates and of intermediates of the HIO_3 reduction. The rate of the first step in the etching reaction, in which an In—P bond is broken by an HIO_3 molecule (leading to the formation of a first intermediate X_1^+), may be assumed to be determined by the supply of HIO_3 at the surface. Hence, at all surface sites, X_1^+ is formed at the same rate. If, however, one of the subsequent steps is sensitive to local variations in the reaction rate, then the reaction between an intermediate of the HIO_3 reduction and a decomposition intermediate will be slow at sites with a low intrinsic reaction rate, so that intermediates will be able to move along the surface and hence to react selectively at sites with a higher intrinsic rate. At these sites, etch pits

develop. The fact that no pits are observed at the $(\bar{1}\bar{1}\bar{1})$ and (100) faces can be explained by assuming a higher reactivity at these faces, analogously to the etching of GaP, so that at these faces, the intermediates are less likely to move along the surface.

7.2. PROFILE ETCHING

7.2.1. General

In the processing of semiconductors for electronic and optoelectronic device technology, often small parts of a semiconductor sample or layer have to be removed according to well-defined patterns. This selective removal is mostly performed by covering the remainder of the surface with a masking layer that prevents the attack of the semiconductor surface by the wet etchant. The mask may consist either of a photoresist layer or of a dielectric layer (e.g., silicon dioxide or silicon nitride), deposited by techniques such as plasma-enhanced chemical vapor deposition. It is obvious that the etching procedures must meet very specific requirements, depending on the application. A factor of considerable importance is the shape of the etching profiles near the mask edges. Whereas profiles etched near mask edges are usually of micrometer scale size, this type of etching is denoted as microscopic etching. To discuss this type of etching problem, a two- or a three-dimensional approach is necessary. Since the semiconductor material covered by the mask is monocrystalline, the microscopic etching kinetics of all crystallographic planes, in principle, has to be considered near the mask edge; in practice, this is hardly feasible. With III–V compounds that have the zincblende structure, the fact has to be taken into account that a polar face consisting of group III atoms exclusively usually has a much lower etch rate than a polar face consisting of group V atoms. It has been shown from many experimental data that the etching kinetics plays a decisive role in the determination of the profile shape and that the macroscopic etching kinetics of various crystallographic planes constitutes, in many cases, a good guideline for predicting the microscopic profile shape. With etchants operating through a chemical mechanism, certain crystallographic facets are revealed when the dissolution rate of all crystallographic planes is controlled by the surface reaction. However, when the rate of the surface reaction is very high for all faces, then two-dimensional mass transport of etching species becomes rate-determining, generally resulting in rounded profiles. Intermediate profiles, the shapes of which are partly determined by the kinetics of the surface reaction and partly by mass transport, are also found. Although similar rules as for chemical etching hold for etching according to an electroless mechanism, complications may arise in the latter case (see Section 7.2.4.). We now illustrate the preceding principles with some examples.

7.2.2. *Diffusion-Controlled Etching Profiles*

When the etching reaction is controlled by diffusion from solution, a concentration gradient of the etchant builds up at the semiconductor–liquid interface. At a macroscopic surface, one-dimensional diffusion has to be considered. Therefore, the concentration gradient and hence the etch rate is independent of the position at the semiconductor surface. However, in the case of mask etching, two-dimensional diffusion of the etchant has to be taken into account in the neighborhood of the mask edges, so that the concentration gradient depends on the position at the surface. To predict the shape of etch profiles near mask edges, the concentration gradient should, therefore, be calculated as a function of both the etch time and the position with respect to the mask edges. Theoretical models have been developed on this basis [111–114]. Two cases can be distinguished, depending on whether the mask can be considered as "semi-infinite" or is characterized by slits that are so narrow that their width affects the profile shape. As an example, Figure 23 shows experimental and calculated results on the profiles obtained with (100) GaAs in a diffusion-controlled etchant for the face mentioned [H_2O_2–concentrated aqueous HCl (1 : 40)] [12]. A SiO_2 layer aligned in the [110] direction masked half of the sample (semi-infinite mask). Comparison of the experimental and calculated profiles shows that the theory accounts very well for the various features of the profile, including the rounded shape, the underetching of the mask, and the bulge in the profile. No trace of any facet is observed in the scanning electron microscope (SEM) photograph, indicating that not only the (100) face, but also all other crystal planes are etched under diffusion limitation.

7.2.3. *Kinetically Controlled Etching Profiles*

In the case of kinetic control, the macroscopic etching kinetics of the various crystal planes has to be considered to understand and predict the shape of profiles near mask edges. The kinetics of the slowest etching faces is expected to determine the shape of these profiles. In principle, the prediction is anticipated to hold for etching through a chemical as well as through an electroless or a photoetch mechanism. As an example, we consider the case of the photoetching of (100) InP in Fe^{3+}-containing aqueous HCl [56]. To perform the profile etching experiments, the (100) surface was covered by a dielectric mask, where the mask patterns consisted of squares (1.2-mm size) with the sides oriented along the [011] and [$01\bar{1}$] axes (see Fig. 24). These directions are perpendicular to the two faces that can be obtained easily by cleavage, that is, the (011) and ($01\bar{1}$) faces, respectively. The slit width between the squares was 300 μm. The semiconductor was etched for 1 h under uniform illumination. Figure 25 shows typical examples of etched profiles obtained at p-type InP. For the mask edge oriented in the [$01\bar{1}$] direction, a facet is clearly revealed near the edge,

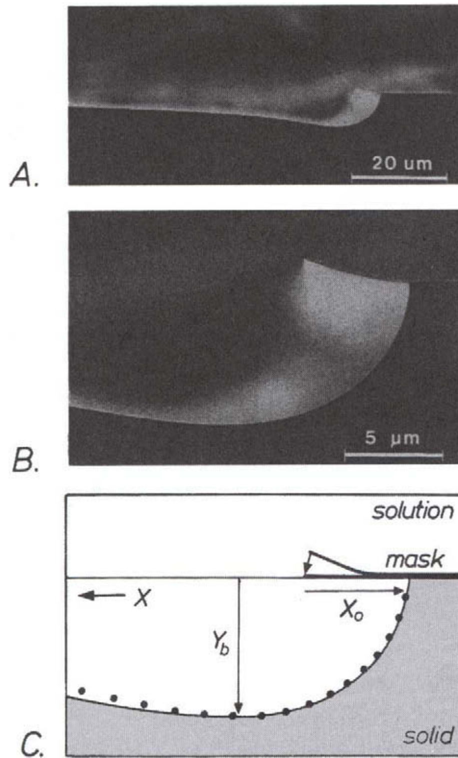

FIG. 23. (A) SEM photograph of a profile etched in GaAs with a semi-infinite SiO_2 mask aligned in the [110] direction. Etching was carried out for 5 min in a H_2O_2–HCl (1 : 40) solution with the wafer placed in a vertical position. (B) A higher magnification of the same profile in the mask edge region. (C) The agreement between the profile measured in (B) (continuous line) and that calculated from theory (filled circles). The underetching and the maximum etched depth are indicated by X_0 and Y_b, respectively. Reprinted from P. H. L. Notten, J. E. A. M. van den Meerakker, and J. J. Kelly, "Etching of III–V Semiconductors: An Electrochemical Approach," ©1991, with permission from Elsevier Science.

making an angle of 55° with the (100) surface (see Fig. 25a). Hence, it can be attributed to the (111) In face [115]. As can be seen, the bottom of the etched groove is flat. A typical example of a profile obtained in the [011] direction is shown in Figure 25b. Again a facet is revealed, in this case making an angle of about 125° with the (100) surface, so that the etch groove has a so-called dovetail shape. From crystallographic considerations, it can be concluded that again the (111) In face is involved [115]. Although a small curvature is observed near the mask edge, the bottom of the groove is flat in the middle.

As mentioned in Section 5.2, the photoetch rate of the (111) InP face in Fe^{3+} is relatively low, which accounts for the facets developed and, hence, for the shapes of the etch profiles. In the case of photoetched n-InP with the mask edge

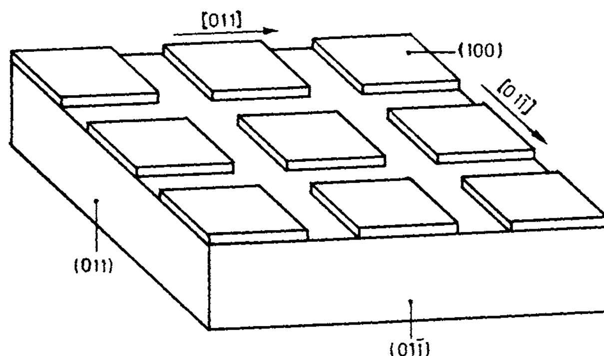

FIG. 24. Schematic representation of a masking pattern on the (100) InP surface. The mask edges are aligned either in the [011] or the [01$\bar{1}$] direction. Reprinted from *J. Electrochem. Soc.* 142, I. E. Vermeir, W. P. Gomes, and P. Van Daele, pp. 3226–3232, 1995. Reproduced by permission of The Electrochemical Society, Inc.

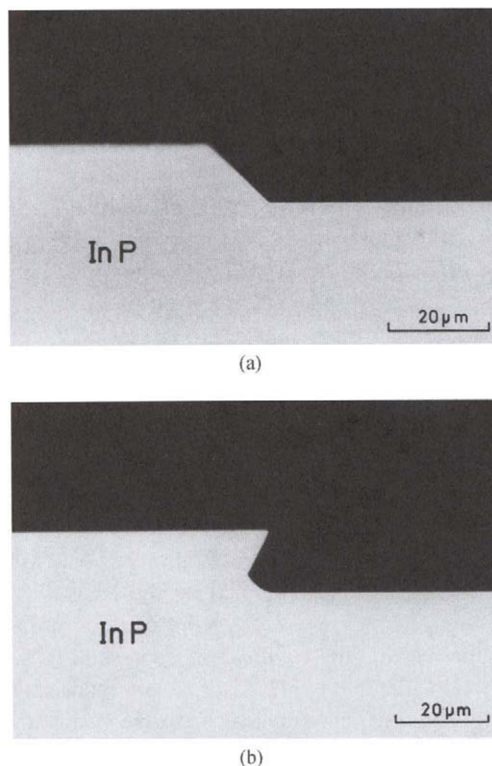

FIG. 25. Photographs of profiles obtained at a silicon nitride mask on (100) p-InP after 1-h etching under illumination in 2-mol l^{-1} $FeCl_3 + HCl$ (pH $\cong$ 0); (a) aligned in the [01$\bar{1}$] direction; (b) aligned in the [011] direction. Reprinted from *J. Electrochem. Soc. 142*, I. E. Vermeir, W. P. Gomes, and P. Van Daele, pp. 3226–3232, 1995. Reproduced by permission of The Electrochemical Society, Inc.

oriented along the $[01\bar{1}]$ direction, the sidewall also makes an angle of about 55° with the (100) face. Here, however, complications arise due to the fact that the bottom of the groove shows a very rough structure. For a discussion on this problem, refer to [56].

It should be mentioned that whereas usually the (100) face of III–V semiconductors is used for mask etching and usually the (111) face is the slowest etching face under kinetic control, sidewalls with inclinations as shown are very common.

7.2.4. Complications Due to Cathodic Protection of Crystal Faces

As mentioned before, when all crystal planes are etched at a diffusion-limited rate, rounded profiles at mask edges are normally expected. This is certainly the case when the etching mechanism is chemical. In the case of electroless etching, however, exceptions with respect to this rule have been observed, namely in cases in which the diffusion-limiting step is the cathodic (hole-injection) reaction. In the electroless etching of n-GaAs in 0.1-mol l^{-1} $Fe(CN)_6^{3-}$ solution at pH = 13, for example, in which diffusion of the $Fe(CN)_6^{3-}$ is the rate-limiting step, the (111) face is clearly revealed near the mask edge [12]. In the same solution but at 0.5-mol l^{-1} $Fe(CN)_6^{3-}$, however, in which the rate-limiting step is not diffusion of $Fe(CN)_6^{3-}$ but that of OH^- ions, a rounded profile is observed. These findings can be rationalized along the same lines as those developed to explain certain material-selectivity phenomena (see Section 6), that is, on the basis of a cathodic protection model. Indeed, as mentioned before, the flat-band potential of a given semiconductor in a solution of given composition may be different for different crystal faces exposed to the electrolyte, due to differences in the structure of the Helmholtz layer. In the case of GaAs, the (111) face appears to have a flat-band potential that is about 200 mV more positive than that of the $(\bar{1}\bar{1}\bar{1})$ and (100) faces (cf. Section 5.3). Taking the case of p-GaAs, this implies that at the same electrode potential, the equilibrium hole concentration at the surface p_s is lower at the (111) face than at the $(\bar{1}\bar{1}\bar{1})$ and (100) faces. Experimentally, this is reflected by the relative positions of the anodic dissolution curves in the sense that the onset is more positive for the (111) face. The observed effect can then be explained on the basis of the same figure as that used for explaining material selectivity by cathodic protection (Section 6, Fig. 19), but with the left and the right curves representing, in the present case, that for the $(\bar{1}\bar{1}\bar{1})$ and for the (111) faces of GaAs, respectively.

When a single crystal is etched at a mask edge, various crystal planes are exposed to the solution, so that the possibility of local element formation between crystallographic faces must be envisioned. Considering Figure 19, it is clear that although the etch rate at all separated faces is controlled by diffusion of the hole-injection agent, with both faces in contact with the solution and in mutual electrical contact, the etch rate of the "more noble" face [the (111) face]

will be diminished and that of the "less noble" face [the $(\bar{1}\bar{1}\bar{1})$ face] will be enhanced. As a consequence, although hole injection at the mask edge takes place at a diffusion-limited rate over the entire semiconductor surface, part of the holes injected at the (111) areas will be transported through the semiconductor to a neighboring less noble area, where they will cause anodic dissolution. This will result in "cathodic protection" of the (111) face; that is, this face will dissolve at a relatively low kinetically controlled rate, so that a (111) facet will develop.

7.2.5. *Complications Due to Native Oxide Layers*

In the foregoing paragraph, a faceted profile was observed, although a rounded profile would be anticipated. The inverse effect appears to exist also. This point will be exemplified by the InP–HIO_3 system [56]. In the experiments that follow, the configuration is again that of Figure 24. Profile etching experiments were performed in aqueous 10^{-3}-mol l^{-1} KIO_3 + HCl (pH = 0) in darkness. Photoresist as well as silicon nitride masks were used. The samples were etched for 30 min. Figure 26 shows examples of etched profiles obtained at p-type samples covered with a photoresist mask. The profile obtained for the photoresist mask edge in the [011] direction does not reveal any crystallographic facet; instead, a rounded profile is observed (Fig. 26a). For the mask edge oriented in the $[01\bar{1}]$ direction, however, a faceted structure is observed (Fig. 26b). The facet makes an angle of about 47° with the (100) face, which implies that either a (221) or a (331) face is involved [116]. These faces are stepped faces that consist of In atoms and can be considered as combinations of (111) and (110) planes [117].

In view of the discussion in the next section, a top view of an etched p-type sample covered with a photoresist mask is shown in Figure 27. The broad white fringe observed at the mask edge in the [011] direction indicates that the underetching is much more important at this edge than at the resist edge oriented in the $[01\bar{1}]$ direction. The same results were obtained at n-type samples.

For the sake of the discussion, it is important to realize that HIO_3 etches InP through a chemical mechanism and that the macroscopic etch rate at the (100), (111), and $(\bar{1}\bar{1}\bar{1})$ faces of InP under the given circumstances is diffusion-controlled [51]. If the same were true for any other face, rounded profiles would be expected, as indeed observed when the mask edge is oriented in the [011] direction. However, with the mask edge oriented in the $[01\bar{1}]$ direction, a facet [either (221) or (331)] is developed, suggesting that the face concerned is etched slowly. Confirmation of this assumption by etching of a (221) or a (331) single crystal face was not possible, since no samples with the given orientation were available. It is important to note that an alternative mechanism that leads to facet development (i.e. galvanic cell formation) can be excluded because the etching mechanism is chemical.

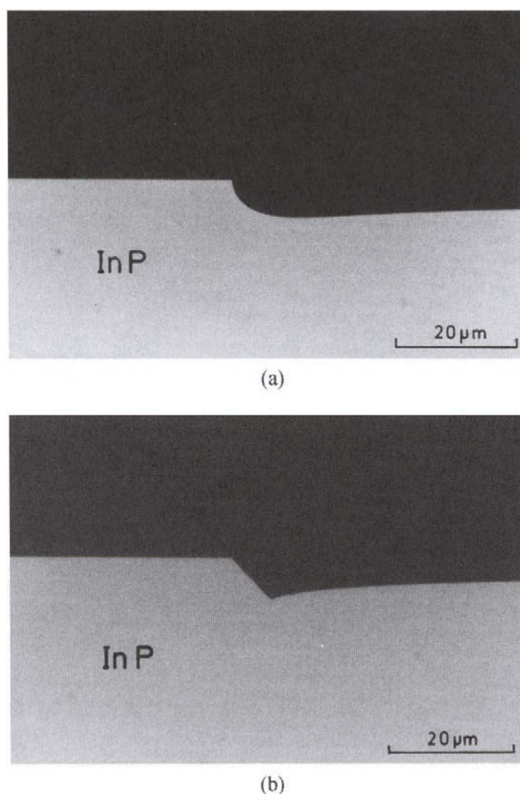

(a)

(b)

FIG. 26. Photographs of profiles obtained at (100) p-InP covered with a photoresist mask after 30-min etching in 10^{-3}-mol l^{-1} $KIO_3 + HCl$ (pH ≅ 0): (a) mask aligned in the [011] direction; (b) mask aligned in the $[01\bar{1}]$ direction. Reprinted from *J. Electrochem. Soc. 142*, I. E. Vermeir, W. P. Gomes, and P. Van Daele, pp. 3226–3232, 1995. Reproduced by permission of The Electrochemical Society, Inc.

The question now arises why, in contrast to the photoetching in $FeCl_3$, the "slow" face is not revealed when the mask edge is oriented in the [011] direction. Notten [118] observed an analogous anisotropy in profile shape when etching InP in $Br_2 + HBr$ and proposed an interpretation for this anisotropy.

It is assumed that on top of the InP sample (i.e., between the InP and the mask), a thin oxide film is present and that an anisotropy exists in the lateral dissolution rate of this film. The anisotropy exists in the sense that the lateral etch rate is high at the mask edge oriented in the [011] direction but low at the mask edge oriented in the $[01\bar{1}]$ direction. This anisotropy is demonstrated experimentally by the pronounced underetching of the [011] oriented mask edge, in contrast to the less pronounced underetching of the $[01\bar{1}]$ oriented edge after etching in HIO_3 solution (see top view in Fig. 27). This anisotropy suggests that the oxide film has an ordered structure.

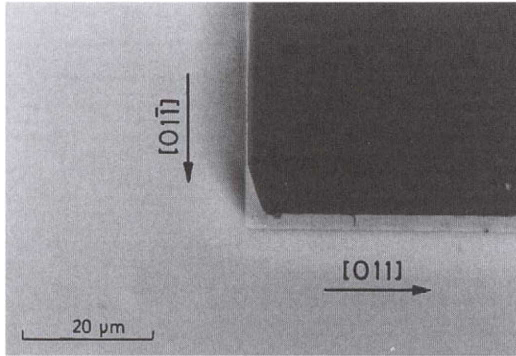

FIG. 27. Photograph of top view of a (100) p-InP sample, partly covered by a photoresist mask, after 30-min etching in 10^{-3}-mol l^{-1} $KIO_3 + HCl$ (pH ≅ 0): [011] direction horizontal. Reprinted from *J. Electrochem. Soc. 142*, I. E. Vermeir, W. P. Gomes, and P. Van Daele, pp. 3226–3232, 1995. Reproduced by permission of The Electrochemical Society, Inc.

The actual situation near the InP surface is shown in Figure 28. The oxide film between the mask edge and the substrate is represented by the lightly shaded area. Consider first the profile obtained for the [01$\bar{1}$] oriented mask edge at which the lateral dissolution of the oxide film is slow (Fig. 28b). The oxide film does not significantly influence the microscopic etch rate and the slow-etching face making a 47° angle with the mask will hence be developed. At a mask edge oriented in the [011] direction, the lateral etch rate of the oxide is assumed to

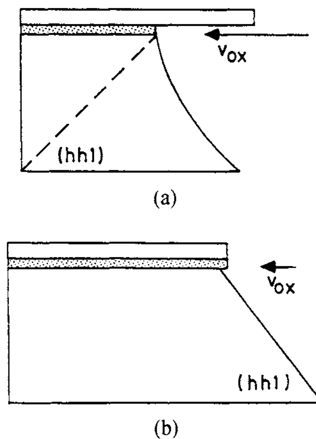

FIG. 28. Model explaining the influence of an oxide top layer on the shape of the profiles etched in InP: (a) mask aligned in the [011] direction; (b) mask aligned in the [01$\bar{1}$] direction. (hhl) denotes either (221) or (331); v_{ox} is the lateral etch rate of the oxide layer. Reprinted from *J. Electrochem. Soc. 142*, I. E. Vermeir, W. P. Gomes, and P. Van Daele, pp. 3226–3232, 1995. Reproduced by permission of The Electrochemical Society, Inc.

be diffusion-limited. In that case, the slow-etching face would then be expected to appear, extending from the oxide edge into the substrate, as symbolized by the dashed line in Figure 28a. This face is, however, not developed: since the lateral etch rate of the oxide is diffusion-limited, the top layer of the InP itself is in direct contact with the etching solution. The etch rate of this (100) face is diffusion-limited as well. Consequently, a rounded profile will be obtained.

When photoetching InP in $FeCl_3 + HCl$, one may wonder why, in contrast to the dark etching by $KIO_3 + HCl$, a dovetail profile at the [011] oriented mask edge is developed, even though the properties of the oxide film and the pH of the solution attacking this oxide are the same in both cases. The crucial point is evidently that in HIO_3, the etching of the (100) face is diffusion-limited, whereas in $FeCl_3$, it is not.

8. Conclusions

From the preceding discussion, it appears that the strategy of combining electrochemical and etch rate measurements constitutes a powerful tool for unraveling the mechanisms of etching reactions at III–V semiconductors, so considerable mechanistic information on these reactions is currently available. Insight into the mechanisms of wet etching reactions provides a fundamental scientific basis for controlling etch rates and for development of new etching procedures, which in the past were established mainly by trial-and-error. This scientific approach is essential in view of the ever-increasing complexity and degree of miniaturization in device fabrication. Understanding and controlling etch rates is particularly important in cases where material-selective etching is involved, as is often the case with III–V multilayer structures used for opto-electronic device fabrication. Insight into the rates and mechanisms of etching reactions at III–V semiconductors also appears to lead to a better understanding of macroscopic and microscopic etch morphologies. Even more detailed (i.e., atomic scale) information on etching mechanisms and on the origin of etch morphologies may be expected in the near future as a result of *in situ* surface studies during etching reactions by surface spectroscopic techniques and by scanning tunneling microscopy. In the case of GaAs, promising results reported recently were obtained from the *in situ* use of these experimental methods in the course of various electrochemical reactions [119, 120, 121].

Acknowledgment

Most of the work performed by the author and his co-workers and cited in the text was performed in the framework of a Gemeenschappelijk Overlegde Actie program, financed by the Ministry of the Flemish Community (Ministerie van de Vlaamse Gemeenschap), Belgium.

References

1. G. E. Thomas, *Philips Tech. Rev.* 44, 51 (1988).
2. C. E. Timmerig, J. M. Langemaat, C. T. Foxon, and J. J. Harris, *Semicond. Sci. Technol.* 3, 1139 (1988).
3. F. A. Ponce and D. P. Bour, *Nature* 386, 351 (1997).
4. S. Nakamura, *Science* 281, 956 (1998).
5. A. Kautek, S. K. Krawczyk, and R. Olier, *J. Electrochem. Soc.* 134, 1859 (1987).
6. J. L. Weyher and J. van de Ven, *J. Cryst. Growth* 78, 191 (1986).
7. R. P. Tijburg and T. van Dongen, *J. Electrochem. Soc.* 123, 687 (1967).
8. H. Gerischer, *Ber. Bunsen-Ges. Phys. Chem.* 69, 578 (1965).
9. H. Gerischer and I. Mattes, *Z. Phys. Chem. NF* 49, 112 (1966).
10. H. Gerischer and I. Willem-Mattes, *Z. Phys. Chem. NF* 64, 187 (1969).
11. H. Gerischer, *Surf. Sci.* 18, 97 (1969).
12. P. H. L. Notten, J. E. A. M. van den Meerakker, and J. J. Kelly, "Etching of III–V Semiconductors: An Electrochemical Approach." Elsevier Advanced Technology, Oxford, 1991.
13. W. P. Gomes and H. H. Goossens, in "Advances in Electrochemical Science and Engineering" (H. Gerischer and C. W. Tobias, Eds.), Vol. 3, Chap. 1. VCH, Weinheim, 1994.
14. H. Gerischer, in "Advances in Electrochemistry and Electrochemical Engineering" (P. Delahay, Ed.), Vol. 1, p. 139. Interscience, New York, 1961.
15. H. Gerischer, in "Physical Chemistry, An Advanced Treatise" (H. Eyring, Ed.), Vol. IX A, p. 436. Academic Press, New York, 1970.
16. S. R. Morrison, "Electrochemistry at Semiconductor and Oxidized Metal Electrodes." Plenum, New York, 1980.
17. Yu. V. Pleskov and Yu. Ya. Gurevich, "Semiconductor Photoelectrochemistry." Consultants Bureau, New York, 1986.
18. Z. Hens and W. P. Gomes, *Phys. Chem. Chem. Phys.* 1, 3607 (1999).
19. H. Gerischer and W. Mindt, *Electrochim. Acta* 13, 1329 (1968).
20. L. M. Peter, J. Li, and R. Peat, *Electrochim. Acta* 35, 1657 (1990).
21. L. M. Peter, A. M. Borazio, H. J. Lewerenz, and J. Stumper, *J. Electroanal. Chem.* 290, 229 (1990).
22. W. J. Albery and M. L. Hitchmann, "Ring-Disc Electrodes." Clarendon, Oxford, 1971.
23. Yu. V. Pleskov and V. Yu. Filinovskii, "The Rotating Disc Electrode." Consultants Bureau, New York, 1976.
24. S. R. Morrison and T. Freund, *J. Chem. Phys.* 47, 1543 (1967).
25. W. P. Gomes, T. Freund, and S. R. Morrison, *J. Electrochem. Soc.* 115, 818 (1968).
26. R. Memming, *J. Electrochem. Soc.* 116, 785 (1969).
27. W. P. Gomes and F. Cardon, *Prog. Surf. Sci.* 12, 155 (1982).
28. A.-M. Van Wezemael, W. H. Laflère, F. Cardon, and W. P. Gomes, *J. Electroanal. Chem.* 87, 105 (1978).
29. Ph. Verpoort, Ph.D. Thesis, University of Ghent, 1997.
30. A. Theuwis, Ph.D. Thesis, University of Ghent, 1998.
31. I. M. Huygens, K. Strubbe, and W. P. Gomes, *J. Electrochem. Soc.* 147, 1797 (2000).
32. R. L. Meek and N. E. Schumacher, *J. Electrochem. Soc.* 119, 1148 (1972).
33. M. J. Madou, F. Cardon, and W. P. Gomes, *Ber. Bunsen Ges. Phys. Chem.* 81, 1186 (1977).
34. P. A. Kohl, C. Wolowodiuk, and F. W. Ostermayer Jr., *J. Electrochem. Soc.* 130, 2288 (1983).
35. S. Preusser, M. Herlem, A. Etcheberry, and J. Jaume, *Electrochim. Acta* 37, 289 (1992).
36. P. J. Verpoort, I. E. Vermeir, and W. P. Gomes, *J. Electrochem. Soc.* 142, 3589 (1995).
37. A. Theuwis and W. P. Gomes, *J. Electrochem. Soc.* 144, 1390 (1997).
38. R. Memming and G. Schwandt, *Electrochim. Acta* 13, 1299 (1968).
39. C. Yontsey, I. Adesida, and G. Bulman, *Appl. Phys. Lett.* 71, 2151 (1997).
40. J. Van de Langemaat, Ph.D. Thesis, University of Utrecht, 1998.
41. M. Pourbaix, "Atlas d'Equilibres Electrochimiques," p. 436. Gauthier–Villars, Paris, 1963.

42. T. Solomun, R. McIntyre, W. Richtering, and H. Gerischer, *Surf. Sci.* 169, 414 (1986).
43. S. Lingier and W. P. Gomes, *Ber. Bunsen Ges. Phys. Chem.* 95, 170 (1991).
44. F. Decker, *Electrochim. Acta* 30, 301 (1985).
45. D. Vanmaekelbergh, J. J. Kelly, S. Lingier, and W. P. Gomes, *Ber. Bunsen Ges. Phys. Chem.* 92, 1068 (1988).
46. D. Vanmaekelbergh and J. J. Kelly, *J. Electrochem. Soc.* 136, 108 (1989).
47. B. H. Erné, D. Vanmaekelbergh, and I. E. Vermeir, *Electrochim. Acta* 38, 2559 (1993).
48. A. Theuwis, I. E. Vermeir, and W. P. Gomes, *J. Electroanal. Chem.* 410, 31 (1996).
49. H. H. Goossens, K. Strubbe, and W. P. Gomes, *J. Electroanal. Chem.* 286, 133 (1990).
50. K. Strubbe and W. P. Gomes, *J. Electrochem. Soc.* 140, 3301 (1993).
51. I. E. Vermeir, H. H. Goossens, F. Vanden Kerchove, and W. P. Gomes, *J. Electrochem. Soc.* 139, 1389 (1992).
52. H. Gerischer, *J. Electroanal. Chem.* 58, 263 (1975).
53. D. Vanmaekelbergh and W. P. Gomes, *J. Phys. Chem.* 94, 157 (1990).
54. D. Vanmaekelbergh, C. W. Hoogendam, and J. J. Kelly, *J. Electroanal. Chem.* 270, 175 (1989).
55. I. E. Vermeir, F. Vanden Kerchove, and W. P. Gomes, *J. Electroanal. Chem.* 313, 141 (1991).
56. I. E. Vermeir, W. P. Gomes, and P. Van Daele, *J. Electrochem. Soc.* 142, 3226 (1995).
57. H. H. Goossens, F. Vanden Kerchove, and W. P. Gomes, *J. Electroanal. Chem.* 261, 89 (1989).
58. H. H. Goossens, W. P. Gomes, and F. Cardon, *J. Electroanal. Chem.* 278, 335 (1990).
59. J. J. Kelly, J. E. A. M. van den Meerakker, P. H. L. Notten, and R. P. Tijburg, *Philips Tech. Rev.* 44, 61 (1988).
60. B. P. Minks, G. Oskam, D. Vanmaekelbergh, and J. J. Kelly, *J. Electroanal. Chem.* 273, 119 (1989).
61. B. P. Minks, D. Vanmaekelbergh, and J. J. Kelly, *J. Electroanal. Chem.* 273, 133 (1989).
62. B. P. Minks, M. Wiegel, and J. J. Kelly, *Electrochim. Acta* 36, 695 (1991).
63. J. J. Kelly, J. van de Ven, and J. E. A. M. van den Meerakker, *J. Electrochem. Soc.* 132, 3026 (1985).
64. J. van de Ven, J. L. Weyher, J. E. A. M. van den Meerakker, and J. J. Kelly, *J. Electrochem. Soc.* 133, 799 (1986).
65. J. van de Ven and H. J. P. Nabben, *J. Electrochem. Soc.* 137, 1604 (1990).
66. J. van de Ven and H. J. P. Nabben, *J. Electrochem. Soc.* 138, 144 (1991).
67. P. H. L. Notten, *Electrochim. Acta* 32, 575 (1987).
68. H. H. Goossens, I. E. Vermeir, F. Vanden Kerchove, and W. P. Gomes, *Electrochim. Acta* 35, 1351 (1990).
69. H. H. Goossens and W. P. Gomes, *Electrochim. Acta* 37, 811 (1992).
70. I. E. Vermeir and W. P. Gomes, *J. Electroanal. Chem.* 365, 59 (1994).
71. F. Decker, B. Pettinger, and H. Gerischer, *J. Electrochem. Soc.* 130, 1355 (1983).
72. J. J. Kelly and P. H. L. Notten, *Electrochim. Acta* 29, 589 (1984).
73. R. M. Feemstra, J. A. Stroscio, J. Tersoff, and A. P. Fein, *Phys. Rev. Lett.* 58, 1192 (1987).
74. K. Strubbe and W. P. Gomes, *J. Electrochem. Soc.* 140, 3294 (1993).
75. P. T. Bowman, E. I. Ko, and P. J. Sides, *J. Electrochem. Soc.* 137, 1309 (1990).
76. F. A. Cotton and G. Wilkinson, "Advanced Inorganic Chemistry." Wiley, New York, 1972.
77. M. Regitz and H. J. Bestmann, "Methoden der Organischen Chemie," 4. Auflage, Band E1, pp. 40, 54. Thieme Verlag, Stuttgart, 1982.
78. H. C. Gatos and M. C. Lavine, in "Progress in Semiconductors" (A. F. Gibson and R. E. Burgess, Eds.), Vol. 9. Temple Press, Brighton, 1965.
79. H. C. Gatos, *Science* 137, 311 (1962).
80. J. J. Kelly and A. C. Reynders, *Appl. Surf. Sci.* 29, 149 (1987).
81. S. Iida and K. Ito, *J. Electrochem. Soc.* 118, 768 (1971).
82. Y. Mori and N. Watanabe, *J. Electrochem. Soc.* 125, 1510 (1978).
83. E. Kohn, *J. Electrochem. Soc.* 127, 505 (1980).
84. P. H. L. Notten and A. A. J. M. Damen, *Appl. Surf. Sci.* 28, 331 (1987).

85. P. H. L. Notten, *J. Electrochem. Soc.* 131, 2641 (1984).
86. A. Theuwis and W. P. Gomes, *J. Electrochem. Soc.* 146, 1903 (1999).
87. T. Tanaka, S. Minagawa, and T. Kajimura, *Appl. Phys. Lett.* 54, 1391 (1989).
88. H. Temkin, M. B. Panish, R. A. Logan, and J. P. van der Ziel, *Appl. Phys. Lett.* 45, 330 (1984).
89. M. Konagai, M. Sugimoto, and T. Takahashi, *J. Cryst. Growth* 45, 277 (1978).
90. E. Yablonovitch, T. Gmitter, J. Harbison, and R. Bath, *Appl. Phys. Lett.* 51, 2222 (1987).
91. P. Demeester, I. Pollentier, L. Buydens, and P. Van Daele, *SPIE Conf. Proc.* 1361 (1990).
92. P. Demeester, L. Buydens, and P. Van Daele, *Appl. Phys. Lett.* 57, 168 (1990).
93. P. Demeester, L. Buydens, I. Moerman, D. Lootens, and P. Van Daele, *J. Cryst. Growth* 107, 161 (1991).
94. A. Malag, J. Ratajczak, and J. Gazecki, *Mater. Sci. Eng., B* 20, 332 (1993).
95. P. J. Verpoort, *Bull. Soc. Chim. Belg.* 105, 805 (1996).
96. H. H. Goossens and W. P. Gomes, *J. Electrochem. Soc.* 138, 1696 (1991).
97. R. Peat, A. Riley, D. E. Williams, and L. M. Peter, *J. Electrochem. Soc.* 136, 3352 (1989).
98. R. Tenne, V. Marcu, and N. Yellin, *Appl. Phys. Lett.* 45, 1219 (1984).
99. R. Tenne and M. Schatkay, *Appl. Phys. B* 35, 243 (1984).
100. R. Tenne, V. Marcu, and Y. Prior, *Appl. Phys. A* 37, 205 (1985).
101. M. M. Faktor and J. L. Stevenson, *J. Electrochem. Soc.* 125, 621 (1978).
102. A. Yamamoto, S. Tohno, and C. Uemura, *J. Electrochem. Soc.* 128, 1095 (1981).
103. B. H. Erné, D. Vanmaekelbergh, and J. J. Kelly, *Adv. Mater.* 7, 739 (1995).
104. B. H. Erné, D. Vanmaekelbergh, and J. J. Kelly, *J. Electrochem. Soc.* 143, 305 (1996).
105. F. Iranzo Marin, M. A. Hamstra, and D. Vanmaekelbergh, *J. Electrochem. Soc.* 143, 1137 (1996).
106. M. M. Faktor, D. G. Fiddyment, and M. R. Taylor, *J. Electrochem. Soc.* 122, 1566 (1975).
107. J. L. Weyher and J. van de Ven, *J. Cryst. Growth* 63, 285 (1983).
108. J. L. Weyher and J. van de Ven, *J. Phys. (Paris)* 43, 313 (1982).
109. J. L. Weyher and L. J. Gilling, *J. Appl. Phys.* 58, 219 (1985).
110. L. R. Plauger, *J. Electrochem. Soc.* 121, 455 (1974).
111. H. K. Kuiken, *Proc. Roy. Soc. London, Ser. A* 392, 199 (1984).
112. H. K. Kuiken, J. J. Kelly, and P. H. L. Notten, *J. Electrochem. Soc.* 133, 1217 (1986).
113. H. K. Kuiken, *Proc. Roy. Soc. London, Ser. A* 396, 95 (1984).
114. C. Vink and C. Cuvelier, *J. Comput. Phys.* 59, 247 (1985).
115. S. Adachi and H. Kawaguchi, *J. Electrochem. Soc.* 128, 1342 (1981).
116. A. Taylor, in "X-Ray Metallography," p. 995. Wiley, Chichester, 1961.
117. J. R. C. Sangster, in "Compound Semiconductors" (R. K. Willardson and H. L. Goering, Ed.) Vol. 1, p. 241. Chapman and Hall, London, 1962.
118. P. H. L. Notten, *J. Electrochem. Soc.* 138, 243 (1991).
119. B. H. Erné, M. Stchakovsky, F. Ozanam, and J. N. Chazalviel, *J. Electrochem. Soc.* 145, 447 (1998).
120. M. Koinuma and K. Uosaki, *J. Vac. Sci. Technol., B* 12, 1543 (1994).
121. C. Kaneshiro and T. Okumura, *Physica B* 227, 271 (1996).